AD-A039 020 TEXAS UNIV AT AUSTIN APPLIED RESEARCH LABS F/G 20/1
EXPERIMENTAL STUDY OF OUTDOOR PROPAGATION OF SPHERICALLY SPREAD--ETC(U)
JAN 77 M A THEOBALD F44620-76-C-0040
UNCLASSIFIED ARL-TR-77-5 AFOSR-TR-77-0521 NL

1 OF 2
AD
A039020

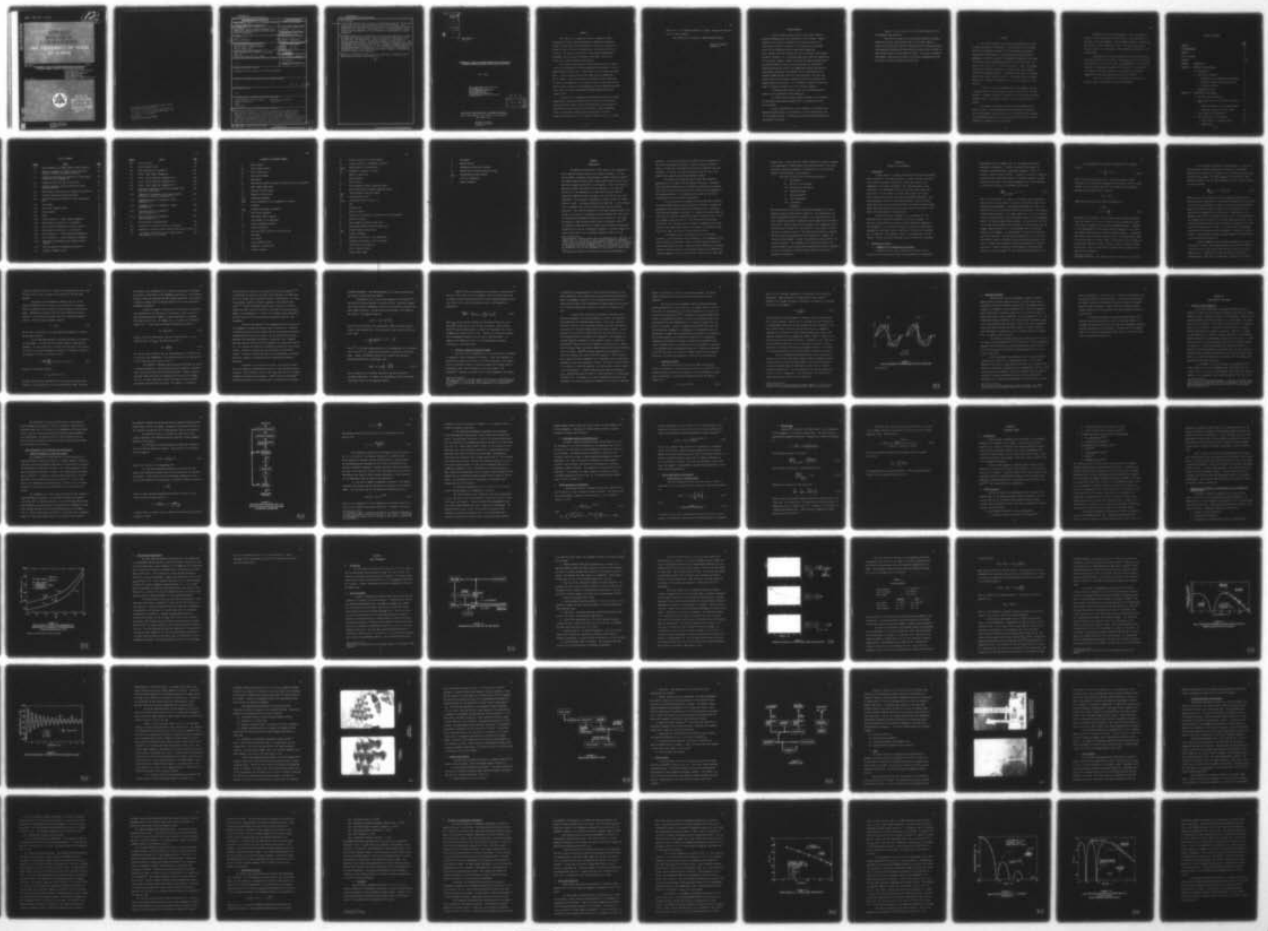

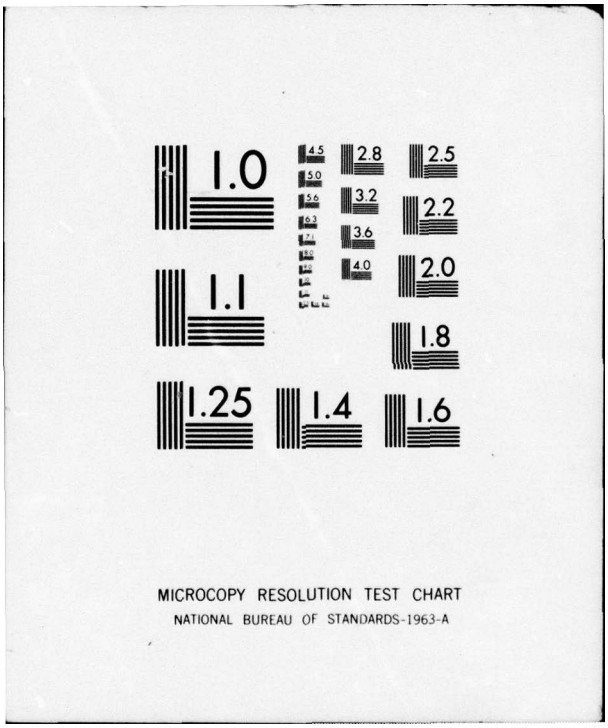
1.0
4.5
5.0
5.6
6.3
7.1
2.8
3.2
3.6
4.0
2.5
2.2
2.0
1.8
1.1
1.25
1.4
1.6
MICROCOPY RESOLUTION TEST CHART
NATIONAL BUREAU OF STANDARDS-1963-A

AFOSR - TR - 77 - 0521

12 NW

AD A039020

APPLIED RESEARCH LABORATORIES

THE UNIVERSITY OF TEXAS AT AUSTIN

ARL - TR - 77 - 5
January 1977

Copy No.

EXPERIMENTAL STUDY OF OUTDOOR PROPAGATION OF SPHERICALLY SPREADING PERIODIC ACOUSTIC WAVES OF FINITE AMPLITUDE

National Aeronautics and Space Administration
Contract NAS1 - 14160,
Air Force Office of Scientific Research
Contract F44620 - 76 - C - 0040,
Office of Naval Research
Contract N00014 - 75 - C - 0867, and
National Oceanic and Atmospheric Administration
Grant 04 - 5 - 022 - 12

Mark A. Theobald

DDC
RECEIVED
MAY 3 1977
D

DDC FILE COPY

APPROVED FOR PUBLIC
RELEASE; DISTRIBUTION
UNLIMITED.

AIR FORCE OFFICE OF SCIENTIFIC RESEARCH (AFSC)
NOTICE OF TRANSMITTAL TO DDC
This technical report has been reviewed and is approved for public release IAW AFR 190-12 (7b).
Distribution is unlimited.
A. D. BLOSE
Technical Information Officer

UNCLASSIFIED

SECURITY CLASSIFICATION OF THIS PAGE *(When Data Entered)*

REPORT DOCUMENTATION PAGE	READ INSTRUCTIONS BEFORE COMPLETING FORM
1. REPORT NUMBER: AFOSR-TR-77-0521	2. GOVT ACCESSION NO. / 3. RECIPIENT'S CATALOG NUMBER
4. TITLE *(and Subtitle)*: EXPERIMENTAL STUDY OF OUTDOOR PROPAGATION OF SPHERICALLY SPREADING PERIODIC ACOUSTIC WAVES OF FINITE AMPLITUDE	5. TYPE OF REPORT & PERIOD COVERED: INTERIM rept.
	6. PERFORMING ORG. REPORT NUMBER: ARL-TR-77-5
7. AUTHOR(s): Mark A. Theobald	8. CONTRACT OR GRANT NUMBER(s): F44620-76-C-0040; N00014-75-C-0867
9. PERFORMING ORGANIZATION NAME AND ADDRESS: Applied Research Laboratories, The University of Texas at Austin, Austin, Texas 78712	10. PROGRAM ELEMENT, PROJECT, TASK AREA & WORK UNIT NUMBERS: 681307, 9781-02, 61102F
11. CONTROLLING OFFICE NAME AND ADDRESS: Air Force Office of Scientific Research/NA, Bldg. 410, Bolling Air Force Base, DC 20332	12. REPORT DATE: January 1977
	13. NUMBER OF PAGES: 152 (169 p.)
14. MONITORING AGENCY NAME & ADDRESS *(if different from Controlling Office)*: —	15. SECURITY CLASS. *(of this report)*: UNCLASSIFIED
	15a. DECLASSIFICATION/DOWNGRADING SCHEDULE

16. DISTRIBUTION STATEMENT *(of this Report)*

APPROVED FOR PUBLIC RELEASE; DISTRIBUTION UNLIMITED

17. DISTRIBUTION STATEMENT *(of the abstract entered in Block 20, if different from Report)*

—

404 434

18. SUPPLEMENTARY NOTES

—

19. KEY WORDS *(Continue on reverse side if necessary and identify by block number)*

Finite-amplitude spherical waves
Outdoor propagation
Siren
Horn arrays
Nonlinear air acoustics
Diffraction

20. ABSTRACT *(Continue on reverse side if necessary and identify by block number)*

The outdoor propagation of spherically spreading sound waves of finite amplitude was investigated. The main purpose of the experiments was to determine the extent to which the outdoor environment, mainly random inhomogeneity of the medium, affects finite amplitude propagation. Periodic sources with fundamental frequencies in the range 6 to 8 kHz and source levels SPL_{1m} from 140 to 149 dB were used. The sources were an array of 7 to 10 horn drivers and a siren. The propagation path was vertical and parallel to

next page

DD FORM 1 JAN 73 1473 EDITION OF 1 NOV 65 IS OBSOLETE

UNCLASSIFIED

SECURITY CLASSIFICATION OF THIS PAGE *(When Data Entered)*

20. Abstract

cont → an 85 m tower, whose elevator carried the traveling microphone. The general conclusions drawn from the experimental results were as follows. The inhomogeneities caused significant fluctuations in the instantaneous acoustic signal, but with sufficient time averaging of the measured harmonic levels, the results were comparable to results expected for propagation in a quiet medium. (U)

Propagation data for the fundamental of the siren approached within 1 dB of the weak shock saturation levels. Extra attenuation on the order of 8 dB was observed. The measurements generally confirmed the predictions of several theoretical models. The maximum propagation distance was 36 m. The narrowbeam arrays were much weaker sources. Nonlinear propagation distortion was produced, but the maximum value of extra attenuation measured was 1.5 dB. The maximum propagation distance was 76 m. The behavior of the asymmetric waveforms received in one experiment qualitatively suggested that beam type diffraction effects were present. (U)

The role of diffraction of high intensity sound waves in radiation from a single horn was briefly investigated. (U)

ESSION for
White Section
Buff Section
ION/AVAILABILITY CODES
AIL. and/or SPECIAL
A

ARL-TR-77-5
January 1977

EXPERIMENTAL STUDY OF OUTDOOR PROPAGATION OF SPHERICALLY SPREADING PERIODIC ACOUSTIC WAVES OF FINITE AMPLITUDE

Mark A. Theobald

National Aeronautics and Space Administration
Contract NAS1-14160,
Air Force Office of Scientific Research
Contract F44620-76-C-0040,
Office of Naval Research
Contract N00014-75-C-0867, and
National Oceanic and Atmospheric Administration
Grant 04-5-022-12

DDC
RECEIVED
MAY 9 1977
D

APPLIED RESEARCH LABORATORIES
THE UNIVERSITY OF TEXAS AT AUSTIN
AUSTIN, TEXAS 78712

APPROVED FOR PUBLIC
RELEASE; DISTRIBUTION
UNLIMITED.

FOREWORD

This report is an adaptation of Mark A. Theobald's thesis "Experimental Study of Outdoor Propagation of Spherically Spreading Periodic Acoustic Waves of Finite Amplitude," which was written for the degree of Master of Science in Engineering at The University of Texas at Austin. Mr. Theobald was enrolled in the Mechanical Engineering Department, and his degree was granted in May 1977. The work was carried out at Applied Research Laboratories.

The research, which began in 1975, represents the first phase in a study of the propagation of finite amplitude sound outdoors. In this phase, periodic sound is used. Random noise is to be used in the second phase. Jointly carrying out the first phase with Mr. Theobald was Don A. Webster. Some of the results not described in this report may be found in the appendices of Mr. Webster's report, "Saturation of Plane Acoustic Waves and Notes on the Propagation of Finite-Amplitude Spherical Waves," Applied Research Laboratories Technical Report ARL-TR-77-4 (January 1977).

The research was supported by the National Aeronautics and Space Administration under Contract NAS1-14160, by the Air Force Office of Scientific Research under Contract F44620-76-C-0040, by the Office of Naval Research under Contract N00014-75-C-0867, and by the National Oceanic and Atmospheric Administration under Grant 04-5-022-12. Technical monitors were Dr. J. M. Seiner for NASA, Lt. Col. R. C. Smith

and Lt. Col. L. W. Ormand for AFOSR, Dr. Logan E. Hargrove for ONR, and Dr. F. F. Hall for NOAA.

This report will be issued as a NASA Contractor Report.

David T. Blackstock
Supervisor

ACKNOWLEDGEMENTS

I wish to thank the many persons on the staff of Applied Research Laboratories who have contributed to this research. Special thanks go to Dr. David T. Blackstock, my research supervisor, for directing the course of this work. I also appreciate his thorough review of this manuscript and his many helpful suggestions.
Don A. Webster worked very closely with me on all phases of the project. William L. Willshire, Jr., contributed many hours toward the construction of the anechoic chamber. James F. Byers and Jack Guyer provided much of the detailed design for the siren and supervised its construction. James Stockton and the staff of the Engineering Services Division provided advice, assistance, and materials for the construction of the anechoic chamber and the use of the tower facilities. The siren and several items for the anechoic chamber were built in the shops of the Engineering Services Division. T. G. Goldsberry, Charles M. Slack, and James J. Truchard provided much of the electronic equipment.

I thank Dila Davis and the staff of the Technical Reports Office for the preparation of this manuscript.

Dr. John M. Seiner kindly arranged for NASA to lend us much of the microphone and analysis equipment used to instrument the tower receive system.

I wish to thank Norris A. Kurio, Assistant to the Director of Balcones Research Center, for permission to use the tower and the room for the anechoic chamber. Red Worley provided technical assistance with maintenance of the tower.

Finally, I wish to thank my wife, Ruth Anne Theobald, for her encouragement and inspiration.

This work was supported by the National Aeronautics and Space Administration under Contract NAS1-14160, the Air Force Office of Scientific Research under Contract F44620-76-C-0040, the National Oceanic and Atmospheric Administration under Grant 04-5-022-12, and the Office of Naval Research under Contract N00014-75-C-0867. It is also a pleasure to acknowledge a scholarship provided by the College of Engineering of The University of Texas at Austin during 1975-1976.

ABSTRACT

The outdoor propagation of spherically spreading sound waves of finite amplitude was investigated. The main purpose of the experiments was to determine the extent to which the outdoor environment, mainly random inhomogeneity of the medium, affects finite amplitude propagation. Periodic sources with fundamental frequencies in the range 6 to 8 kHz and source levels SPL_{lm} from 140 to 149 dB were used. The sources were an array of 7 to 10 horn drivers and a siren. The propagation path was vertical and parallel to an 85 m tower, whose elevator carried the traveling microphone. Measurements were made in late summer under a wide range of weather conditions. The ground level wind speeds were from 0 to 24 km/h. Measurement error was of the order 0.5 dB for calm air.

Several theoretical approaches were used to explain the data. A graphical method is used to gauge the expected importance of nonlinear effects. A computer algorithm is described for use with finite amplitude spherical waves in lossy media. Several ad hoc propagation models are applied.

The general conclusions drawn from the experimental results were as follows. The inhomogeneities caused significant fluctuations in the instantaneous acoustic signal, but with sufficient time averaging of the measured harmonic levels, the results were comparable to results expected for propagation in a quiet medium.

Propagation data for the fundamental of the siren approached within 1 dB of the weak shock saturation levels. Extra attenuation on the order of 8 dB was measured. The measurements generally confirmed the predictions of several theoretical models. The maximum propagation distance was 36 m. A power output at the fundamental frequency of 410 W was estimated.

Experiments using the narrowbeam arrays showed that nonlinear propagation distortion was produced. The maximum value of extra attenuation measured was 1.5 dB. This value was approximately 1.5 dB less than predicted. The maximum propagation distance was 76 m. The behavior of the asymmetric waveforms received in one experiment qualitatively suggested that beam type diffraction effects were present.

The role of diffraction of high intensity sound waves in radiation from a single horn was briefly investigated.

TABLE OF CONTENTS

		Page
FOREWORD		ii
ACKNOWLEDGEMENTS		iv
ABSTRACT		vi
LIST OF FIGURES		xi
GLOSSARY		xiii
CHAPTER I	INTRODUCTION	1
CHAPTER II	REVIEW OF THE LITERATURE	4
	A. Introduction	4
	B. Theoretical Literature	4
	1. Propagation in a Homogeneous, Quiet Medium	4
	2. Effects of Random and Stratified Media	14
	3. Diffraction Effects	16
	C. Experimental Studies	19
CHAPTER III	APPLICATION OF THE THEORY	21
	A. Effective Source Parameters	21
	B. Theory Applicable to Both Moderate and Strong Waves	24
	1. Computer Propagation by Weak Shock Theory	24
	2. Merklinger, Mellen, and Moffett Model	29
	C. Theory Applicable to Weak Waves	29
	D. Theory Applicable to Strong Waves	30
	1. Naugol'nykh et al. (Burgers) Model	30
	2. Rudnick Model	31

		Page
CHAPTER IV	EXPERIMENT DESIGN	33
	A. Introduction	33
	B. Source Selection	33
	C. Estimate of the Importance of Nonlinearity on the Propagation of Spherical Waves	35
	D. Other Design Considerations	39
CHAPTER 5	ARRAY EXPERIMENTS	41
	A. Introduction	41
	B. Array Development	41
	C. Array Transmit System	56
	D. Receive System	58
	1. Tower	60
	2. Source Monitor	62
	3. Traveling Microphone and Anemometer	64
	4. Signal Measuring Equipment and the Enclosure	66
	a. Experimental Accuracy	69
	b. Enclosure	70
	E. Procedure for Propagation Experiments	71
	F. Small Signal Behavior	72
	G. Finite Amplitude Behavior	79
	1. Array No. 1	79
	2. Array No. 2	83
CHAPTER VI	SIREN EXPERIMENTS	94
	A. Siren	94
	B. Siren Transmit System	95

		Page
	C. Siren Operation	99
	D. Evaluation of the Siren as a Sound Source	100
	E. Propagation Experiments at Finite Amplitude	103
CHAPTER VII	CONCLUSIONS	123
APPENDIX A	AN ANECHOIC CHAMBER FOR USE AT HIGH AUDIO FREQUENCIES	127
	A. Introduction	127
	B. Construction	130
	C. Performance Test	132
	D. Chamber Instability	134
APPENDIX B	RADIATION OF HIGH INTENSITY SOUND WAVES FROM A HORN	135
REFERENCES		145

LIST OF FIGURES

Figure	Title	Page
2-1	Axial Waveforms in a Narrow Beam of Finite Amplitude	18
3-1	Computer Propagation of Spherical Waves of Finite Amplitude Including Atmospheric Absorption	26
4-1	Design Curve To Assess the Importance of Nonlinearity on Spherical Wave Propagation	38
5-1	Progressive Wave Tube Test of Horn Driver	42
5-2	Frequency Response of JBL 375 Horn Driver under Various Conditions	45
5-3	Axial Pressure Distribution for Single Horn and Driver	49
5-4	Pressure Distribution Across Horn Mouth	51
5-5	Acoustic Resistance at Throat of Finite Exponential Horn	52
5-6	Horn Arrays	55
5-7	Horn Driver Transmit System	57
5-8	Receive System	59
5-9	Tower	61
5-10	Driver Array No. 2 - Small Signal Propagation	63
5-11	Beam Pattern for Array No. 1 (7 elements)	75
5-12	Axial Pressure in Nearfield of Driver Array No. 1	76
5-13	Beam Pattern for Array No. 2 (10 elements)	78
5-14	Driver Array No. 1 - Finite Amplitude Propagation	80
5-15	Driver Array No. 2 - Finite Amplitude Propagation	84
5-16	Comparison of Experimental and Computed Results Array No. 2	87
5-17	Extra Attenuation of Fundamental--Array No. 2	91
6-1	Schematic Diagram of Siren	96

Figure	Title	Page
6-2	Siren with Horn	97
6-3	Siren Transmit System	98
6-4	Siren Beam Pattern (Fundamental)	102
6-5	Siren - Small Signal Propagation	104
6-6	Siren - Finite Amplitude Propagation No. 1	105
6-7	Siren - Finite Amplitude Propagation No. 2	106
6-8	Siren - Finite Amplitude Propagation No. 3	107
6-9	Qualitative Comparison of Received Waveforms from Three Siren Experiments	109
6-10	Comparison of Experimental and Computed Results Siren-Finite Amplitude Propagation No. 3	112
6-11	Propagation Curve for Fundamental - Siren Experiment No. 2	117
6-12	Propagation Curve for Fundamental - Siren Experiment No. 3	118
6-13	Extra Attenuation of Fundamental Siren Experiment No. 2	120
6-14	Extra Attenuation of Fundamental Siren Experiment No. 3	121
A	Inverse Square Law Measurements	133
B-1	Diffraction of A Spherical Wave by An Aperture	137
B-2	Apparatus To Measure Acoustic Signal on the Axis of a Horn	139
B-3	Oscillograms of Received Acoustic Signal versus Axial Distance for f=7.36 kHz	140

GLOSSARY OF IMPORTANT SYMBOLS

a	piston radius
A_d	area of driver throat
A_m	area of horn mouth
A_o	area of horn throat
b	beam radius
B_n	dimensionless Fourier pressure coefficient for the nth harmonic
c_o	small signal sound speed
d_d	diameter of driver throat
d_t	diameter of horn throat
$E_1(x)$	exponential integral
EXDB	extra attenuation of the fundamental in decibels
f	frequency
f_{kHz}	frequency expressed in kilohertz
f_o	horn cutoff frequency
g	acceleration due to gravity
G	scale height of the atmosphere
H	double exponential integral
$\vec{I}$	acoustic intensity
J_n	nth order Bessel function of the first kind
k	wavenumber
L	horn length
m	flare constant of horn
N	parameter of diffraction
p	acoustic pressure

p_n	acoustic pressure at the nth harmonic
p_1	acoustic pressure at fundamental frequency
p_{peak}	peak pressure of a sawtooth wave
p_{10}	fundamental amplitude at source
q	radius of ring source
r	radial distance
r_o	source radius
$\bar{r}$	shock formation distance--spherical waves
$\hat{r}$	well-formed sawtooth distance--spherical waves
r_{max}	old age distance--spherical waves
SFL	source frequency level
SPL_{1m}	extrapolated source level at 1 m
t	time
t'	retarded time
u	particle velocity
U_n	particle velocity Fourier coefficient for the nth harmonic
x	plane wave distance
$\bar{x}$	shock formation distance--plane waves
$\hat{x}$	well-formed sawtooth distance--plane waves
x_{max}	old age distance--plane waves
Z	acoustic impedance
α	absorption coefficient of the fundamental
α_n	absorption coefficient of the nth harmonic
β	coefficient of nonlinearity
γ	ratio of specific heats
ϵ	acoustic Mach number

λ	wavelength
ρ_o	ambient density
σ	dimensionless distortion variable
σ_o	dimensionless reference distance ($=\beta\epsilon k r_o$)
σ_{max}	dimensionless old age distance
φ	time (as a parameter)
ω	angular frequency

CHAPTER I

INTRODUCTION

The general research topic of this report is the propagation of finite amplitude airborne sound in the outdoor environment. Jet and rocket engines, explosions, and atmospheric sounders ("acoustic radar")* are common sources that may produce sound intense enough to cause finite amplitude propagation distortion to be important. Only a few studies of spherical periodic sound waves of finite amplitude in air have been carried out in the laboratory; even fewer have been done outdoors. (Underwater measurements have been made in the field as well as in the laboratory.) Thus, because our ignorance is great, the need for outdoor studies is great. Two sample problems may be mentioned. (1) The attenuation of broadband noise from jet aircraft cannot now be precisely calculated. The effective attenuation of the high frequency spectral components of jet noise is considerably less than expected when only spherical spreading and atmospheric absorption are accounted for. The lower attenuation at high frequencies might be due to nonlinear effects.[1]** (2) Nonlinear losses may limit the range and effectiveness of atmospheric sounding just as they do in underwater sounding. On the other hand, nonlinear effects may not be as important outdoors as they are in the

---

*The atmospheric acoustic sounder has been operational since 1968 (see, for example, Ref. 3). The device is used to detect atmospheric inhomogeneities, such as wind shear layers and thermal inversions, by receiving sound pulses reflected from the inhomogeneities. The acoustic source is a group of compression horn drivers feeding a common horn or parabolic reflector; an alternative source is the arrangement of the drivers in a plane array.

**References are listed in numerical order following the appendices.

laboratory. It has been speculated, for example, that inhomogeneity of the outdoor medium might neutralize or inhibit nonlinear distortion effects. In any case, very high sound levels are encountered ever more frequently. It is time to replace speculation about the role of nonlinearity with analysis and firm experimental evidence.

The reason for performing outdoor rather than laboratory measurements is, of course, that the medium is different. Turbulence, wind, and thermal gradients are not normally encountered in the laboratory; we do not know very much about their effects on the propagation of finite amplitude waves. Our experiments are an initial step toward experimentation in an uncontrolled environment.

Our objectives were to measure the finite amplitude distortion of a high intensity audio frequency sound wave outdoors, to compare the measurements with existing theoretical predictions, and to record any other nonlinear phenomena encountered. To simplify the interpretation of our results, we kept the experiment as simple as possible; thus, a vertical propagation path was chosen to avoid complications from ground reflections. The experiments were restricted to conditions of low wind speeds to keep random medium effects to a minimum. Two different sound sources were used: an array of horn drivers and a siren.

Our research was motivated partly by two very practical questions. (1) Are nonlinear effects important in the propagation of jet noise? Because the experiment needed to be kept simple, we decided to use periodic waves, not noise. Since the results obtained in the present study were positive, that is, that nonlinear effects can be important in outdoor propagation, the next step will be to employ a source that emits

intense noise. (2) Are nonlinear effects important for acoustic sounding of the atmosphere? Because arrays of horn drivers similar to ours have been used for acoustic sounding in this application, our results may indicate a partial answer to this question.

The report is divided into the following chapters.

I. Introduction

II. Review of the Literature

III. Application of the Theory

IV. Experiment Design

V. Array Experiments

VI. Siren Experiments

VII. Conclusions

Appendices

The reader familiar with theory concerning the propagation of finite amplitude spherical waves may omit chapter II. The considerations in directly applying the theoretical models to our experiments and a computer algorithm applicable to spherical wave propagation are described in chapter III. General criteria for the design of our propagation experiment are given in chapter IV. The evolution of the acoustic sources is described in chapters V and VI. The experimental methods are explained and our results are compared with the existing theory. Chapter VII contains closing remarks. Finally, the appendices contain material of a specialized nature. The performance and construction details of an anechoic chamber for use at high audio frequencies are given in Appendix A. The role of diffraction in high amplitude radiation from a horn is discussed in Appendix B.

CHAPTER II

REVIEW OF THE LITERATURE

A. Introduction

In this chapter we consider existing theoretical and experimental results relevant to the research problem. We seek to describe the distortion and extra attenuation suffered by a directional spherical wave propagating in an outdoor environment. The extra attenuation is the diminution of the fundamental over and above which a small signal wave would suffer. In this report, the terms "small signal" and "linear theory" denote both spherical spreading and atmospheric absorption. Any other atmospheric effects are mentioned separately. There are several analytical as well as ad hoc models available to describe nonlinear propagation under various conditions, but we shall limit our discussion to the models that were applied to the experiments.

In most theoretical treatments of the propagation of finite amplitude waves, a perfectly sinusoidal source wave is assumed. In practice, source distortion or effective source distortion compromises this assumption. It is therefore necessary to find ways of modifying or applying the theoretical results so that more realistic source waveforms may be considered. This question, however, is postponed until the next chapter. For now only purely sinusoidal source waveforms are considered.

B. Theoretical Literature

1. Propagation in a Homogeneous, Quiet Medium

We begin the review with a qualitative description of the distortion of an initially sinusoidal wave propagating in a homogeneous,

quiet medium (see, for example, Ref. 4). We assume that ordinary absorption is negligible. To further simplify the discussion, we initially confine ourselves to plane wave propagation. First, it is helpful to define the term "wavelet." A wavelet is a point on a waveform; a specific value of particle velocity u or acoustic pressure p is associated with this point. Each wavelet propagates with a speed depending on its particle velocity, as expressed in the formula

$$\left.\frac{dx}{dt}\right|_{u=\text{constant}} = c_o + \beta u \quad . \tag{2-1}$$

Here, x is the position, t is time, c_o is the small signal sound speed, and β [$=(\gamma+1)/2$ for air, where γ is the ratio of specific heats] is the coefficient of nonlinearity. The physical mechanisms that lead to the second term in Eq. 2-1 are convection and the nonlinearity of the medium's pressure density relation. For a small signal wave ($u \ll c_o$), all wavelets travel at the same speed. But for increasing values of u, the propagation speed of the wavelets departs from constancy. In particular we see from Eq. 2-1 that the wave peaks (positive values of u) travel faster than the troughs (negative values of u). Our sinusoidal wave will therefore distort as it propagates. At some distance $\bar{x}$, a shock or discontinuity will form in the wave. The unrestricted application of Eq. 2-1 beyond this distance leads to difficulty because a multivalued waveform is predicted. Because such a waveform is physically disallowed for acoustic waves, Eq. 2-1 must be modified. Before taking up the modification, however, let us first examine the wave equation associated with Eq. 2-1.

The approximate wave equation for plane waves in a lossless fluid is

$$u_x - \frac{\beta}{c_o^2} uu_{t'} = 0 \quad , \tag{2-2}$$

where t' is the retarded time $t-x/c_o$. (The exact equation is less convenient for our purposes and negligibly more accurate, even up to sound pressure levels of the order 165 dB).* The solution of this equation satisfying the boundary (source) condition

$$u(0,t) = g(t) \quad ,$$

(where $g(t)=u_o \sin \omega t$ for the present discussion) is

$$u = g(\varphi)$$

$$\varphi = t' + \frac{\beta u x}{c_o^2} \quad . \tag{2-3}$$

The notation is as follows: φ is the time at which a particular wavelet leaves the source (i.e., $t=\varphi$ at $x=0$) and u_o is the peak particle velocity at the source. Equation 2-3 is called the Earnshaw solution. (Actually, it is an approximation of the solution given by Earnshaw.[5]) It is valid for distances $x<\bar{x}$, where $\bar{x}$ is the shock formation distance. A sinusoidal wave forms a shock at $\bar{x}=1/\beta\epsilon k$, where $\epsilon[=u_o/c_o]$ is the acoustic Mach number at the source and k is the wave number. At this point it is convenient to introduce the distortion distance variable σ, which is defined for plane waves as $x/\bar{x}$. Thus for a wave from a sinusoidal source, $\sigma=\beta\epsilon kx$, and $\sigma=1$ signifies shock formation.

---

*Throughout this work, sound pressure levels are referred to 2×10^{-5} N/m^2.

We now consider the question of modifying Eqs. 2-1 and 2-3 so that wave trains containing shocks may be described. The Earnshaw solution (Eq. 2-3) may still be applied to the continuous portions of the waveform between shocks. The Rankine-Hugoniot shock relations, which express conservation laws for shock propagation, may be combined to yield the useful relation

$$\left.\frac{dx}{dt}\right|_{shock} \doteq c_o + \frac{\beta}{2}(u_a+u_b) \quad , \tag{2-4}$$

where u_a and u_b are the particle velocities immediately ahead of and behind the shock, respectively. The expression indicates that the velocity of the shock is approximately the mean of the wavelet speeds immediately ahead of and behind the shock. Equation 2-4 then replaces Eq. 2-1 in describing the propagation of the shock front. Descriptions of the merging of shock waves are provided by Refs. 4 and 5. The combination of the Earnshaw solution with Eq. 2-4 is termed "weak shock theory." Few initial waveforms are simple enough for analytical solutions of the weak shock theory equations to be found. On the other hand, the equations themselves are conceptually simple and amenable to solution by computer methods. Pestorius[6] has developed a computer algorithm that may be used for an arbitrary source waveform.

In the propagation of an initially sinusoidal wave, the wave will distort to form a full-fledged sawtooth at the position $\hat{x}=3\bar{x}(\sigma=3)$.[4] The sawtooth is the most nearly stable periodic waveform for a finite amplitude wave. Dissipation occurs at the shocks in the sawtooth. Simultaneously, energy from the fundamental is pumped into the higher

harmonics. This process keeps the wave a sawtooth. The sawtooth waveshape is approximately maintained out to a distance $x_{max}=1/\alpha-\bar{x}$, (σ_{max}), where α is the attenuation coefficient for ordinary absorption in the medium. From approximately this point on, the wave becomes a quasi-sinusoid. Linear theory is then roughly sufficient to predict the propagation.

The major weakness encountered with weak shock theory in our application is that the only dissipation included is caused by irreversible processes at the shocks. Ordinary small signal absorption is ignored. In practice, there are many instances in which ordinary absorption is not negligible for waves containing weak shocks. In fact, absorption may prevent shock and/or sawtooth formation by damping the wave very quickly. Weak shock theory should not be applied to waves too weak to form shocks (see, for example, Ref. 4). Thus the problem of simultaneously accounting for both nonlinear and ordinary absorptive losses must be considered and will be discussed in more detail later in the chapter.

The application of weak shock theory is restricted to pressure levels for which the underlying approximations are valid. The upper limit for plane waves in air is a sound pressure level of approximately 165 dB.[7] This restriction was of minor importance in our experiments.

Turning now to the propagation of diverging spherical waves, we note that the approximate (lossless) wave equation analogous to Eq. 2-2 is

$$u_r + \left(\frac{1}{r}\right) u - \left(\frac{\beta}{c_o^2}\right) uu_{t'} = 0 \quad , \tag{2-5}$$

where the retarded time is now $t'=t-(r-r_o)/c_o$ and r_o is the source radius. The nonlinear distortion process slows down dramatically for spherical

waves, as compared to the distortion process for plane waves. The reason for the slackening is the reduction in amplitude caused by spherical spreading. The mechanisms causing the distortion are the same as the mechanisms for plane waves, but their effect is lessened by spherical spreading. The Earnshaw solution, Eq. 2-3, and weak shock theory may be applied to spherical propagation by making the replacements $u \rightarrow ru/r_o$ and $x \rightarrow r_o \ln(r/r_o)$. For spherical waves from a sinusoidal source, the expression for σ is

$$\sigma = \beta \epsilon k r_o \ln\left(\frac{r}{r_o}\right) \quad ,$$

which shows that σ increases much more slowly with distance than it does for plane waves. The inverse relation is

$$r = r_o e^{\sigma/\beta\epsilon k r_o} \quad .$$

The values $\sigma=1$ and $\sigma=3$ still indicate shock and sawtooth formation, respectively. For example, shocks form at the distance

$$\bar{r} = r_o e^{1/\beta\epsilon k r_o} = r_o e^{\bar{x}/r_o} \quad .$$

Therefore, if the equivalent plane wave shock formation distance $\bar{x}$ is much greater than the source radius, the spherical wave must travel a very great distance to distort into a shock wave. As in the case of plane waves, there is also a distance r_{max} (σ_{max}) beyond which nonlinear effects become approximately negligible. The formula for r_{max} is given in chapter III. Directional sources may be treated for the farfield case by

a procedure described in Ref. 9. Because our measurements were made along the axis of the sources, we ignore directionality in the following material.

Included in the approximations leading to Eq. 2-5 is the farfield assumption, that is, $kr \gg 1$. In the farfield of a spherical source, the particle velocity and the acoustic pressure p are nearly in phase. Although the solution of Eq. 2-5 is most naturally written in terms of u, the condenser microphones used in our experiments measure pressure. The small signal impedance relation

$$p = \rho_o c_o u \tag{2-6}$$

may be used to relate p and u for the sound levels amenable to solution by weak shock theory.[6]

In the preceding discussion, nonlinear distortion was viewed in the time domain. The view from the frequency domain is often equally important. In other words, given a source waveform, what is the spectrum of the wave at a certain propagation distance? We consider a solution to this question in terms of the Fourier series

$$p = \frac{r_o p_{10}}{r} \sum_{n=1}^{\infty} B_n \sin n[\omega t - k(r-r_o)] \quad , \tag{2-7}$$

subject to the boundary condition

$$p = p_{10} \sin \omega t \text{ at } r=r_o \quad .$$

We shall discuss several approaches for calculating the harmonic amplitudes B_n. We first define the often used abbreviation EXDB. The extra

attenuation of the fundamental due to nonlinear effects may be expressed as the ratio (in decibels) of the fundamental amplitude p_1 to the combined effects of spherical spreading and small signal absorption. This quantity is denoted by EXDB, where the acronym stands for the "extra attenuation expressed in decibels."

Perhaps the simplest expressions for the harmonic amplitudes are the expressions for the amplitudes of strong waves, that is, waves in which ordinary absorption compared to shock dissipation is negligible. The Fubini solution (see, for example, Ref. 4) is valid in the preshock region ($\sigma \leq 1$). In this case, the harmonic amplitudes are given by

$$B_n = \frac{2}{n\sigma} J_n(n\sigma) \quad , \tag{2-8}$$

where J_n is the nth order Bessel function of the first kind. In the sawtooth region ($3 \leq \sigma \leq \sigma_{max}$), the weak shock result is

$$B_n = \frac{2}{n(1+\sigma)} \quad . \tag{2-9}$$

(We note for later reference that the second harmonic of a sawtooth wave is 6 dB below the fundamental.) The expression valid in the region $1 < \sigma < 3$ is more complicated and is given in Ref. 8.

The analysis of moderate and weak waves must include the effects of ordinary absorption. Several models have been proposed to simultaneously consider nonlinear distortion and absorption. Burgers' equation describes simple wave flow in a thermoviscous fluid (see, for example, Ref. 4). No exact solutions are known for spherical waves, but some approximate solutions have been found. For example, a perturbation

solution has been obtained for the range prior to shock formation.[10,11] In describing the results of our first array experiments, we shall make use of the second order perturbation solution. Naugol'nykh et al. found an approximate solution of Burgers' equation for the sawtooth wave region.[12] Tepper[13] approximated Naugol'nykh's solution by a Fourier series, and Cary[13] used this solution to calculate the extra attenuation (EXDB) of the fundamental. In chapter VI we compare values predicted by Cary with values of the extra attenuation measured during our siren experiments.

Pestorius[6] and Anderson[14] have programmed weak shock theory for the propagation of plane and spherical waves, respectively. Pestorius corrected the particle velocity values for tube wall attenuation and dispersion during the distortion process. The calculations were in good agreement with experiments performed in a plane wave tube. Anderson generated computer solutions for the propagation of a spherical N wave in air. The solution was improved by including air absorption in the calculations. Anderson's computations closely matched his experimental results. To predict received waveforms for our experiments, we modified Pestorius' program by including spherical spreading and atmospheric absorption.

In addition to the models given above, several ad hoc models have been proposed to simultaneously account for both absorption and nonlinearity. These models are ad hoc in the sense that they are not direct attempts at solving the wave equation. Safar[15] and Pernet and Payne[16] present models valid in the preshock region for absorption of arbitrary

frequency dependence. The sound generated by our sources was generally too intense to apply these two models.

Merklinger et al.[17] used a method suggested by Westervelt[18] to calculate the extra attenuation for spherical waves. Westervelt assumed that energy from the fundamental is used in second harmonic generation and small signal absorption. Interactions involving higher order harmonics are ignored. The suggested model is

$$\text{div } \vec{I} = -2\alpha I + \left\langle p^{(1)} q \right\rangle \quad ,$$

where $\vec{I}$ is the intensity of the fundamental, $I \equiv |\vec{I}|$, the angle brackets denote a time average, and q is the nonlinear acoustic source density per unit volume

$$q = \frac{\beta}{\rho_o^2 c_o^4} \frac{\partial}{\partial t} \left(p^{(1)} + p^{(2)} + \ldots \right)^2 \quad .$$

Here $p^{(1)}$ is the small signal solution for the fundamental at the retarded time t' and $p^{(2)}$ is a second order correction involving the second harmonic. Using a perturbation solution due to Safar[15] and solving a Bernoulli equation for I, Merklinger found

$$\text{EXDB} = 10 \log_{10} \left(1 + \frac{\sigma_o^2 H}{2} \right) \quad , \qquad (2\text{-}10)$$

where $\sigma_o = \beta \epsilon k r_o$ and H is a double exponential integral that must be evaluated numerically. We compare our experimental results with predictions based on Eq. 2-10 in chapters V and VI.

Rudnick,[19] while investigating the attenuation of plane sawtooth waves in a duct, made the ad hoc assumption that the sawtooth decay rate is simply the sum of the decay rates due to small signal attenuation (tube wall effects in his case) and nonlinear effects. The assumption is expressed as

$$\frac{dp_{peak}}{dx} = -\left(\alpha_t p_{peak} + \frac{\beta k}{\pi \rho_o c_o^2} p_{peak}^2\right) \quad , \qquad (2\text{-}11)$$

where p_{peak} is the acoustic pressure at the sawtooth peak and α_t is an absorption coefficient for the tube wall attenuation. More recently, Webster[11] used the Rudnick model to predict the saturation level of the fundamental for plane waves in a tube. Webster also presented a solution for the fundamental amplitude for the case of spherical waves. In chapter VI we compare data from our siren experiments with predictions based on the Rudnick model.

2. Effects of Random and Stratified Media

Two basic types of inhomogeneity of the medium must be considered in planning an outdoor propagation experiment. First, the atmosphere is stratified or layered with respect to the fluid parameters. The stratification is especially evident in vertical propagation at heights that are nonnegligible when they are compared to the scale height of the atmosphere.* (Because we consider only vertical propagation, the effects

*The scale height G is the basic length scale related to stratification of the atmosphere. It is $c_o^2/(\gamma g)$ (about 8 km), where g is the acceleration due to gravity; G is the height of the atmosphere if the density were constant.

of refraction are neglected here.) Second, random fluctuations of the medium parameters often accompany wind turbulence and other disturbances. While the propagation distance for the experiments described in this thesis was very short, future experiments at longer ranges are envisioned. It is therefore appropriate to mention the effects of inhomogeneities here.

A sizeable body of theoretical literature describing finite amplitude propagation in stratified media has evolved. The atmosphere is often modeled as an isothermal medium subject to the force of gravity. The ambient density for an isothermal atmosphere decreases exponentially with height, but the small signal sound speed remains constant. For an analysis of the effects of stratification for this case (and a list of other Russian works on the subject), see Romanova.[20] The assumption of constant (ambient) temperature is not required, however. Carlton and Blackstock[21] treated the vertical propagation of plane waves in a medium where the small signal sound speed, ambient density, and fluid nonlinearity vary with height. Nayfeh[22] described quasiplane wave propagation in ducts with varying cross section and fluid properties. Both references may be applied to plane propagation in the atmosphere when the functional dependence of the fluid parameters is known. The effect of stratification is to amplify or reduce the amplitude u_o of the particle velocity relative to the sound speed c_o. Because finite amplitude distortion depends on u_o/c_o, stratification has the effect of either speeding up or slowing down the distortion. For example, for a wave propagating vertically in the atmosphere, the distortion generally accelerates if the wave is traveling

upward but decelerates if the wave is traveling downward. The details depend ultimately on the specific medium conditions and the source amplitude.

The theory of linear propagation through a medium containing random inhomogeneities is well known (see, for example, Refs. 23 and 24). The effect of a random medium on nonlinear propagation is the subject of several recent publications.[25,26] A difficulty in applying random medium theory to an experimental situation is that the distribution function in time and space for the inhomogeneities is, in general, unknown and very difficult to measure. However, Fridman and Pelinovsky[26] state that, for finite amplitude propagation, the amplitudes of all harmonics above the fundamental are larger than the amplitudes in the absence of fluctuations. The increase depends on the distribution functions of the parameters. Lacking the instrumentation required to estimate the distribution functions, we assumed that, by confining our initial experiments to conditions of low windspeeds and by averaging the data over a sufficiently long time span,[27] we could ignore the effects of random fluctuations on nonlinear distortion. We found this assumption to hold true in our experiments.

3. Diffraction Effects

Some recent theoretical work from the USSR concerning the effects of diffraction on strong acoustic beams is of interest.[28-30] The theoretical models describe the propagation of a well-collimated circular beam of plane waves. The amplitude distribution across the beam is assumed to be

$$p = p_{10} \exp(-r^2/b^2) \quad , \qquad (2\text{-}12)$$

where r is the coordinate transverse to the beam and b is the effective beam radius. (This assumption is commonly made in radar theory.) Rudenko et al.[28] gauge the relative importance of diffraction to nonlinear distortion by the parameter

$$N = \frac{2}{\beta\epsilon(kb)^2} \quad . \tag{2-13}$$

As $N \to 0$, nonlinear effects dominate the behavior while, for $N \to \infty$, diffraction is most important. Analysis for the lossless case where diffraction is nonnegligible shows that the beam diverges after $\hat{x}$ is surpassed.* The most intense section of the beam (on and near the axis) is damped by dissipation at the shocks. The wave becomes asymmetrical, that is, the peaks are sharpened and the troughs are rounded. Figure 2-1 shows the on-axis solutions for the cases N=0 and N=0.4. Bakhvalov et al.[29] show theoretical waveform variations on and off the axis as functions of source amplitude, the distance off-axis, and propagation distance. No solutions of the governing equations for arbitrary source waveforms are available.

The well-collimated beam described above is not encountered in practice, but the model may apply to highly directive radiators at large distances where the waves are nearly planar. The received waveforms in our array experiments may show qualitative evidence for the "peaked" waveform described above. In our discussion of the data we estimate the value of N for our experiments. For a discussion of the diffraction of high intensity waves from a horn, see Appendix B.

---

*The definition of the discontinuity buildup length σ_d in Ref. 28 corresponds to the "well-formed sawtooth distance" $\hat{x}(\sigma=3)$ in our notation.

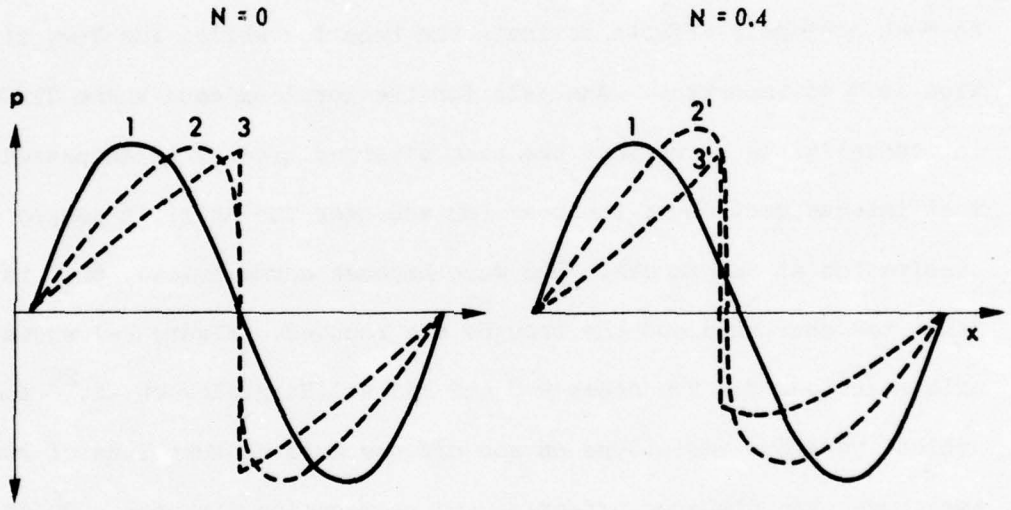

1: $\sigma = 0$
2, 2′: $\sigma = 1$
3, 3′: $\sigma = 2$

FIGURE 2-1
AXIAL WAVEFORMS IN A NARROW BEAM OF FINITE AMPLITUDE

(Taken from Ref. 30.)

C. Experimental Studies

There have been very few experimental studies of periodic spherical waves of finite amplitude in air.* The only known outdoor measurements were made by Widener and Muir,[34] who investigated the performance of a parametric array operating in air. (The term "parametric array" describes the nonlinear interaction of two collinear single frequency sound beams of finite amplitude. See, for example, Ref. 35.) The difference frequency generated by the interaction was investigated along a 20 m long horizontal path over water. While other outdoor experiments using very powerful sources have been reported, no attempt was made in these experiments to quantify the role of nonlinear effects on the data (see, for example, Refs. 36 and 37).

The laboratory (indoor) studies most nearly related to our work are those of Allen and Rudnick,[38] Allen,[39] and Shin.[40] Allen and Rudnick measured the beam patterns for a siren generating an acoustic output of 84 to 176 W and pointed out several interesting characteristics of the intense sound field.

Allen investigated the radiation from a St. Clair generator[41] operating at 14.6 kHz in a 2 m long anechoic space. The St. Clair generator functioned as a plane baffled piston and, as a resonant device, generated a nearly pure sinusoidal wave at a maximum SPL of 161 dB. Allen recorded such finite amplitude effects (now commonly known) as acoustic saturation, blunted beam patterns, and poor side lobe suppression. Saturation is the limiting process whereby the received level at a field

*We duly note the large literature on sonic booms (see, for example, Refs. 31 and 32) and explosion sounds (see, for example, Ref. 33).

point is independent of the source level. Increases in the source level are nearly nullified by extra attenuation. The directivity alterations are caused by the extra attenuation incurred at sections of the sound field with higher intensity. A major lobe that is normally rounded becomes squared off as the amplitude in the center decreases relative to the side lobes.

To study the attenuation of spherical sawtooth waves, Shin utilized a siren and conducted the study in an anechoic chamber. He corrected the weak shock decay rate for spherical spreading and obtained excellent agreement with his experiment. The data cover the frequency range 8.5 to 11 kHz for extrapolated source levels of 139 to 143 dB at 1 m, over distances as great as 1 m.

CHAPTER III

APPLICATION OF THE THEORY

A. Effective Source Parameters

One of the difficulties in applying the models described in chapter II is that the source conditions assumed in the models are usually different from the conditions realized in the experiments. Except for the computer algorithm described in section B.1. of this chapter, the models used here are restricted to sound that is a pure sine wave at a reference point r_o in the farfield. In practice, however, the wave is usually already distorted when it reaches the farfield. There are two reasons for such distortion. (1) There is inherent distortion in the transducer. Inherent distortion was particularly strong in our siren source. (2) The signal is subject to finite amplitude distortion as it travels through the nearfield. Our method of dealing with "source distortion" is to measure the distorted waveform at an initial point $r=r_i$ just outside the nearfield and to extrapolate backward until we reach an effective source radius r_o at which the waveform is a pure sinusoid.* The dimensionless amplitude at this point is denoted ϵ.

Our estimates of r_o and ϵ are based on a measurement of the sound pressure levels of the fundamental and second harmonic at the initial point r_i. We use the second harmonic rather than other harmonics because, in our experiments, more energy was present there than in the

*For piston sources operating underwater, it has been found empirically that a value of r_o between $R_o/3$ and $3R_o/4$ is acceptable. Here R_o is the Rayleigh distance given by the piston area divided by the wavelength. See, for example, Ref. 2.

higher harmonics. Consider again Eq. 2-7 and let p_n denote the pressure amplitude of the nth harmonic. We write

$$p_1 = \frac{r_o p_{10}}{r} B_1$$

and

$$p_2 = \frac{r_o p_{10}}{r} B_2 \quad ,$$

where B_n is given by the appropriate formula (for example, Eq. 2-8 or 2-9), depending on whether shocks are present and at what stage of development. A measurement of p_1 and p_2 is made at the distance r_i. We are left, therefore, with a system of two equations in two variables (r_o and p_{10}). In principle, we may solve the system to yield the desired source parameters. For example, if r_i is in the preshock region, that is, $\sigma_i < 1$, we have

$$p_{1i} = \frac{r_o p_{10}}{r_i} \frac{2}{\sigma_i} J_1(\sigma_i) \tag{3-1}$$

and

$$p_{2i} = \frac{r_o p_{10}}{r_i} \frac{1}{\sigma_i} J_2(2\sigma_i) \quad . \tag{3-2}$$

Forming the ratio of p_{2i} to p_{1i}, we obtain

$$\frac{p_{2i}}{p_{1i}} = \frac{J_2(2\sigma_i)}{2J_1(\sigma_i)} \quad , \tag{3-3}$$

from which the value of σ_i may be found. The smallest value of σ_i satisfying Eq. 3-3 is selected. Equation 3-1 may then be solved for $r_o p_{10}$.

Using this value and the expression for σ_i $[=\beta\epsilon k r_o \ln(r_i/r_o)]$, we obtain the source radius

$$r_o = r_i \, e^{-\sigma_i/\beta\epsilon k r_o} \quad . \tag{3-4}$$

Finally, p_{10} (and therefore ϵ) is computed from the value of $r_o p_{10}$. If shocks are present, one must use the sawtooth or transition expressions for p_1 and p_2 in order to find σ_i.

In the extrapolation procedure described here, it is tacitly assumed that the fundamental and second harmonic are in phase. In general, this condition is not guaranteed to hold. In addition, a source may produce an asymmetrical waveform. We are therefore justified in the extrapolation procedure only to the extent that agreement with the experiment warrants.

The range parameters for our experiments are calculated by[8]

$$\bar{r} = r_o \exp\left\{\frac{1}{\sigma_o}\right\} \quad , \tag{3-5a}$$

$$\hat{r} = r_o \exp\left\{\frac{3}{\sigma_o}\right\} \quad , \tag{3-5b}$$

and

$$r_{max} = \left(\frac{\sigma_o}{\alpha}\right)\left[1 + \sigma_o \ln\left(\frac{r_{max}}{r_o}\right)\right]^{-1} \quad , \tag{3-5c}$$

where $\sigma_o = \beta\epsilon k r_o$. Equation 3-5c is transcendental and must be solved by iteration. Range parameters based on an effective source are listed with the propagation curves (shown in chapters V and VI). The parameters are subscripted "eff" to suggest the effective source.

The calculation of extra attenuation based on the effective source parameters also warrants a word of explanation. Measured extra attenuation must refer to the level of the fundamental at the source position r_i, that is, the point from which the effective source parameters were extrapolated. The predicted value of extra attenuation for our source is then the difference between the values predicted by the models for the distance $r(r>r_i)$ and r_i.

B. Theory Applicable to Both Moderate and Strong Waves

1. Computer Propagation by Weak Shock Theory

The propagation of a spherical wave of finite amplitude in a lossy medium may be described by means of a computer program. We modify Pestorius' weak shock propagation algorithm for plane waves[6] by correcting the computations for spherical spreading. For a loss mechanism, we substitute atmospheric absorption in place of the boundary layer attenuation used by Pestorius. D. Watson of Applied Research Laboratories provided additional, more flexible input and output schemes.[42] Only the basic steps in the computations are outlined below. See Ref. 6 for a detailed discussion of the techniques and algorithms used to perform the calculations.

The propagation of a finite amplitude spherical wave consists of three simultaneous processes: (1) spherical spreading, (2) nonlinear distortion, and (3) ordinary absorption. For a sufficiently small propagation distance, one may consider the processes to be independent of each other and may calculate their effects sequentially (see, for example, Ref. 6). While a process may be described in either the time or frequency domain, the functional representation in one domain is often simpler.

The computer's forward and inverse fast Fourier transforms (FFT and FFT^{-1}, respectively) link the two domains. Because of the restriction $kr \gg 1$, we are justified in using Eq. 2-6 to relate particle velocity and pressure.

The flowchart in Fig. 3-1 provides an overall view of the computer algorithm. The functional form for each part of the propagation process is listed below.

(1) The particle velocity decreases by spherical spreading at a rate of 6 dB per doubling of distance. This relation is expressed in the time domain as

$$u(r+\Delta r) = \frac{r}{r + \Delta r}\, u(r) \quad , \tag{3-6}$$

where Δr is the size of the propagation step.

(2) The finite amplitude distortion is viewed in the time domain as an amplitude dependent shift in the arrival time for a particular wavelet. If the wavelet were of infinitesimal amplitude or were a zero of the waveform, the time required to traverse a distance Δr would be

$$t_o = \frac{\Delta r}{c_o} \quad .$$

But for a finite amplitude wavelet whose particle velocity is u, the travel time for the same distance is

$$t_f = \frac{\Delta r}{c_o + \beta u} = t_o - \frac{\beta u \Delta r}{c_o^2 + c_o \beta u} \quad .$$

To first order in ϵ (where $u \ll c_o$), we may drop the term $c_o \beta u$ in the above equation to obtain

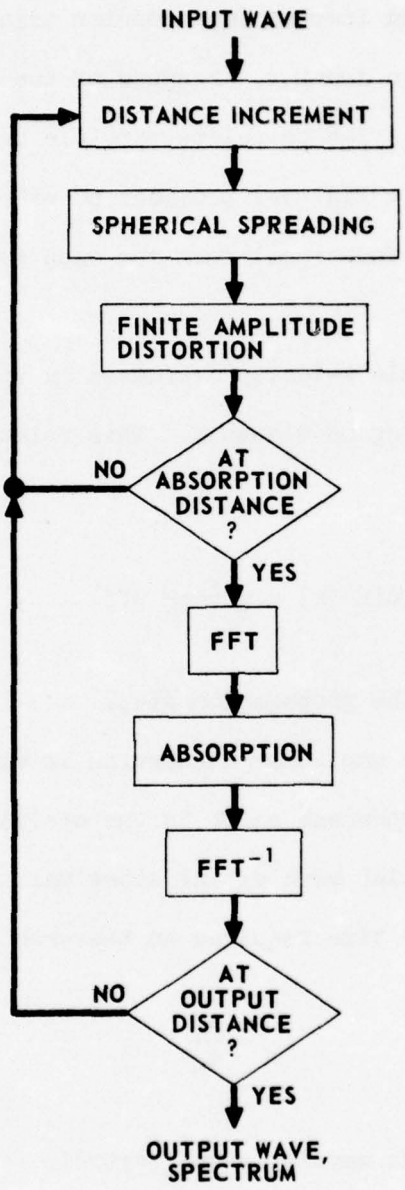

FIGURE 3-1
COMPUTER PROPAGATION OF SPHERICAL WAVES OF FINITE AMPLITUDE INCLUDING ATMOSPHERIC ABSORPTION

$$t_f = t_o - \frac{\beta u \Delta r}{c_o^2} \quad . \tag{3-7}$$

The analogous form for the arrival time t_s of a weak shock front is (see Eq. 2-4)

$$t_s = t_o - \frac{\beta(u_a+u_b)\Delta r}{2c_o^2} \quad . \tag{3-8}$$

The computations required for the merging of shocks are given in Ref. 6. Our version of the computer program is not included in this report because the published version by Pestorius may be easily modified by including spherical spreading (Eq. 3-6)* and by replacing tube wall losses by atmospheric absorption. Because nonlinear distortion depends on the ratio of the particle velocity to the small signal sound speed and our measurements were taken at widely varying temperatures, we were careful to use the appropriate speed of sound in the calculations.

(3) The wave is damped by atmospheric absorption. The damping increases with frequency and the calculation is performed in the frequency domain. The functional form for the atmospheric absorption alone is

$$U_n(r+\Delta r) = U_n(r)\, e^{-\alpha_n \Delta r} \quad , \tag{3-9}$$

where U_n is the magnitude of the nth harmonic in the Fourier series for u and α_n is the respective absorption coefficient. Dispersion need not be

*An appropriate place to insert the calculation for spherical spreading in the published program is following step C40, p. 173 of Ref. 6. The accumulated propagation distance prior to calling the subroutine is required for the calculation.

considered, because in atmospheric propagation it is negligibly small at normally encountered frequencies.

In our experiments atmospheric absorption is a much weaker effect than spherical spreading and is often weaker than nonlinear distortion. The absorption calculation occurs in the frequency domain while both the distortion and spreading calculations are made in the time domain (see Fig. 3-1). Thus, computer time is saved (the FFT operation is comparatively slow) by correcting for absorption at larger distance increments than those used for distortion and spreading. The absorption coefficients are calculated from a formula given by Bass.[43] The resulting coefficients are accurate to ±5% over the temperature range 273 to 313°K, the relative humidity range 0 to 100%, and the frequency range 50 Hz to 10 MHz at a pressure of 1 atm. The addition of an algorithm based on Bass' formula is an improvement over the procedure used by Anderson,[14] who assumed that the coefficients simply increase with the square of the frequency. The improvement should be significant at frequencies where relaxation effects are important.

By repeatedly applying Eqs. 3-6, 3-9, and 3-7 or 3-8 to every wavelet, one may simulate the propagation of the wave.

The input waveform to the program was taken from a measurement at $r=r_i$. The point r_i was in the farfield of the source but was as close to the source as feasible. A Hewlett-Packard 9810A programmable calculator with a 9864A digitizer was used to digitize the oscillogram. The minimum resolution was 0.25 mm. The waveform was smoothed by the calculator to minimize digitizing jitter. The resulting data were filtered to remove any dc pressure bias (dc bias would cause problems

during program execution) and were scaled to match the time-averaged level of the fundamental. Discussion of further details related to program execution is delayed until chapter V.

2. Merklinger, Mellen, and Moffett Model

In order to apply the method developed by Merklinger et al. for the calculation of the extra attenuation of the fundamental (Eq. 2-10) to our work, we use the effective source parameters as explained in section A of this chapter. The double exponential integral H required for the solution is written in terms of single exponential integrals by Fenlon.[44] Merklinger et al. state that Fenlon's expression is an approximation accurate to 20% for $\bar{\alpha}r_o \leq 0.1$ dB, where $\bar{\alpha}$ is the absorption coefficient expressed in dB/unit distance. The inequality is easily satisfied in our experiments. We calculate the single exponential integrals by using a polynomial approximation given in Ref. 45. The expansion has a maximum error of 2×10^{-7} for $\bar{\alpha}r \leq 4.3$ dB.

C. Theory Applicable to Weak Waves

A perturbation solution of Burgers' equation for spherical waves may be applied to a wave in which no shocks are present. The solution for the second harmonic, accurate to second order in ϵ, for a sinusoidal signal at r_o is[10]

$$p_2 = \frac{p_o r_o}{r} \frac{\sigma_o}{2} I_{22} e^{-4\alpha(r-r_o)} , \qquad (3\text{-}10)$$

where

$$I_{22} = \int_{r_o}^{r} \frac{e^{2[\alpha(r'-r_o)]}}{r'} dr' = e^{-2\alpha r_o} \int_{r_o}^{r} \frac{e^{2\alpha r'}}{r'} dr', \quad \sigma_o = \beta\epsilon k r_o .$$

It may be shown that, to second order in ϵ, any second harmonic source distortion at r_o does not enter the perturbation solution; rather, the initial second harmonic distortion diminishes by linear theory as[11]

$$p_2(r,t) = p_2(r_o,t)\left(\frac{r_o}{r}\right)e^{-\alpha_2(r-r_o)} \quad . \tag{3-11}$$

The use of α_2 instead of $4\alpha_1$ allows for the possibility of relaxation effects in the medium. Effective source parameters are not required because the initial distortion does not affect the nonlinear behavior. In general, the phase difference between the two signals represented by Eqs. 3-10 and 3-11 is nonzero. The total second harmonic is the vector sum of the signals. The fundamental component decays according to linear theory in this approximation.

D. Theory Applicable to Strong Waves

1. Naugol'nykh et al. (Burgers) Model

The extra attenuation calculated by Cary using the model of Naugol'nykh et al. is applied directly to our work. The extra attenuation is

$$\text{EXDB} = -\,20\,\log_{10}\left[\frac{rV_1}{r_o\,e^{-\alpha r}}\right] \quad , \tag{3-12}$$

where

$$V_1 = \frac{2\alpha/\beta\epsilon k}{\sinh \alpha r\left[1/\sigma_o + \ln(r/r_o)\right]} \quad . \tag{3-13}$$

An effective source must be defined and applied as in section A of this chapter. The solution is valid only in the sawtooth region of propagation.

2. Rudnick Model

Blackstock[46] has applied the Rudnick model for the fundamental to the propagation of a spherical sawtooth wave. For such a wave the dimensionless fundamental amplitude (compensated for spherical spreading) is

$$B_1 = \frac{2}{1+\sigma} = \frac{2}{1+\beta\epsilon k r_o \ln(r/r_o)} \quad .$$

The nonlinear decay rate is therefore

$$\left(\frac{dB_1}{dr}\right)_{\text{nonlinear}} = -\left(\frac{\beta\epsilon k r_o}{2r}\right) B_1^2 \quad , \qquad (3\text{-}14a)$$

while the rate of decay due to ordinary absorption is

$$\left(\frac{dB_1}{dr}\right)_{\substack{\text{small}\\ \text{signal}}} = -\alpha B_1 \quad . \qquad (3\text{-}14b)$$

Adding Eqs. 3-14 gives the total decay rate

$$\frac{dB_1}{dr} = -\left(\alpha B_1 + \frac{\beta\epsilon k r_o}{2r} B_1^2\right) \quad . \qquad (3\text{-}15)$$

Equation 3-15 is a nonlinear ordinary differential equation valid in the region $r > \hat{r}$. We integrated Eq. 3-15 numerically by the second method of Runge-Kutta (see, for example, Ref. 47). In chapter VI the results are compared with measured data. Effective source parameters are again required (see section III.A.).

Webster[11] later found the analytic solution to Eq. 3-15 subject to the boundary condition of sinusoidal excitation at r_o with a pressure amplitude of p_{10}. The solution is

$$p_1 = \frac{r_o}{r} \frac{2p_{10}\, e^{-\alpha(r-r_o)}}{1 + \beta\epsilon k r_o\, e^{\alpha r_o} [E_1(\alpha r_o) - E_1(\alpha r)]} \quad , \qquad (3\text{-}16)$$

where the exponential integral $E_1(x)$ is defined (see, for example, Ref. 45) as

$$E_1(x) = \int_x^\infty \frac{e^{-y}}{y}\, dy \quad .$$

The integral must be evaluated numerically. Useful polynomial approximations to the integral are given in Ref. 45.

CHAPTER IV

EXPERIMENT DESIGN

A. Introduction

Certain general considerations in the design of our propagation experiment are discussed in this chapter. Of special concern was the selection of an acoustic source which could produce measurable nonlinear effects within the physical confines of our vertical propagation path. A tower 85 m high, equipped with an elevator which could be used to carry a traveling microphone, was available. This tower fixed the length scale of the propagation experiment.

Several sources capable of producing periodic sound of finite amplitude in air have been reported in the literature. A few seemed well suited for our purposes. To quickly evaluate their effectiveness, we used a graphical method for predicting the nonlinear effects associated with spherically spreading sound waves. This method has been described elsewhere[48,11] but is repeated here for completeness.

B. Source Selection

The sources used in our experimental work were chosen on the combined bases of (1) operating frequency range and bandwidth, (2) projected output levels, (3) materials and equipment already at hand, (4) cost, and (5) construction time. The devices considered for possible selection are listed below.

1. electroacoustic driver(s) in three configurations:
   a. an array of drivers, each with its own small horn[49]

b. a single large horn fed by several drivers[50]

c. a dish reflector fed by several drivers[49,50]

2. resonance devices in one of the above configurations

a. St. Clair generator[39,41]

b. stepped-plate transducer[51]

3. aeroacoustic or air modulated sources

a. siren[37,38]

b. electropneumatic driver[52]

c. whistle[53]

d. Hartmann generator[53,54]

The references cited in the list above point out some of the important operating characteristics associated with the sources. Our desire for a source of easily variable frequency (with perhaps the ability to produce narrowband noise for later experiments) quickly eliminated the resonance devices, whistle, and Hartmann generator as possible candidates. The need to use high audio frequencies, because of their generally favorable effect on the development of nonlinear phenomena (see section C), caused us to drop the electropneumatic driver from consideration. The acoustic signal from a large horn fed by several electroacoustic drivers may be more susceptible to nonlinear distortion within the horn itself than is the signal from an array of drivers with individual horns. A large horn is also difficult to construct, as is a large reflecting dish. We therefore concentrated our efforts on the development of a horn driver array.

From several standpoints, arrays of horn drivers are attractive for use in experiments such as ours. Commercially available drivers, which, at least in theory, are reliable uniform devices, may be used. The

frequency of operation is easily varied. All electronic control of the source is possible, in contrast to the mechanical apparatus required for several of the devices listed above. We were fortunate to have on hand a large number of horn drivers of exceptionally wide bandwidth. Their use was attractive not only because of cost but because the wide bandwidth feature could be utilized in subsequent experiments on finite amplitude noise.

When it turned out that the horn arrays generated less intense sound than desired, a siren was constructed as an alternate, much stronger source. An electrically driven siren as used here may cover a wide range of operating frequencies. Sirens with conversion efficiencies approaching 50% may be built. A siren is less convenient to use than a driver array because of the air compressor required. The much higher sound levels obtainable from the siren more than compensate, however, for the added inconvenience. The horn driver arrays and siren are discussed in detail in chapters V and VI, respectively.

C. Estimate of the Importance of Nonlinearity on the Propagation of Spherical Waves

We sought to evaluate and maximize the nonlinear effects expected for a given source by specifying the design parameters. By examining Eqs. 3-5, one recognizes the importance of the two dimensionless quantities $\beta\epsilon kr_o$ and αr_o. These quantities determine the severity of the nonlinear behavior. Nonlinear effects may be increased by

1. raising the source amplitude ϵ,
2. increasing the frequency f,
3. increasing the effective source radius r_o, which generally

depends on frequency as well as actual source size,

4. increasing β, i.e., switching to a more nonlinear medium, and/or
5. decreasing the attenuation coefficient α, which depends strongly on humidity and frequency.

Because several of the factors in this list are coupled, it is not immediately obvious how to optimize a particular experiment for the greatest nonlinear effects. A convenient graphical display of the conditions required for a certain level of nonlinear behavior may be constructed as follows.

Consider a sinusoidal wave spreading from a spherical source of effective radius r_o. For a very weak wave, atmospheric absorption damps the wave before shocks can form. Quantitatively, this means that the computed quantities $\bar{r}$ and r_{max} have the following relation to each other: $r_{max} \ll \bar{r}$. In a very strong wave, on the other hand, shocks form quickly and the wave travels a significant distance before small signal behavior begins, that is, $\bar{r} \ll r_{max}$. Thus the condition $\bar{r}=r_{max}$ is a dividing criterion, marking the approximate threshold of the importance of nonlinear effects. If the computed quantities $\hat{r}$ and r_{max} are equal, then more serious nonlinear effects are expected to be present. These two conditions may be written in terms of $\beta\epsilon kr_o$ and αr_o as follows:

$$\bar{r}=r_{max} \rightarrow 2\alpha r_o = \beta\epsilon kr_o \, e^{-1/\beta\epsilon kr_o}$$

$$\hat{r}=r_{max} \rightarrow 4\alpha r_o = \beta\epsilon kr_o \, e^{-3/\beta\epsilon kr_o} \quad . \tag{4-1}$$

It is convenient here to define a quantity closely related to $\beta\epsilon kr_o$. The

"source frequency level," SFL, is defined as[48]

$$SFL = SPL_{1m} + 20 \log_{10} f_{kHz} \quad , \tag{4-2}$$

where SPL_{1m} is the extrapolated source level at 1 m and f_{kHz} means the frequency in kilohertz. This level is equivalent to the "scaled source level" used by Merklinger et al.[17] For air at 20°C, the relation between SFL and $\beta\epsilon kr_o$ is

$$SFL = 20 \log_{10} \beta\epsilon kr_o + 167.2 \text{ (dB)} \quad .$$

A plot of Eqs. 4-1 cuts the SFL-αr_o plane into three regions. Nonlinear effects for a particular source may then be read as very important, of possible importance, or unimportant for operating points above, between, or below the two curves, respectively. The SFL chart in Fig. 4-1 shows the operating points for the sources used in our experiments. All operating points are measured values. The values of r_o were taken as equal to $R_o/2$ for each source, respectively.* Judging by the position of point A, for example, we expect array No. 1 (seven horn drivers) to be a moderate source in terms of nonlinear effects. Array No. 2 (ten horns) should be a stronger source. The siren is indicated to be a very strong source. The propagation experiments to be described generally confirm these expectations. We return to this subject in chapters V and VI.

*While R_o is commonly applied to piston sources, we also use it in this thesis with our horn arrays and siren. For consistency, we agree to calculate R_o on the basis of the "active area" of the source (e.g., the sum of the areas of the horn mouths in an array).

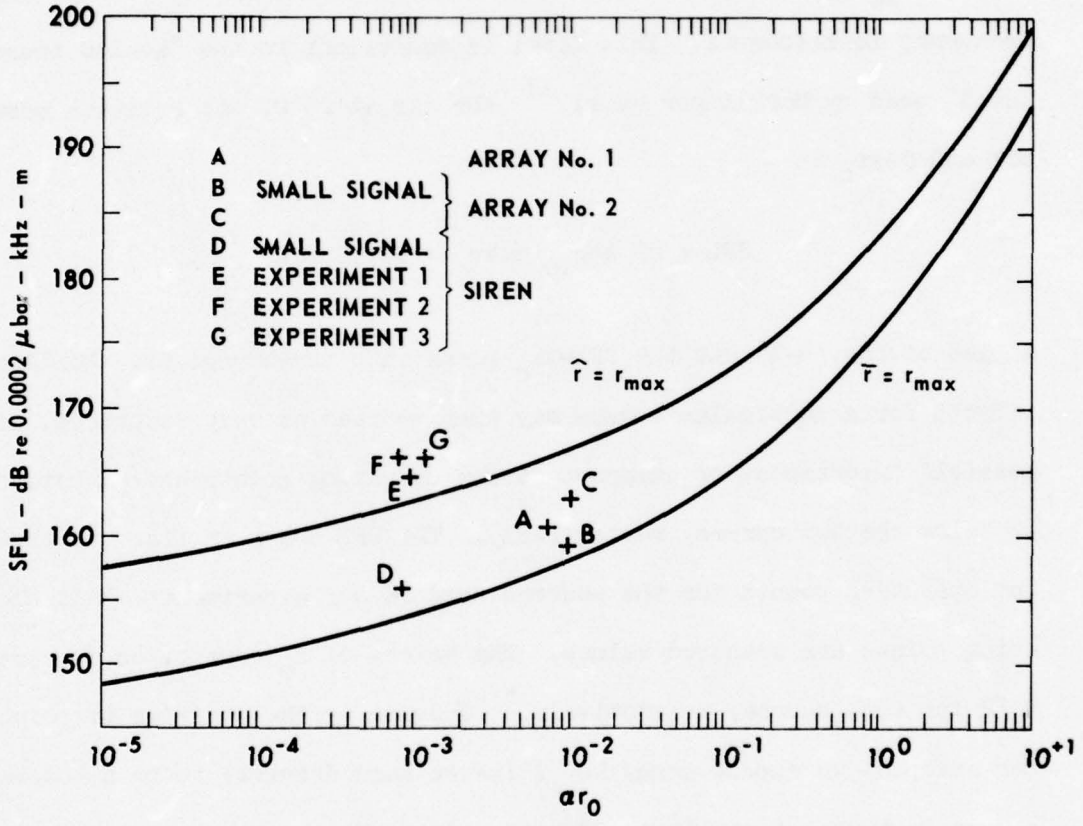

FIGURE 4-1
DESIGN CURVE TO ASSESS THE IMPORTANCE OF NONLINEARITY ON SPHERICAL WAVE PROPAGATION
(CONDITIONS ARE FOR AIR AT 20°C)

Adapted from Theobald, Webster, and Blackstock (1976).

ARL - UT
AS-75-2391-P
DAW - DR
12 - 17 - 75
REV. 12-2-76

D. Other Design Considerations

Two other important design considerations were the length scale of the experiment and the effects of source and receiver directivity. Use of the SFL chart gives a quick indication of the magnitude of the nonlinear effects expected but yields no information about the distances over which these effects occur. Once a design for a source appeared promising, therefore, it was then necessary to compute the actual values of $\bar{r}$, $\hat{r}$, and r_{max} (see Eqs. 3-5). It was important that some or all of these distances be within the limited propagation range available to us. On the other hand, an experiment in which all interesting effects occur within a short distance (e.g., within 1 m) would not demonstrate whether nonlinear propagation effects are indeed observable in the inhomogeneous medium.

As for directivity, there were three main considerations. First, high source directivity is desirable to boost the SFL (note that αr_o is also affected). Second, the serious effects of refraction by atmospheric irregularities on a beam that is too narrow may render the microphone measurements very difficult. Finally, although high frequency is favorable with respect to SFL, an upper limit is set by the receiving microphone, which becomes very directional at frequencies above approximately 42 kHz. At higher frequencies, both phase and amplitude response are poor. The time waveforms are therefore inaccurate. The sources were thus selected and designed to meet the following minimum requirements: (1) shock formation should occur within reach of our microphone, (2) the fundamental frequency of the sources should be in the 8 to 12 kHz range,

and (3) the beamwidth should not be less than about 10°. These requirements were approximately satisfied by the arrays and the siren that were actually used.

CHAPTER 5

ARRAY EXPERIMENTS

A. Introduction

In this chapter an account of the evolution of the horn arrays and the experimental results obtained through their use is given. The component testing and selection process is explained. The array transmit system and the receive system used for all of the propagation experiments are described. Finally, experimental results are compared with theoretical predictions.

B. Array Development

A number of commercially available high power horn drivers were considered for possible use as array elements. Eventually three drivers were selected for detailed tests: the James B. Lansing, Inc., models No. 2470 (rated at 25 W electrical input*) and No. 2482 (60 W) and a 375-H retrofitted with an aluminum diaphragm (30 W). Several of these were ruled out as being too low in power handling ability, being too limited in frequency response, or having excessive internal distortion. The frequency response, efficiency, and (unclamped) electrical input impedance were measured by coupling each driver to a 5 cm i.d., 30 m long progressive wave tube. The tube was terminated anechoically and is described in detail in Ref. 6. See Fig. 5-1. The tube's first nonplanar mode occurred at approximately 3950 Hz. The receiving microphone was

*Manufacturer's ratings are for an rms power input for a continuous 1 kHz sine wave.

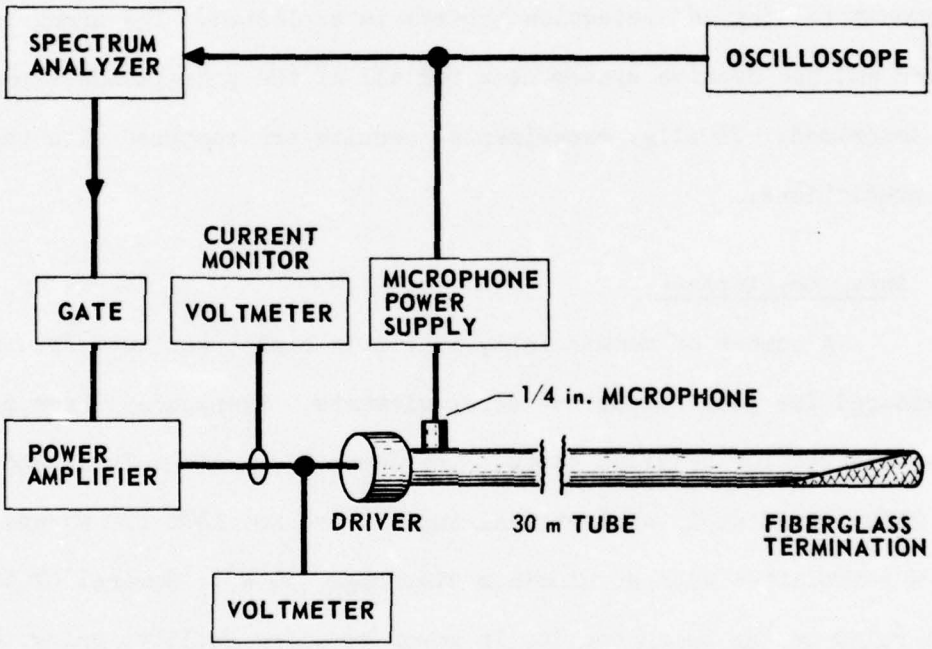

FIGURE 5-1
PROGRESSIVE WAVE TUBE TEST OF HORN DRIVER

ARL - UT
AS-76-1336
MAT - DR
11 - 19 - 76

13 cm from the driver mouth. The equipment involved in the tests included the following.

1. Hewlett-Packard 3580A spectrum analyzer with a camera. The spectrum analyzer's sweep oscillator provided a swept or fixed frequency sine wave of constant voltage that tracked with the analyzer center frequency. Measurements were made using a 30 Hz bandwidth. Rated analyzer accuracy was ±0.3 dB for the frequency range 20 Hz to 20 kHz.

2. B&K 4136 1/4 in. pressure microphone and cathode follower. The response was rated as flat to within ±1 dB from 45 Hz to 50 kHz, but the integration effect caused by flush mounting the microphone in the tube wall moved the high frequency 1 dB point down to approximately 18 kHz.[6]

3. B&K 2108 microphone power supply.

4. Hewlett-Packard 355D step attenuator. Not shown in Fig. 5-1, the attenuator reduced the sweep oscillator signal to avoid overloading the power amplifier input.

5. DRL pulser. This signal gate was activated during pulsed mode tests of the driver's power handling capabilities.

6. Altec 250-B power amplifier. The unit's measured frequency response was flat to within ±0.2 dB from 500 Hz to 10 kHz. The maximum rms power output was 250 W into a 2.5 Ω load.

7. Pearson model No. 110 current transformer. The current transformer, when followed by a voltmeter, provided ac current data for impedance measurements. It also provided an indication of driver overload.

8. Hewlett-Packard 400EL ac voltmeter. The voltmeter alone also monitored the potential applied for impedance measurements.

All three drivers failed at their rated input powers after various periods of operation. Two kinds of damage resulted. Either the voice coils physically distorted from overheating and shorted out or the fusible link in the voice coil circuit opened. The voice coil was ruined in either case. Pulse operation was also tried. The drivers were pulsed at approximately double their continuous power rating; some failures occurred in this operating mode. The 375-H driver eventually chosen as the element for the arrays was derated to 25 Wrms input with fair reliability.

The driver found to have the smoothest frequency response (constant voltage drive) in the 5 to 10 kHz range, the greatest bandwidth, and the highest efficiency at these frequencies was the 375-H. An added advantage of this driver was the availability (from government surplus) of approximately 20 units in various stages of disrepair. Fifteen of these units were cleaned and refitted with aluminum diaphragm voice coils at the James B. Lansing, Inc., factory in Los Angeles. The frequency response for a typical 375-H driver coupled to the plane wave tube is shown in Fig. 5-2(a) (the response curves in Figs. 5-2(b) and 5-2(c) are discussed later in this section). The test was conducted at low levels. It is seen that the response is flat to within ±2 dB over the range 6 to 8.5 kHz and is flat to within ±4 dB over the range 0.5 to 8.5 kHz. At 8 kHz the electric-to-acoustic conversion efficiency (at low levels) was found to be approximately 17%. The efficiency varied from unit to unit. For example, another driver was 13% efficient under the same conditions. This difference reflects a 1 dB decrease in SPL.

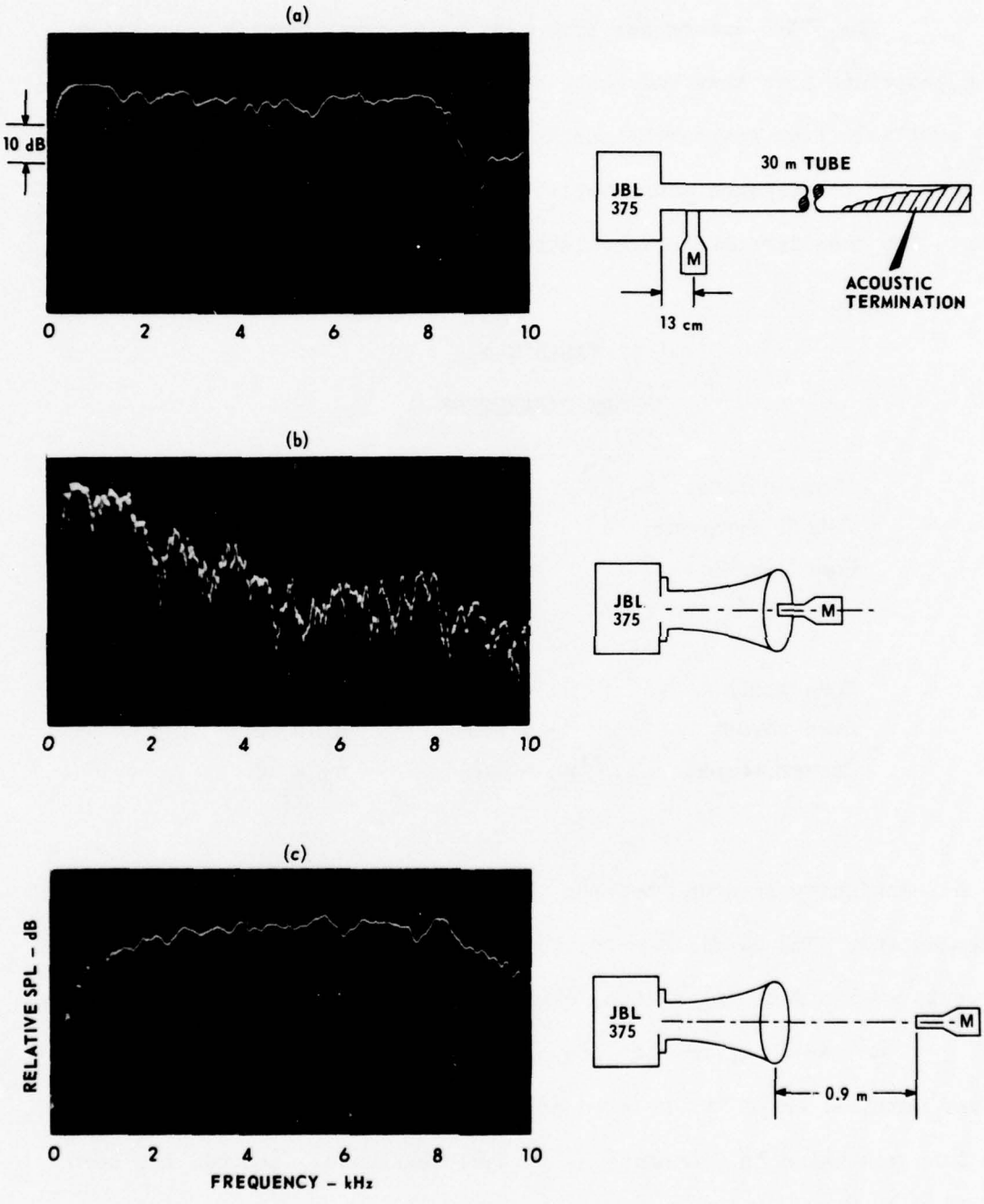

FIGURE 5-2
FREQUENCY RESPONSE OF JBL 375 HORN DRIVER UNDER VARIOUS CONDITIONS

ARL - UT
AS-76-2283
MAT - DR
12 - 14 - 76

The 375-H driver was selected for the propagation experiment. An appropriate horn then had to be chosen. A circular exponential horn was available from government surplus in sufficient quantities for an array. The performance characteristics of the horn required investigation. The horn parameters are listed below.

TABLE V-1

HORN PARAMETERS

Flare constant		$m = 0.047\ cm^{-1}$
Cutoff frequency		$f_o = 260$ Hz
Horn length		$L = 20$ cm
	Diameter	*Area*
Horn mouth	$2a = 16$ cm	$A_m = 190\ cm^2$
Horn throat	$d_o = 6.0$	$A_o = 28$
Driver throat	$d_d = 4.8$	$A_d = 18$

The discontinuity in areas between the driver and horn is ignored in our calculations. The farfield acoustic output was later seen to actually decrease when a matching section was added to eliminate the discontinuity.

We based our predictions of the acoustic output of the horn-horn driver combination on two related assumptions. First, the sound within the horn was taken to propagate as a quasiplane wave. Second, the horn mouth was assumed to radiate sound as if it were a uniformly vibrating baffled piston. Both assumptions are commonly used in analyzing the radiation from horns (see, for example, Ref. 55). Use of the first assumption reveals that, when the transmitted wave reaches the horn mouth,

its SPL should be

$$SPL_m = SPL_d - 20 \log_{10} \sqrt{A_m/A_d} \quad ,$$

where SPL_d is the level at the horn throat. If the pressure due to the transmitted wave then causes the layer of air at the horn mouth to vibrate as a piston, as implied by the second assumption, the SPL at a distance r in the farfield should be

$$SPL_{ff} = SPL_m - 20 \log_{10} \left(\frac{r}{R_o} \right) \quad ,$$

where R_o $(=ka^2/2)$ is the Rayleigh distance. At R_o itself, the SPL is expected to be

$$SPL_{R_o} = SPL_m - \Delta \quad ,$$

where Δ is the difference, expressed in decibels, between the true axial pressure at R_o (see Ref. 56) and the farfield asymptote.

Unfortunately, measurements did not confirm the predictions based on the two assumptions. Measurements were made at 8 kHz, at which frequency Δ=1 dB. If one starts with the value SPL_o=154 dB projected on the basis of measurements in the progressive wave tube, the values expected from the formulas above are SPL_m=144 dB and SPL_{R_o}=143 dB. The values actually measured were SPL_m=143 dB and SPL_{R_o}=131 dB. Although the predicted and measured values of SPL_m seem close, the good agreement is largely fortuitous. The microphone at the horn mouth picked up not only the transmitted wave but also the wave diffracted from the mouth rim. The strong effect of the diffracted wave was observed: the measured SPL was

extremely sensitive to microphone position. In any case, however, the discrepancy between the predicted and measured values of SPL_{R_o} was 12 dB, a very serious loss. Extrapolating this same loss to an array of seven elements operating at 8 kHz, one finds that the value of SFL is reduced from an expected value of 172 dB to 160 dB. Point A in Fig. 4-1 corresponds to the 160 dB value. It can thus be seen that, if the 12 dB loss had not occurred, the 7-element array would have qualified as a strong source.

In the hope of diagnosing and curing the cause of the low acoustic output, we examined in some detail the axial pressure distribution and the pressure distribution across the mouth of a single horn and driver. These experiments were performed in an anechoic chamber.* The axial pressure distributions for the single horn and for a uniform baffled piston equal in area to the horn mouth are shown in Fig. 5-3. Data set 1 was taken with an 1/8 in. microphone (see section D.4.) mounted on an optical bench; data set 2 was taken using a 1/4 in. microphone mounted on the overhead monorail support of the anechoic chamber. The theory and data are matched in the farfield because of our uncertainty of the behavior of both in the nearfield region. The 12 dB discrepancy between predicted and received levels is therefore not evident in the figure. It is, however, obvious that the measured nearfield behavior does not correspond to the nearfield behavior for a uniform piston. The theoretical series of maxima and minima predicted by theory were replaced in practice by a monotonic decay in the pressure. Trouble with our use of the uniform

*See Appendix A for the construction and performance details of the chamber.

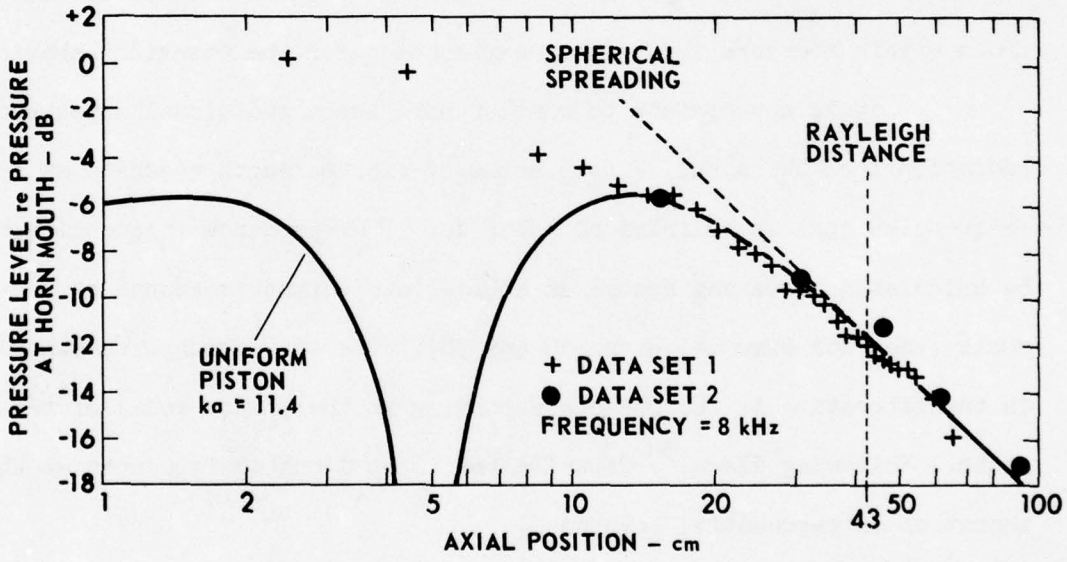

FIGURE 5-3
AXIAL PRESSURE DISTRIBUTION FOR SINGLE HORN AND DRIVER
(THEORY MATCHED TO DATA IN FARFIELD)

ARL - UT
AS-76-1345
MAT - DR
11 - 19 - 76

piston model is indicated. The Rayleigh distance is, however, confirmed as indicating the onset of spherical spreading.

The pressure distribution across the mouth of the horn is compared with the distribution expected[57] for a uniform piston at a slightly lower frequency (7.3 kHz) in Fig. 5-4. The asymmetry of the data in comparison with theory is glaring. Evidently we do not have uniform excitation of the air layer at the horn mouth. The existence of cross-modes within the horn is a likely explanation for the observed behavior.

It is appropriate to mention here three additional aspects of radiation from the horn. First, horns of finite length resonate at certain frequencies just as cylindrical tubes do. The resonance frequencies may be calculated if we may assume an appropriate output impedance at the horn mouth (see, for example, Refs. 55 and 58). The only assumption considered in the literature is the one corresponding to the piston model of the horn mouth. Following Olson,[58] we write the input acoustic impedance at the throat of an exponential horn as

$$Z = \frac{\rho_o c_o}{A_o} \frac{A_m Z_m [\cos(bL+\theta)] + j\rho_o c_o [\sin(bL)]}{jA_m Z_m [\sin(bL)] + \rho_o c_o [\cos(bL-\theta)]} \quad ,$$

where θ=arctan (m/2b), $b=1/2\sqrt{4k^2-m^2}$, and Z_m is the acoustic impedance at the horn mouth. The driver throat is effectively an extension of the horn back to the diaphragm. By examining a defective driver's internal structure, we found that the throat area at the diaphragm is 11 cm^2. Ignoring the discontinuity at the driver horn connection, we plot in Fig. 5-5 the input resistance for an equivalent horn, beginning at the diaphragm. The resonance peaks predicted at 6470 and 8350 Hz are very close to measured

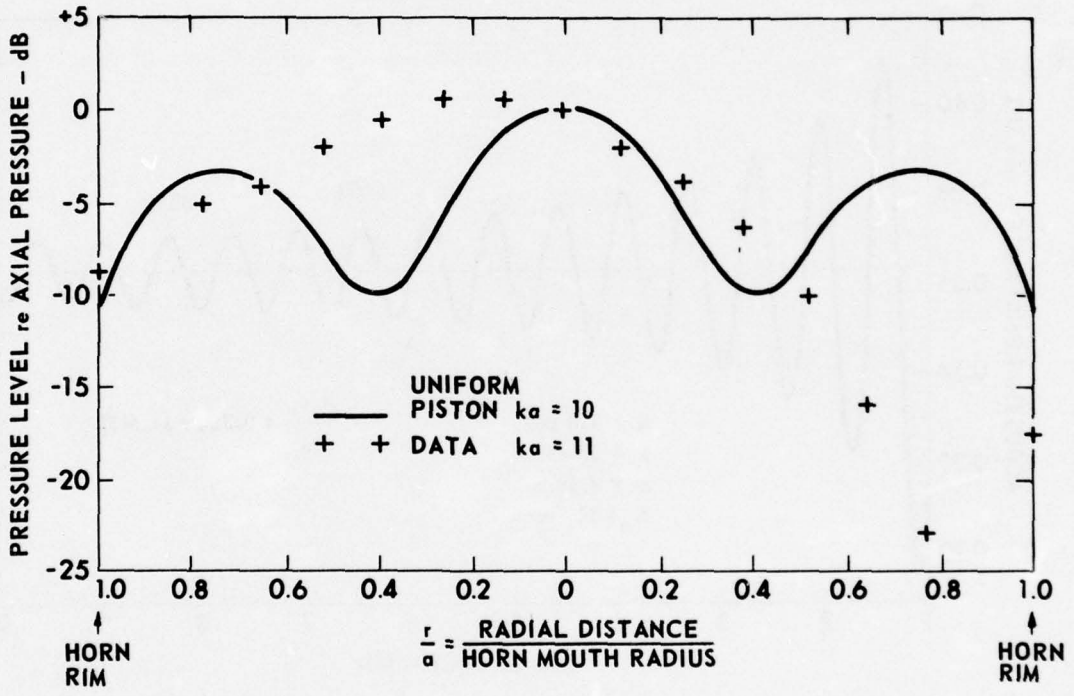

FIGURE 5-4
PRESSURE DISTRIBUTION ACROSS HORN MOUTH

ARL - UT
AS-76-1334
MAT - DR
11 - 19 - 76

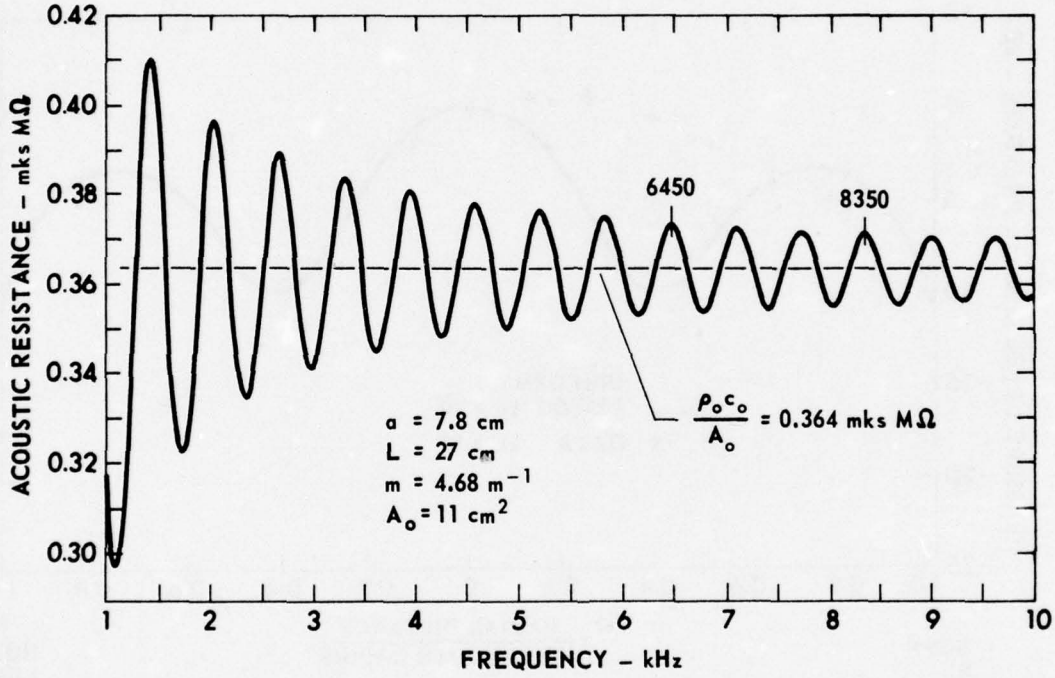

FIGURE 5-5
ACOUSTIC RESISTANCE AT THROAT OF FINITE EXPONENTIAL HORN

ARL - UT
AS-76-1333
MAT - DR
11 - 19 - 76

response peaks of the driver arrays. A response peak at 6655 Hz was evident when ten drivers were packed together in an array. A peak centered at 8250 Hz appeared in the frequency response for a single driver (see Fig. 5-2(c)) and also for an array of seven drivers. Of course in our calculation we have ignored the driver characteristics, which strongly influence the relative magnitudes of the observed peaks.

The second additional aspect of horn radiation is the possibility of nonlinear losses within the horn. If quasiplanar propagation within the horn is again assumed, it may be shown[4] that the nonlinear loss should not exceed 0.1 dB in our case.

Finally, we must give some comment to the two very different frequency response curves exhibited in Fig. 5-2(b) and (c). The presence of a diffracted wave from the mouth rim of the horn in combination with the direct wave through the horn allows a pleasing qualitative explanation for the characteristics shown. Because the relative phase of the two waves within the nearfield varies widely with the product ka, we are not surprised to see the many peaks and valleys shown in Fig. 5-2(b). The relative phase changes are much smaller in the farfield and thus the frequency response is smoothed (Fig. 5-2(c). It may be shown (see Appendix B or Ref. 56) that the direct and diffracted waves combine on the axis of a uniform piston to form the time derivative of the source signal. For a sinusoidal source, differentiation amounts to a multiplication of the source signal by $j\omega$, where ω is the angular frequency. The result is a 6 dB/octave increase in the frequency response.

It is concluded from the tests and analyses of radiation from the horn that, at the high operating frequency we wished to use,

crossmodes probably exist within the horn. Because propagation through the horn is not planar, the excitation of the air layer at the horn mouth is not uniform. Therefore the uniform piston model for the horn mouth is not reliable. However, the Rayleigh distance still approximately indicates the onset of spherical spreading.

The disappointing performance of the horn-horn driver combination touched off a search for an alternative design. Various horn modifications and substitutions were tried, including

(1) shortening the horn to reduce any antiresonance effects,

(2) switching to a conical horn,

(3) adding a sectoral divider in an attempt to control crossmodes,

(4) adding a matching section to eliminate the mismatch between driver and horn (this modification actually degraded performance by 2 dB), and

(5) switching to a one-quarter wavelength tubular coupler.[59]

None of these devices yielded more than a 2 dB improvement over the original horn. This result was attributed to the high frequencies involved. At 8 kHz the wavelength, about 4 cm, is small compared to the mouth diameter, 16 cm, and to the horn length, 20 cm.

Despite the disappointing performance of the horn-loaded 375-H drivers, it was still felt that such an array offered promise as a high intensity source. The source level could be increased by increasing the number of elements. The limit to the size of the array was set by cost and the requirement that the beam not be too narrow. Groups of seven and ten drivers were operated as high intensity arrays. See Fig. 5-6. Because of the size of the driver cases, the horns could not be packed

(a) ARRAY No. 1
(7 ELEMENTS)

(b) ARRAY No. 2
(10 ELEMENTS)

FIGURE 5-6
HORN ARRAYS

with their mouths touching one another. The arrays were therefore arranged to provide the most dense packing of the horns possible. Seven drivers (array No. 1) were formed in a circular array, 0.5 m in diameter. The beam from this array was expected to be axisymmetric and similar in angular dependence to the beam from a circular piston of area equal to $7\ A_m$. Ten horns were assembled in an equilateral triangle formation, 0.5 m on a side. The beam from this array (array No. 2) was expected to be asymmetric and somewhat narrower than the beam from array No. 1. The gaps between the horns in array No. 1 were initially filled by a plane circular baffle (1.1 m in diameter). The measured farfield SPL on axis actually increased, however, when the baffle was removed. No completely satisfactory explanation has been offered for this fact. We speculate that a resonance may have been "detuned" by the presence of the baffle. In any case, no propagation experiments were conducted with baffled arrays. Array No. 1 was operated at 8.2 and 6.6 kHz, while array No. 2 was operated at 6.6 kHz. These frequencies corresponded to peaks in the frequency responses of the arrays. The respective source levels are cited in sections F and G of this chapter.

C. Array Transmit System

The electronic equipment comprising the transmit system for the arrays is described below. The block diagram appears in Fig. 5-7.

1. Hewlett-Packard 3580A spectrum analyzer. The sweep oscillator of this device served as an extremely stable variable frequency oscillator. This device is labeled "oscillator" in Fig. 5-7.

2. Hewlett-Packard 350C step attenuator.

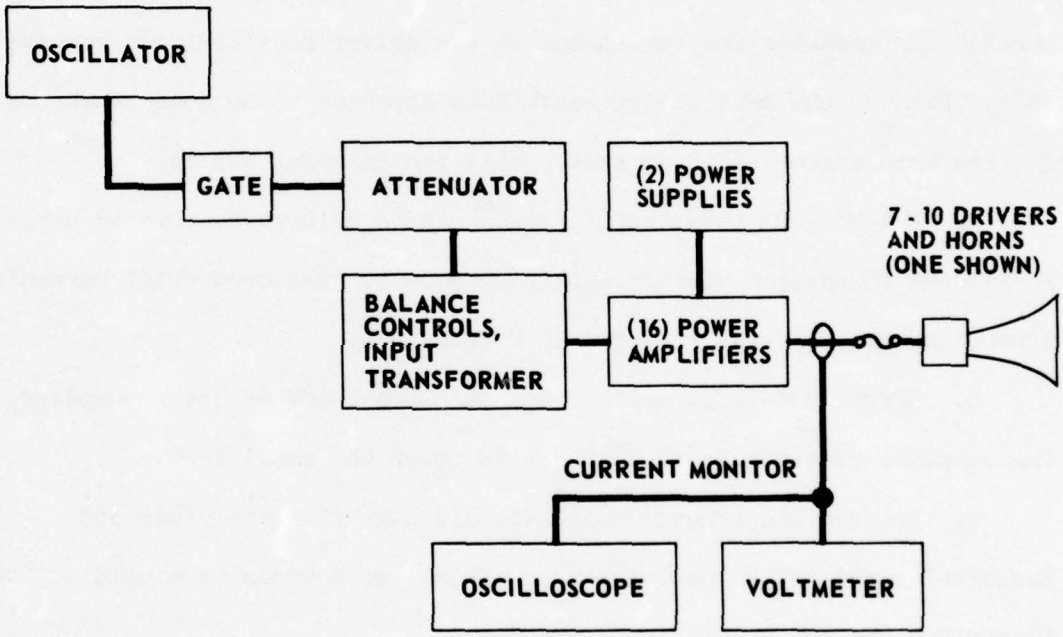

FIGURE 5-7
HORN DRIVER TRANSMIT SYSTEM

ARL - UT
AS-76-1329
MAT - DR
11 - 19 - 76

3. DRL pulser. This signal gate was activated when pulsed measurements were desired.

4. Balance controls and input transformer. The input transformer was needed to prevent the floating ground buss of the amplifiers from shorting to earth ground through other equipment. The balance controls allowed individual gain adjustments for each amplifier channel. Thus partial compensation for variations in the driver sensitivities was available. Because the sensitivity variations appeared to decrease when the drivers were assembled in an array, this feature went unused.

5. RCA HC 200H power amplifiers.[60] Each driver was powered by an individual integrated circuit amplifier module. Measured total harmonic distortion at 1 kHz was 1.4% for 39 W into 15 Ω.

6. Trygon model No. RS40-10 and Harrison 6438B dc power supplies. The supplies provided ±37.5 V at 5 A to power the amplifiers.

7. Pearson Electronics model No. 110 current transformer and Hewlett-Packard 400 EL ac voltmeter. These two devices were used together to monitor the input current to the drivers.

8. Tektronix RM45A oscilloscope.

D. Receive System

A block diagram of the receive system used for both the array and siren experiments is shown in Fig. 5-8. The receive system performed several functions. The absolute harmonic levels and the time waveform were measured at each designated propagation distance. The acoustic output of the source was also monitored against possible equipment drift and failure. Beam patterns of the sound from the various sources were recorded.

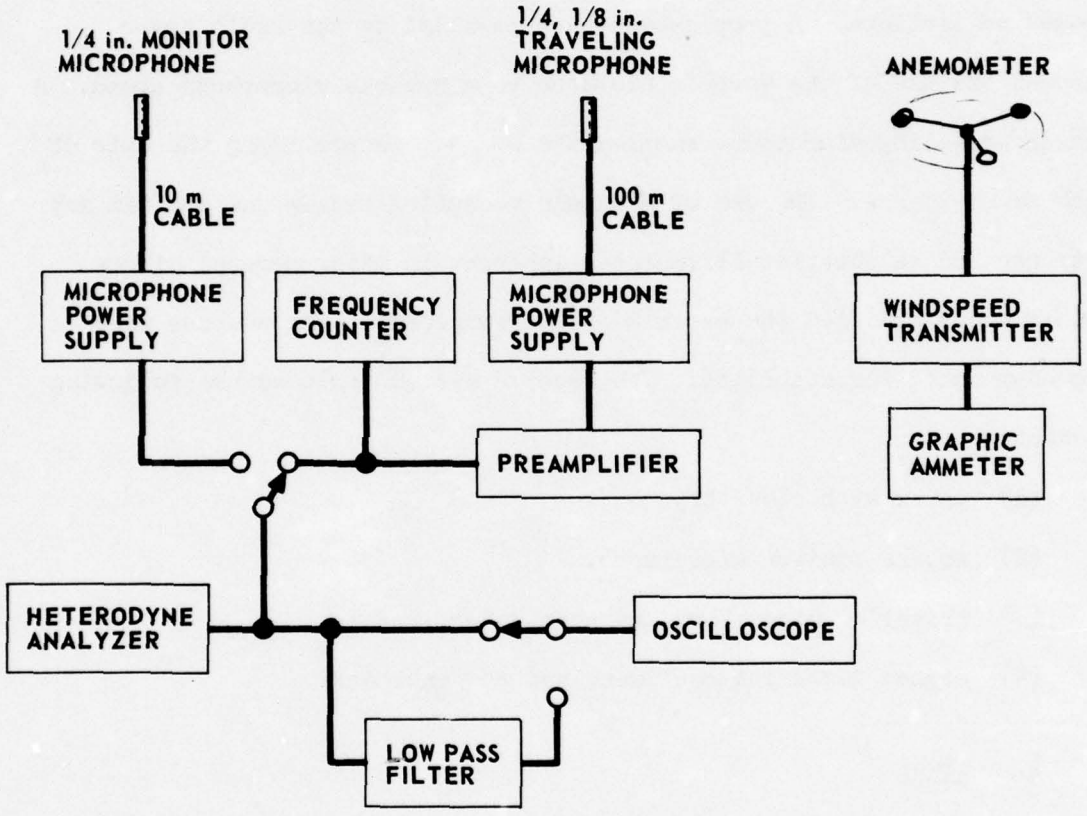

FIGURE 5-8
RECEIVE SYSTEM

ARL - UT
AS-76-1331
MAT - DR
11 - 19 - 76

Because of the size of the sources and the anticipated long duration of the experimental program, simplicity and stability were important factors in the experimental arrangement selected for the system. As stated earlier, a vertical propagation path was chosen to minimize ground reflections. A propagation path parallel to the radio tower allowed the use of the tower's elevator as a movable microphone stand. A single traveling microphone sampled the sound pressure along the axis of each sound source. The use of a single measuring microphone avoided any response and calibration differences inherent in using several microphones and simplified the experimental arrangement. The sources were ground-mounted for stability. The receive system included the following elements:

(1) tower with elevator,

(2) source monitor microphone,

(3) traveling microphone and anemometer, and

(4) signal measuring equipment and the enclosure.

1. Tower

The tower defined the propagation path by supporting the elevator on which the receiving microphone was mounted. See Fig. 5-9. The tower was of tubular steel construction and had a triangular cross section with 0.75 m sides. Guy wires were secured to the tower at mid-height and near the top. The maximum allowable propagation distance was 85 m.

The elevator was an open car of dimensions 0.8 m in width by 0.9 m in depth by 1.2 m in height. The maximum gross load was conservatively rated at 136 kg. The car was powered by a ground-mounted winch;

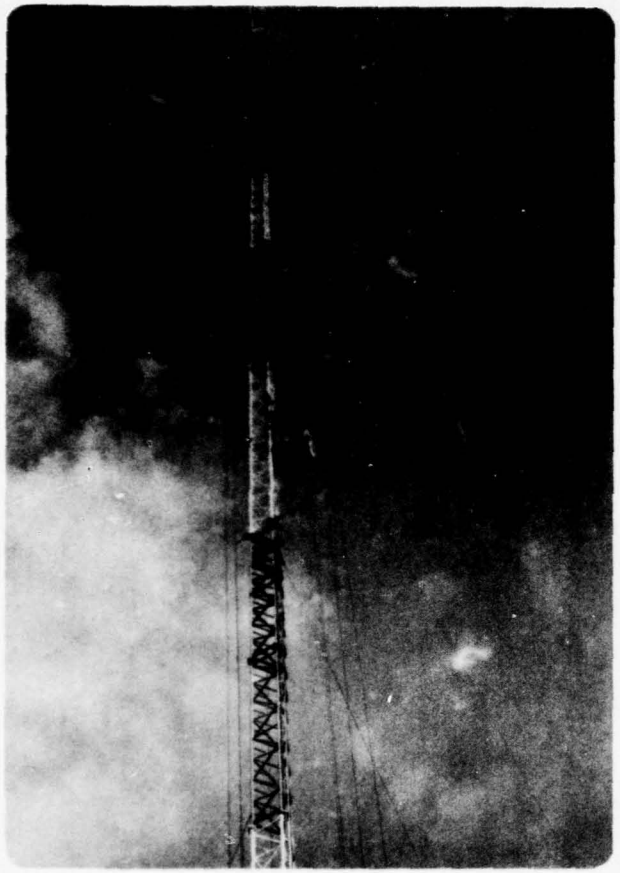

(a) TOWER AND ELEVATOR WITH MICROPHONE BOOM

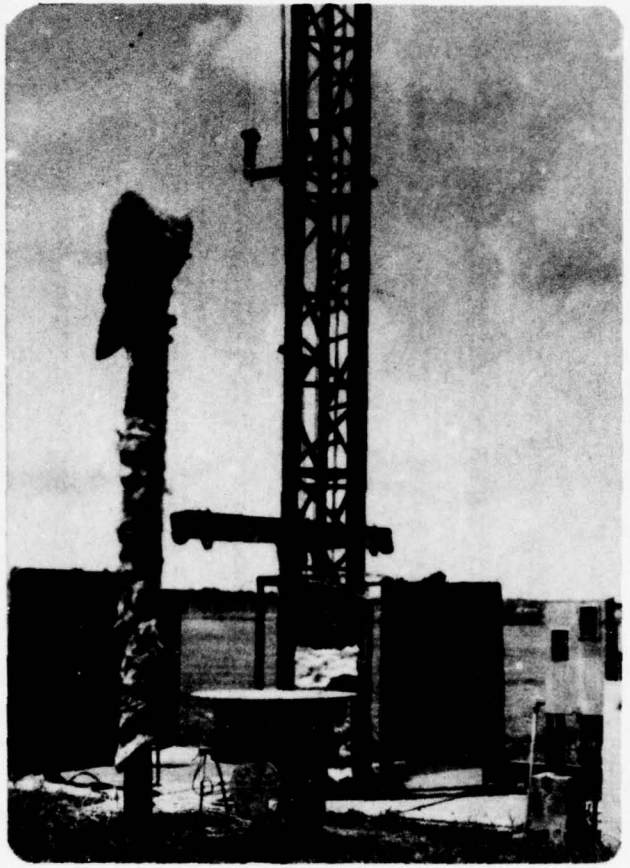

(b) BASE OF TOWER, INDEXING TABLE, AND ARRAY No. 1 (WITH BAFFLE ATTACHED)

FIGURE 5-9
TOWER

all elevator controls were at ground level. The elevator door was of perforated steel. We covered the door with 15 cm thick industrial fiberglass (Owens Corning R-19) to minimize sound reflections to the microphone. The elevator's position, and therefore the propagation distance, were determined in a crude yet reliable way. A light 100 m long cable was calibrated against a measuring tape. This cable was then clamped to the elevator and allowed to dangle to the ground where it provided a direct measure of the microphone height above the source. Height measurement error is estimated as 1% under calm conditions, increasing to perhaps 4% under the strongest winds encountered. The elevator was unfortunately too noisy and moved too fast to allow a continuous-tracking mode of operation.

The sound source mount was an indexing table, 91 cm in diameter, that was located at the base of the tower. The table could be rotated and tilted for adjusting alignment and for measuring beam patterns of the sources. The angles of the measured beam patterns were corrected for the small displacement of the pivot point below the source. A baffled array is shown in place on the indexing table in Fig. 5-9(b).

2. Source monitor

A fixed monitor microphone (1/4 in. B&K model No. 4136) was mounted off-axis in the farfield of the source. The purpose of the monitor was to indicate variations in the acoustic output. Depending on the source dimensions, the monitor was mounted either on a ring stand that stood on the indexing table or on a 1.2 m boom that projected from the adjacent utility pole. The utility pole (4.5 m high) was covered with fiberglass to prevent reflections. The monitor microphone output was

checked by switching it into the signal measuring branch equipment just before a measurement was made with the traveling microphone.

3. Traveling Microphone and Anemometer

The traveling microphone was mounted on a boom extending 2.6 m from the elevator car. The boom was used to remove the microphone from the reflection field of the elevator and tower. The microphone-tower separation was 3.5 m. Thus when the microphone was midway up the tower the minimum time delay of signals reflected from the tower was 1.7 msec. No definitive reflection tests were made. However, if reflections were indeed important in the propagation experiments, they would have been manifested as anomalies in the received cw signals. Because the measured time waveforms agree quite well with computer predictions (see Figs. 5-16 and 6-9), the role of reflections in the data was probably negligible.

The traveling microphone was a 1/4 in. B&K type No. 4136 or a 1/8 in. B&K type No. 4138 mounted in such a way that the sound waves impinged at grazing (90°) incidence. The microphone was calibrated absolutely to within ±0.2 dB by using a B&K type No. 5220 pistonphone. The output signal was fed to the electronic equipment on the ground by way of 100 m of B&K microphone cable. The cable had negligible losses.[61] The sections of microphone cable were clamped together to reduce strain on the cable connectors caused by the substantial cable weight. Windscreens were not used because the ones available to us required large freefield corrections at high frequencies.[62]

The microphone boom included provisions for mounting a small laser to aid in source-receiver alignment. However, the laser available to us proved to be too weak for daylight use. Therefore, we used another

alignment scheme which was simple yet effective. With the traveling microphone 3 m above the 7-element driver array source, a plumb bob was used to bring the source (and indexing table) in line with the microphone. The microphone was then sent to a height of approximately 76 m. The table was tilted to maximize the received sound level. The table was then rotated 90° and the received sound level was maximized again. This position was defined as a 0° tilt with respect to the tower; the table was locked there. This same position was used for the siren. Acoustic alignment of the siren was difficult because its major lobe was so broad. On the other hand, because of the siren's broad beam, alignment of the siren was less critical than it was for the array.

To measure wind speed near the microphone position, we mounted an anemometer on the elevator car. This anemometer, an Electric Speed Indicator Co. model No. F420C, is a wind-driven dc generator whose output potential is proportional to the wind speed. By means of 92 m of stranded cable, which had negligible losses, the output signal was relayed to the ground, where it was connected to a calibrated Esterline-Angus model No. AW graphic ammeter. The accuracy of the wind speed measurement was approximately ±0.5 km/h. The time-averaged (by eye) wind speed was noted at each propagation distance. Although more accuracy could have been obtained by integrating the time record output, it was not deemed worthwhile to do so.

The air temperature and relative humidity at ground level were measured with a Bacharach sling psychrometer. Several times when the wind was fairly calm, the temperature along the tower was found to be essentially the same as the temperature at the ground. Isothermal (ambient)

conditions were therefore assumed for our data analysis. An electronic thermometer (Yellow Springs Instruments model No. 43) with remote readout will be added to the elevator in the near future to allow a more careful measurement of ambient temperature.

We note that knowing temperature and wind speed as a function of propagation distance is not exactly equivalent to knowing the wind and temperature profiles as functions of time. We were forced to assume that the gross profile features were stationary with respect to the time required to run the propagation experiment.

4. Signal Measuring Equipment and the Enclosure

Figure 5-8 and the equipment list below describe the electronic portions of the receive system.

(1) Two 1/4 in. B&K 4136 pressure microphones with cathode followers. These comprised the monitor and traveling microphones for the driver array experiments. The microphone pressure response was nominally flat from 50 Hz to 50 kHz (1 dB down points) for grazing (90°) incidence. Because the 4136 was a pressure response microphone but operated under freefield conditions, the following manufacturer's rated freefield corrections were added to the microphone response:[61]

Without protective grid: -0.2 dB (9 to 14 kHz)
+0.5 dB (19 to 38 kHz)

With protective grid: +1 to 3 dB (17 to 40 kHz)

Spectral measurements in these frequency ranges were corrected accordingly. Time waveforms were not corrected, although they could have been when the signals were processed by the computer. The justification for not making the corrections is described in section G of this chapter.

(2) 1/8 in. B&K 4138 pressure microphone. This was the traveling microphone used for the later siren experiments. Its shorter rise time was useful in obtaining more faithful oscillograms of the sawtooth waves encountered. The 4138 microphone was rated as flat to within ±1 dB from 20 Hz to 100 kHz. No freefield corrections were required to 70 kHz.[63]

(3) Two B&K 2108 microphone power supplies.

(4) Ad Yu 20 dB transistor preamplifier. The preamplifier improved the signal-to-noise ratio for the traveling microphone. The measured gain was 20±0.1 dB from 500 Hz to 200 kHz. The phase distortion was negligible above 100 Hz.

(5) B&K 2010 heterodyne analyzer. The frequency domain measurements were made with this device. Either overall or bandpass levels were selectable. The frequency response (linear) was rated at ±0.2 dB for the range 10 Hz to 50 kHz and ±0.5 dB for the range 2 Hz to 200 kHz. Bandwidth was selectable from 3.16 to 1000 Hz in steps of 10 dB. The variable bandwidth feature was helpful in reducing wind noise and wind-induced fluctuations. The overall SPL measurements did, however, include a contribution due to wind noise. The analyzer also contained much needed averaging circuitry. The pressure signal was first converted to its true rms value, then was RC (resistor-capacitor integration) averaged, and finally was log converted for direct meter display in decibels. The level displayed was thus the pressure signal average (an arithmetic mean), not the average of the pressure levels (a geometric mean). The effective averaging time was selectable from 0.1 to 100 sec in 10 dB steps. The analyzer filter required manual tuning for each harmonic. The tuning was expedited by using the frequency counter to monitor the analyzer's beat frequency

oscillator output, which tracks with the filter center frequency. When an averaging time of 10 sec could be used, about 3 min were required to measure the overall and first three harmonic levels.

(6) Hewlett-Packard 5380A frequency counter. The frequency counter fulfilled several needs. It was used to monitor the oscillator frequency for the driver array (at which time it was connected to the array transmit system) or the siren frequency. It was also used to indicate the analyzer bandpass frequency, as described in No. (5).

(7) Tektronix RM45A oscilloscope with camera. The received signal fluctuated because of wind and turbulence. The oscilloscope records an instantaneous waveform, not a time averaged waveform. Thus there is a variability among waveforms measured at the same distance. Because the wind and turbulence increased with height and because of the cumulative effect of propagation through a random medium, the variability also increased with height. Therefore the waveforms recorded at the larger distances (see Figs. 5-16 and 6-10) are, in particular, to be regarded only as representative. The computer algorithm requires a measured waveform for its input. Because slightly different input waveforms might lead to rather greatly different computed waveforms at long distances, we desired a very stable source waveform. Since little variability was found at distances of less than 15 m, a waveform from this region was acceptable as the computer input.

(8) Low pass (100 kHz cutoff) filter (constructed by D. A. Webster). When the traveling microphone was set at the longer propagation distances (above approximately 45 m), the long microphone cable, acting as a radio antenna, picked up signals from a local AM radio transmitter (carrier

frequency of 1.2 MHz). The tower was within the nearfield of the station and also within a standing wave field caused by the Balcones Fault. Radio reception was unpredictable but varied with the time of day and the weather conditions. Although the radio signal was very strong at times, it did not interfere with the frequency analysis of the acoustic signal. It did, however, greatly affect the time waveform displayed on the oscilloscope. To retrieve the time waveform for the oscilloscope camera, we added the low pass filter at the oscilloscope input whenever it was required. The filter effectively blocked the radio frequency carrier but faithfully passed the acoustic signal. The overall SPL measurements may have been affected by the radio frequency component. Because the overall SPL measurements were of minor importance and were also affected by wind noise, the radio frequency component was not filtered from the input signal to the analyzer.

a. Experimental Accuracy

We estimate here the accuracy of the absolute SPL measurements to be described. For this analysis, we assume that the air is absolutely calm. Several components of equipment were involved, either directly or indirectly, in each SPL measurement. If we assume that the measurement errors attributed to the various components are independent and that each error is normally distributed, the standard deviation of a measurement is

$$S = \left[s_1^2 + s_2^2 + \ldots + s_n^2 \right]^{1/2} ,$$

where s_1, s_2, ..., s_n are the standard deviations associated with the individual components. These standard deviations were the following:

(s_1) pistonphone output: 0.2 dB*

(s_2) polarization potential deviation from 200 Vdc: 0.2 dB*

(s_3) heterodyne analyzer frequency response: 0.2 dB*

(s_4) heterodyne analyzer calibration: 0.2 dB*

(s_5) meter reading: 0.05 dB

(s_6) preamplifier frequency response: 0.1 dB.

The standard deviations associated with the total receive system were therefore 0.4 dB. In other words, the probability of measurement errors less than 0.4 dB was 68%. The probability of errors greater than 0.7 dB was 10% (90% confidence limits). But we must also concern ourselves with the total experiment accuracy. That is, still assuming calm air, we must also account for deviations in the transmitted acoustic signal. The deviation of the source output measured by the monitor microphone was no greater than 0.05 dB for the driver array and 0.3 dB (3 sec average) for the siren experiments. Including these deviations yields a standard deviation for the complete system of 0.4 dB for the array experiments and 0.5 dB for the siren experiments.

b. Enclosure

The electronic equipment was housed in a 2.1 x 2.7 x 2.1 m (outside dimensions) Craig Systems' Helicop-Hut. The hut provided storage space and equipment protection against inclement weather. Because of its potentially airtight construction, the hut may be used in the future to protect the experimenters from unbearably loud sources.

*Manufacturers' ratings.

E. Procedure for Propagation Experiments

This section applies to propagation experiments conducted by using either type of sound source. The experimental methods were identical. The receive system was first calibrated absolutely using the pistonphone. The procedure for making a measurement at a given distance from the source was as follows. The elevator was moved to the desired distance. The source was activated and the output allowed to stabilize. In the case of the siren, stabilization required about 1 min. The driver arrays exhibited no drift following activation. The relative pressure level of the source was then measured by the monitor microphone. We then switched to the traveling microphone and used the heterodyne analyzer to measure the SPLs of the overall, fundamental, second harmonic, and sometimes the third harmonic signal. For small signal experiments, only the overall and fundamental levels were measured. Simultaneously, an oscillogram was taken and the wind speed was recorded. This process was repeated as quickly as possible at the next distance in order to minimize weather (mainly wind speed) variations during the experiment.

In general, the averaging time required for the spectral measurements increased with propagation distance from a minimum of 0.1 sec to a maximum of 30 sec. This increase reflected wind speeds which also generally increased with height. But the values of wind speed measured at a fixed propagation distance occasionally varied by as much as ±4 km/h.

The propagation experiments were conducted under a wide range of wind, temperature, and humidity conditions. The measured wind speeds ranged at the ground from 0 to 4 km/h and, at the greatest propagation distances, from 5 to 21 km/h. Several of the experiments took place before

the anemometer was obtained. We estimate the wind speed range at the ground for these experiments as 0 to 24 km/h. The wind speeds at greater heights are unknown. The propagation experiments took place within the temperature range of 24 to 35°C and the relative humidity range 38 to 80%.

The source was shut down between measurements to protect the experimenters from high level sound. The sources operated at levels dangerous to hearing, if the exposure is long, even when both earplugs and earmuff-type hearing protectors are worn.

A special problem was encountered during the siren experiments. The siren's high sound intensity prohibited experimentation during laboratory working hours. During the night, small line voltage fluctuations (2 to 3 V) caused by the tower's flashing beacon made the siren output unstable. We were thus restricted to taking data between 5:00 and 6:30 p.m., approximately. For these reasons, no data are included here at distances greater than 36 m. Improved wiring will be installed at the tower site to eliminate the line voltage fluctuations at night.

F. Small Signal Behavior

Small signal experiments were performed to establish a basis against which the finite amplitude propagation experiments could be compared.

We first needed to determine whether fluctuations due to wind and turbulence would so dominate the measurements as to disqualify our homogeneous medium theories. Some of our early propagation experiments with the arrays provided an answer to this question. We restrict our present discussion to small signal measurements. It was found that, if a sufficiently long averaging time were used, the data agreed very well with

predictions based on spherical spreading and atmospheric attenuation alone. Agreement was good even though wind gusts of at least 21 km/h occasionally occurred at the greater propagation distances and even though the array beams were relatively narrow. Thus, it was not necessary to account for turbulent scattering and other random media effects. For this reason the terms "small signal" and "linear theory" have been used here to imply the effects of spherical spreading and atmospheric absorption in an homogeneous medium. Two of the small signal propagation experiments are now discussed in some detail.

One of these experiments is reported in Ref. 11. The source was array No. 1. Data were taken over the range 6.1 to 76 m. The operating parameters were f=8.25 kHz, R_o=3.2 m (calculated value), SFL=160 dB, αr_o=0.046, and SPL_{1m}=141.5 dB, where $r_o=R_o/2$. These conditions define a point below the lower curve on the SFL chart (Fig. 4-1). Thus very little, if any, extra attenuation would be expected. This expectation is fulfilled. The propagation data for the fundamental confirm the linear theory curve very well. Some second harmonic distortion was observed, but it was not strong enough to draw appreciable energy from the fundamental. Similar behavior for the fundamental is shown by another experiment with array No. 1, described in section G of this chapter.

The results of a propagation experiment using array No. 2 are shown in Fig. 5-10. The operating parameters were f=6.6 kHz, R_o=3.6 m (calculated value), SFL=159 dB, αr_o=0.032, and SPL_{1m}=143 dB, where $r_o=R_o/2$. The maximum wind speed recorded, 21 km/h, occurred at a distance of 61 m. Point B on the SFL chart (Fig. 4-1) corresponds to this experiment. The point is seen to lie in the intermediate region of the SFL

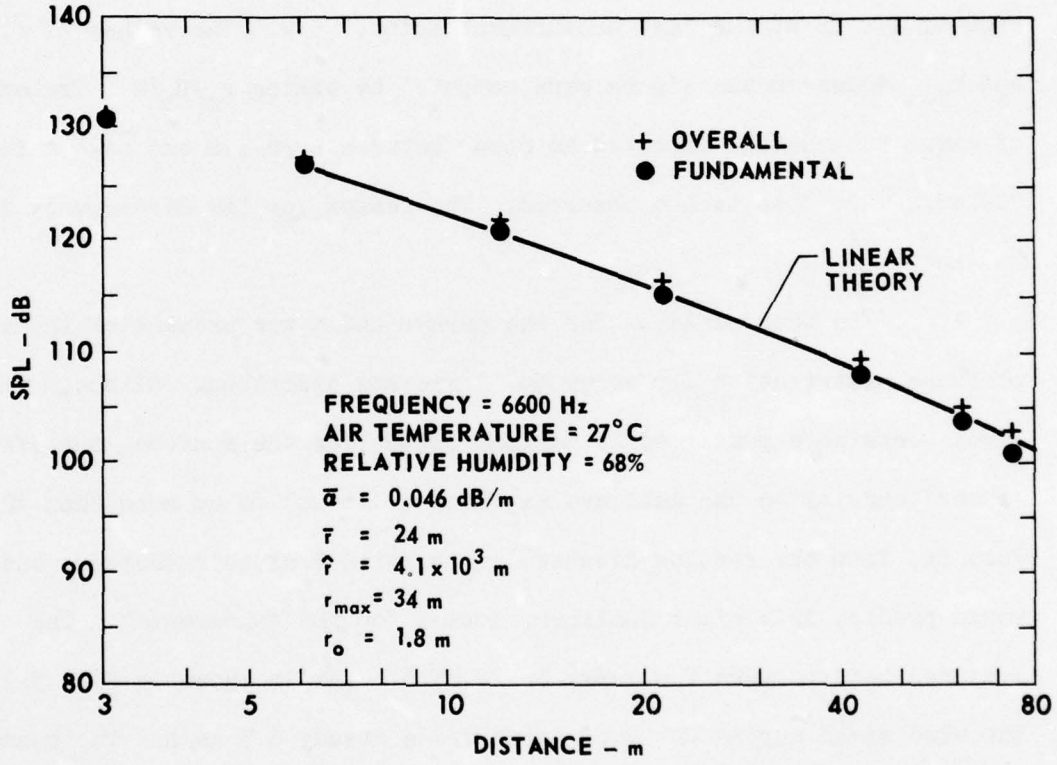

FIGURE 5-10
DRIVER ARRAY No. 2 – SMALL SIGNAL PROPAGATION

chart, yet near the lower limit. One might therefore question whether this is in fact a small signal experiment. The solid curve in Fig. 5-10 represents the small signal prediction. It is begun at the 6.1 m measurement because that is a point definitely in the farfield. The data fit the solid curve quite well out to a distance of about 61 m. There is a deviation of 1.2 dB at the last measurement point, 73 m. The values of $\bar{r}$, $\hat{r}$, and r_{max} shown in the figure were computed by taking $r_o=R_o/2$. The amount of extra attenuation expected to occur between $r_i=6.1$ m and $\bar{r}=24$ m is 0.9 dB. This loss is not observed. The reason for the discrepancy is not known.

The beam patterns for the arrays and a measurement of the axial pressure distribution for array No. 1 are now described. Although these experiments were performed at maximum output for the sources, the effects of nonlinearity on the data are expected to amount to no more than ±2 dB. That is, from the results discussed in section G of this chapter, one would predict only minor nonlinear losses for the fundamental. The measured beam pattern for array No. 1 at 6.6 kHz is shown in Fig. 5-11. The wind speed during the experiment was a steady 6.5 km/h. The beamwidth (the angular separation between the -3 dB points) is seen to be 8° at 6.6 kHz. This figure compares very well with the beamwidth of a uniform circular piston with an area equal to the array's active area. The theoretical and measured directivity patterns correspond well only for the major lobe. The first side lobe of the array is 10 dB below the major lobe. The array was axisymmetric and a symmetric beam pattern is assumed.

The acoustic pressure on the axis of array No. 1 when it was operating at a frequency of 8.25 kHz is shown in Fig. 5-12. The

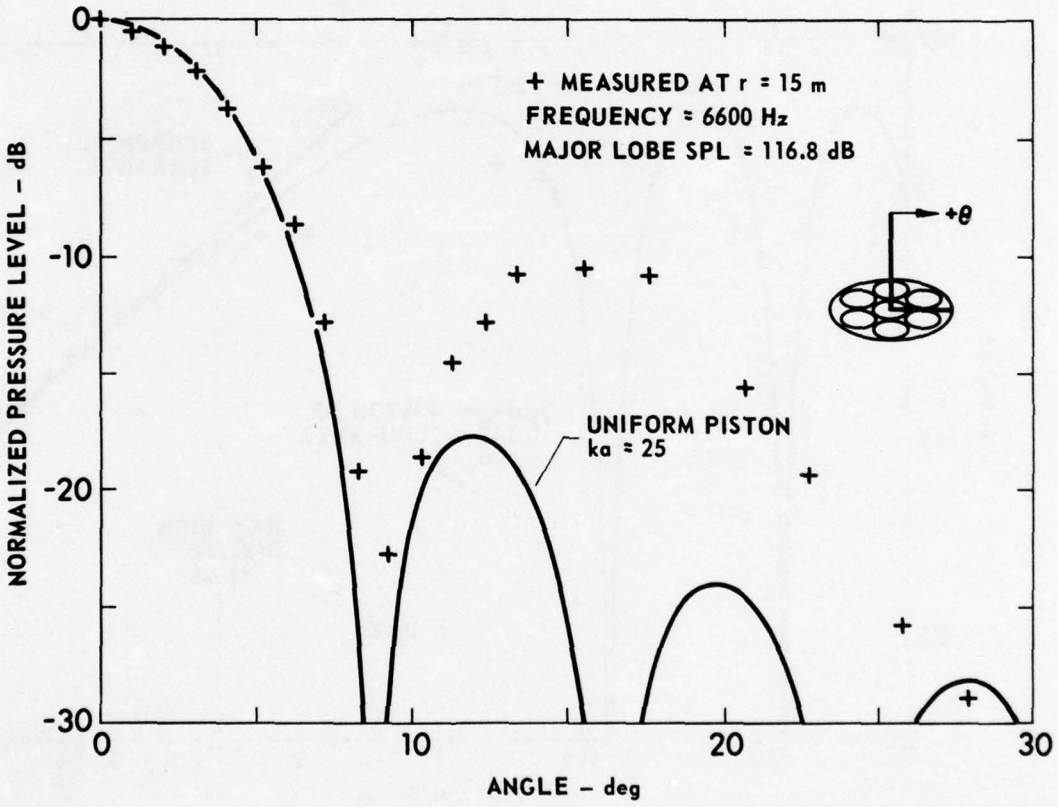

FIGURE 5-11
BEAM PATTERN FOR ARRAY No. 1 (7 ELEMENTS)
(FUNDAMENTAL)

ARL - UT
AS-76-1573
MAT - DR
12 - 3 - 76

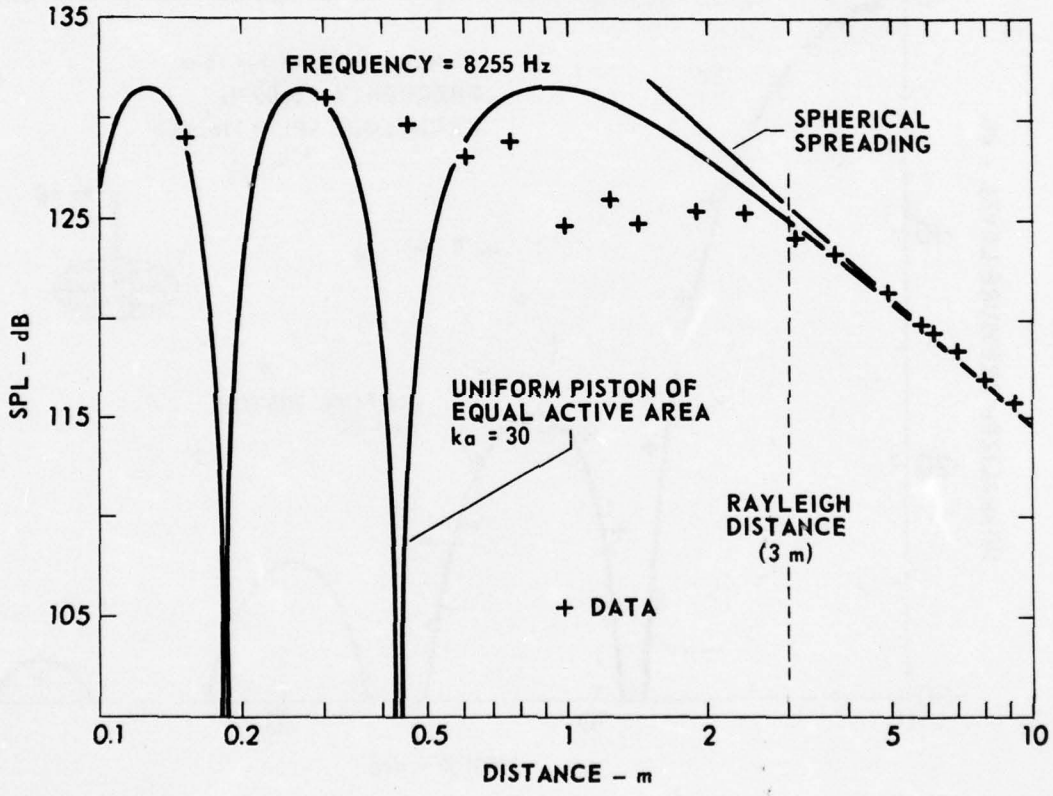

FIGURE 5-12
AXIAL PRESSURE IN NEARFIELD OF DRIVER ARRAY No. 1
(BAFFLE ATTACHED)
THEORY MATCHED TO DATA IN FARFIELD

ARL - UT
AS-76-957
MAT - RFO
8 - 11 - 76

theoretical pressure distribution for a uniform piston of equal active area is also shown. The theory and data have been matched in the far-field. The Rayleigh distance (3.2 m at this frequency) approximately indicated the beginning of the farfield zone. The pressure distribution in the nearfield deviated substantially from the predicted values, much as it was observed to do for a single horn (see Fig. 5-3). We attribute this deviation to the nonuniformity of excitation at the surface of the array. In turn, the nonuniformity is presumed to be at least partly due to the presence of crossmodes in the horns. The nearfield irregularities appear to average out in the farfield, just as they do when the source is a single driver (see section B of this chapter). Nonlinear effects are not expected to severely influence the nearfield pressure distribution because of the short distances and merely local concentrations of high level sound involved. We did not investigate the question of finite amplitude effects in the nearfield more thoroughly because of a lack of time.

The measured beam pattern for array No. 2 is shown in Fig. 5-13. The wind speed recorded during this experiment varied from 2.5 to 9.5 km/h. The array had a beamwidth of approximately 6° at 6.6 kHz through the planes shown in the figure. The array was not axisymmetric and the asymmetry is markedly reflected in the beam pattern. The narrow major lobe may have made the received signal quite sensitive to variation caused by wind convection.

AD-A039 020 TEXAS UNIV AT AUSTIN APPLIED RESEARCH LABS F/G 20/1
EXPERIMENTAL STUDY OF OUTDOOR PROPAGATION OF SPHERICALLY SPREAD--ETC(U)
JAN 77 M A THEOBALD F44620-76-C-0040
UNCLASSIFIED ARL-TR-77-5 AFOSR-TR-77-0521 NL

2 OF 2
AD
A039020

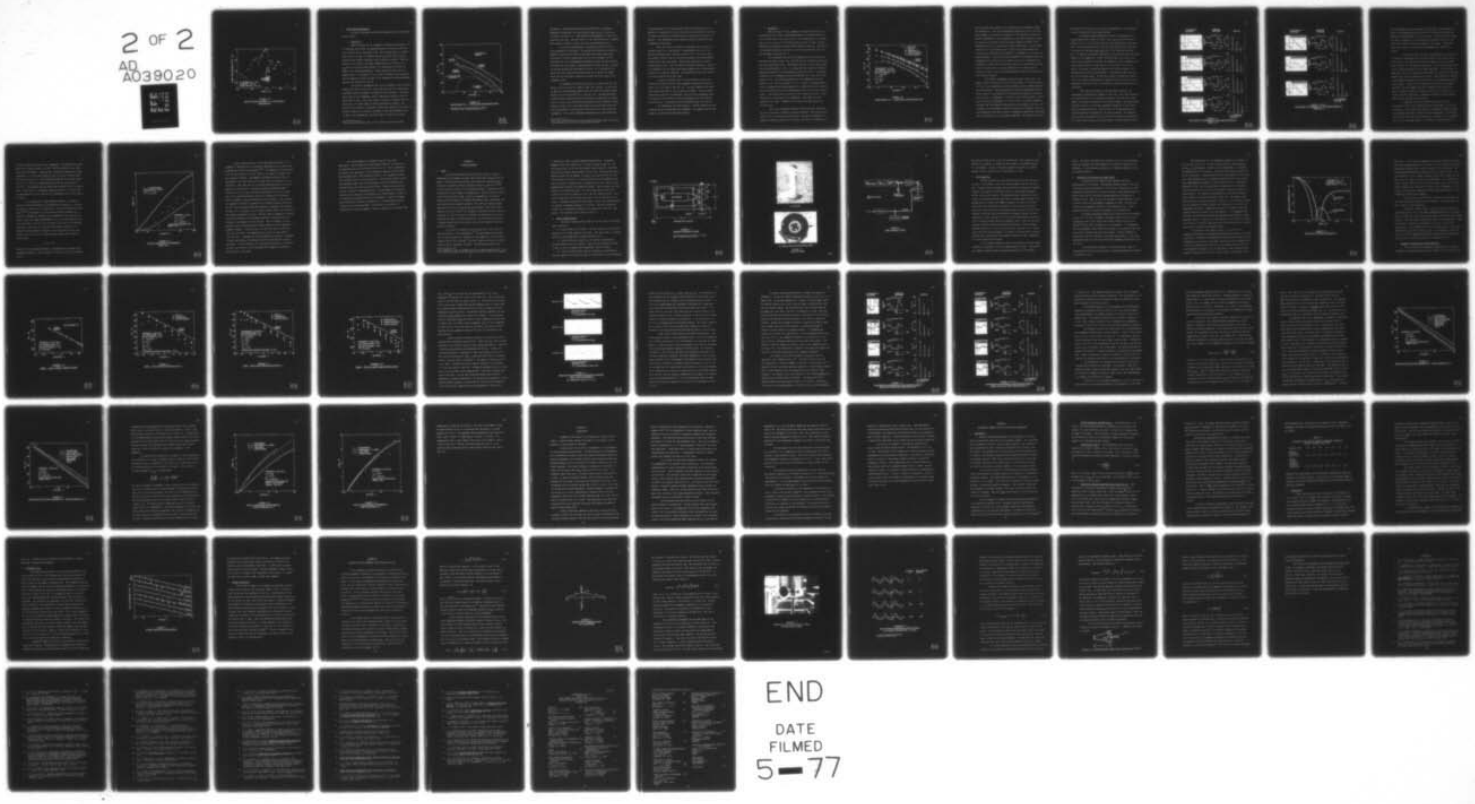

END

DATE
FILMED
5-77

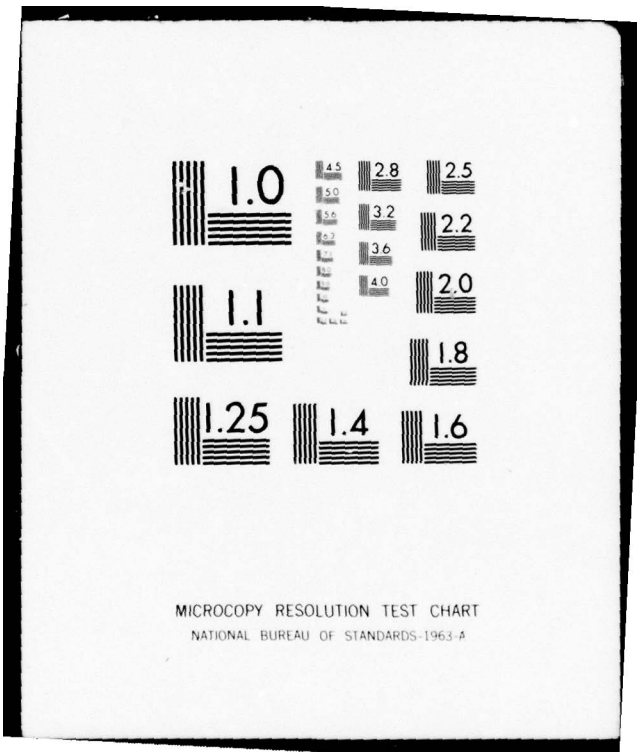
1.0
1.1
1.25
1.4
1.6
1.8
2.0
2.2
2.5
2.8
3.2
3.6
4.0
4.5
5.0
5.6
6.3
7.1
8.0
9.0
MICROCOPY RESOLUTION TEST CHART
NATIONAL BUREAU OF STANDARDS-1963-A

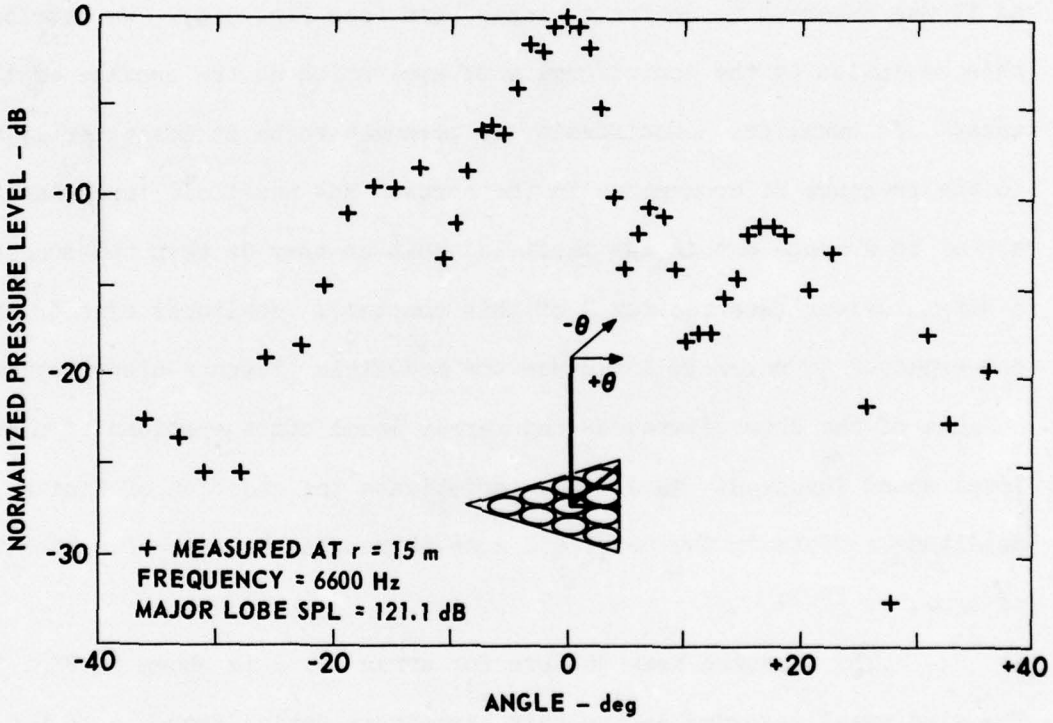

FIGURE 5-13
BEAM PATTERN FOR ARRAY No. 2 (10 ELEMENTS)
(FUNDAMENTAL)

ARL - UT
AS-76-1574
MAT - DR
12 - 3 - 76

G. Finite Amplitude Behavior

Two array experiments performed at maximum output are described in this section.

1. Array No. 1

When the source for the propagation experiment was array No. 1,* the frequency was 6.6 kHz, the Rayleigh distance (calculated value) was 2.5 m, and the source level was 144 dB. The operating point on the SFL chart, point A in Fig. 4-1 (SFL=161 dB and αr_o=0.0070, where r_o=R_o/2), indicates that moderate nonlinear effects should be expected. Moreover, because of the values of the range parameters--$\bar{r}$=11 m, $\hat{r}$=850 m, and r_{max}=33 m--we expected these effects to be observable well within the range of our traveling microphone. These expectations were borne out qualitatively. At a distance of 9.1 m, both the measured time waveforms and the separation between the SPLs of the fundamental and second harmonic indicated the presence of a shock.

The specific propagation data for the fundamental and the second harmonic are shown in Fig. 5-14. Also shown are predicted curves based upon models that are probably too simple for the experiment. The propagation data for the fundamental show no significant deviation from the linear theory curve. (Note that, again, this curve is begun at the 6.1 m data point.) In other words, no extra attenuation is evident. Yet, because of the evidence of nonlinear effects (for example, the presence of shocks at least by 9.1 m and the proximity of the second harmonic curve to that of the fundamental), one would expect to observe some extra

*The traveling microphone was a 1/4 in. model with protective grid.

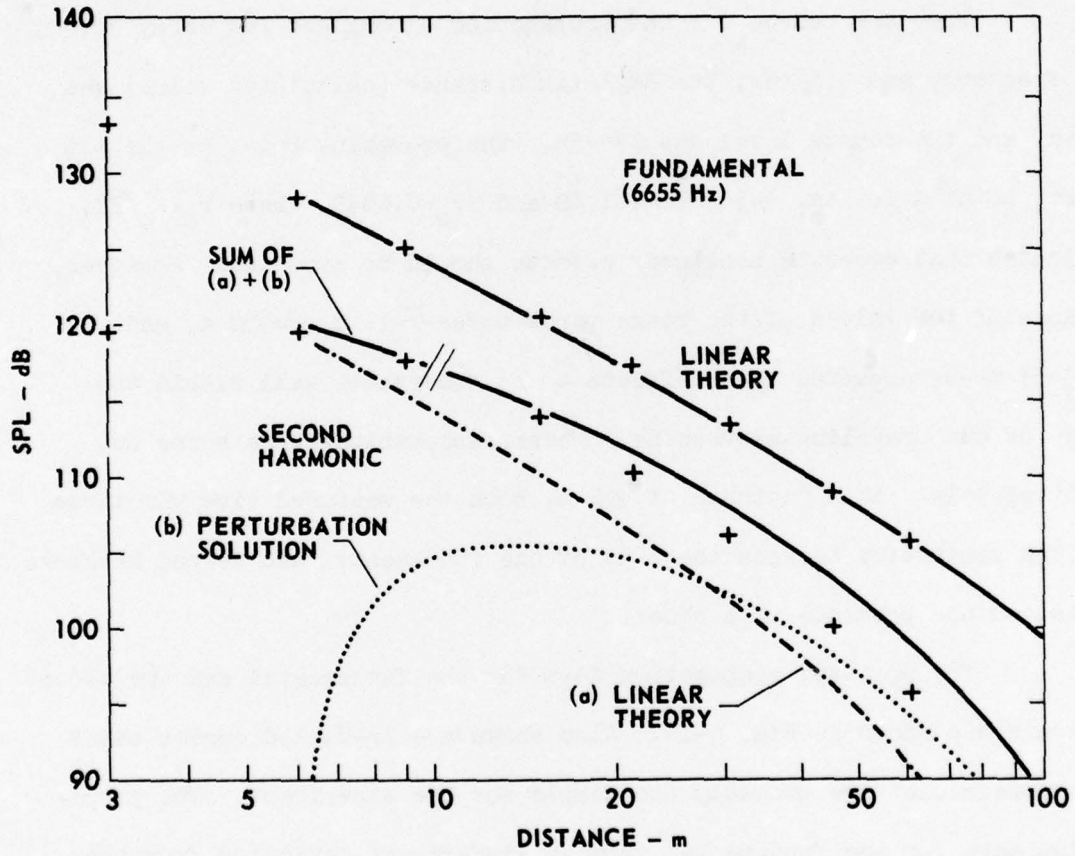

FIGURE 5-14
DRIVER ARRAY No. 1 – FINITE AMPLITUDE PROPAGATION

Adapted from figure previously reported by M. A. Theobald, D. A. Webster, and D. T. Blackstock (1976), Ref. 48

ARL - UT
AS-76-969
MAT - RFO
11 - 23 - 76
REV 12-16-76

attenuation. Using ordinary weak shock theory[8] (that is, ignoring atmospheric attenuation), one would predict EXDB values of 0.57 dB at 6.1 m and 0.91 dB at 9.1 m. The increase of approximately 0.3 dB is not observed in the data. The fact that it is not observed may not be significant, however, because 0.3 dB is less than the experimental error.

As for the second harmonic, no analytical prediction that is really applicable is available. The second order perturbation solution to Burgers' equation may be used for weak waves and ordinary weak shock theory may be used for strong waves, but the wave strengths for this experiment are in the embarrassing intermediate region for which analytical results are very sparse. Nevertheless, an attempt was made to explain the data by applying the perturbation results. It is admitted at the outset that these results are relevant only in the shock free region, which for this experiment represents only about the first tenth of the propagation path.

In applying the perturbation results, we started with Eq. 3-10 and let r_o=6.1 m; curve (b), shown in Fig. 5-14, results. To this curve we added the second harmonic signal [curve (a)] that was already present because of source distortion* at r_o; see Eq. 3-11. The second harmonic caused by finite amplitude effects is generated in phase with the fundamental. If the source distortion were caused by finite amplitude effects within the horns, use of the piston model for the horn mouth shows that the second harmonic in the farfield would be 90° out of phase with the fundamental. Since direct measurement showed that the phase difference

*Note that "source distortion" here includes distortion that took place in the nearfield as well as in the horns and the drivers.

was approximately 0°, we conclude that either the piston model of the radiation is inapplicable or that little distortion occurred in the horns. The latter conclusion is consistent with our calculation (section B of chapter V) that negligible extra attenuation should be associated with propagation in the horns.

While the solution obtained by combining curves (a) and (b) provides a good fit to the data out to approximately 15 m, it is not strictly applicable past a distance of about 9.1 m. The second order perturbation solution does not accurately represent the second harmonic signal after a shock has formed. Data and the perturbation solution diverge beyond r=15 m. The only method of solution available to describe the propagation for the region past shock formation (for a nonsinusoidal source) is the computer algorithm. The algorithm was not used, however, to provide predictions for this case.

A much more suitable test of the perturbation solution was provided by the data from the first propagation experiment described in section F of this chapter (see Ref. 11). (In that experiment the waves were sufficiently weak, so that no shock was formed.) The perturbation results are expected to be applicable over the entire propagation path. It turned out that the data for the second harmonic fit the predicted curve very well. The predicted curve was based on Eqs. 3-10 and 3-11.

The experiments for which array No. 1 was the sound source were completed before the anemometer was installed. We estimate that the wind speeds at the ground were less than 24 km/h.

2. Array No. 2

When the source for the propagation experiment was array No. 2, the frequency was 6.6 kHz, the Rayleigh distance (calculated value) was 3.6 m, and the source level was 146.5 dB. The operating point on the SFL chart, point C in Fig. 4-1 (SFL=163 dB and $\alpha r_o = 9.6 \times 10^{-3}$, where $r_o = R_o/2$), indicates that moderate nonlinear effects should be expected. The effects of nonlinearity should be expected to be more pronounced than those for the experiment using array No. 1.

The propagation data for the fundamental and second and third harmonics are shown in Fig. 5-15. The data for the fundamental fall below the small signal prediction. The maximum deviation from the small signal curve is approximately 1.7 dB. It is seen that the second and third harmonics grow relative to the fundamental before they recede. The minimum separation of the fundamental and second harmonic is 5.4 dB, which value occurs at 18 m. The minimum separation of the fundamental and third harmonic is 11.4 dB at a distance of 9.1 m. Because the minimum separation of fundamental and second harmonic for a sawtooth wave (the limiting form of strong waves) is 6 dB, the measured value of 5.4 dB is a curious result. Other data from the vicinity of 18 m confirm this value. Thus, random error is discounted as an explanation. The reason for this behavior is not clear. Asymmetry of the source wave may explain the recorded value.

Theoretical propagation results for the experiment described above were generated by using the computer algorithm. The received waveform at $r_i = 6.1$ m served as the source wave. Because this distance is outside the Rayleigh distance of the array, the effect of diffraction at

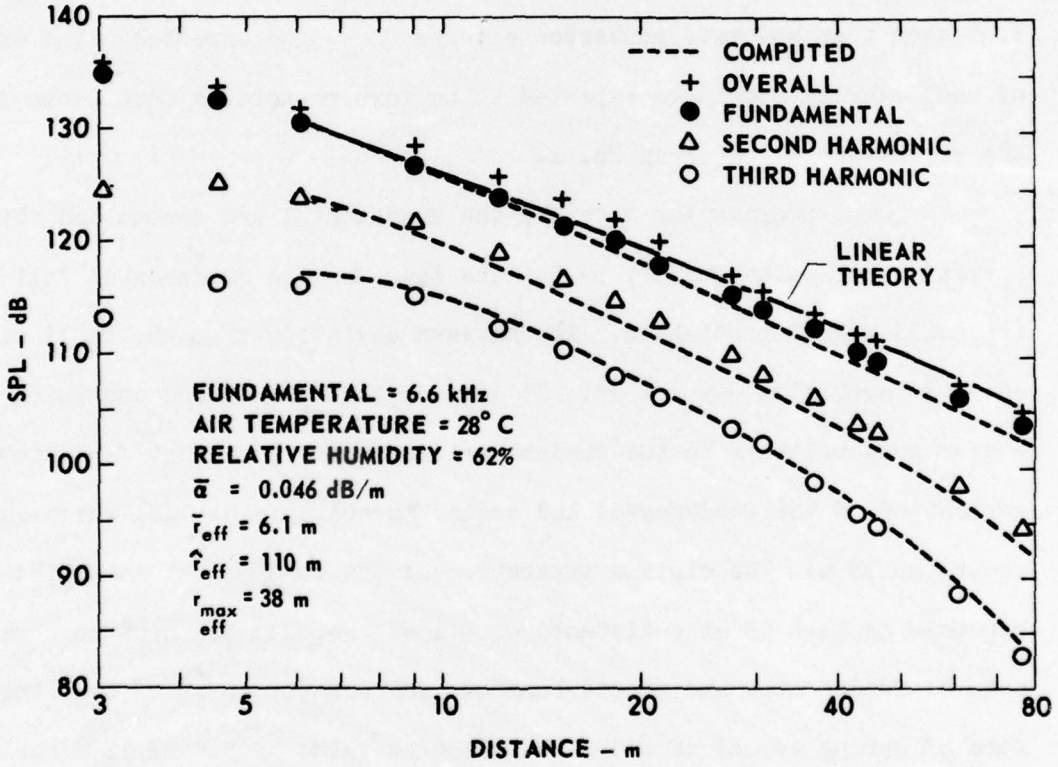

FIGURE 5-15
DRIVER ARRAY No. 2 – FINITE AMPLITUDE PROPAGATION

ARL - UT
AS-76-1324
MAT - DR
11 - 19 - 76

the horn mouths was expected to be excluded from the propagation region (see Appendix B). The source waveform was prepared for use in the computer program, as described in chapter III. The waveform was then fast Fourier transformed to allow examination of the relative harmonic levels. The levels of the second, third, and fourth harmonics relative to the fundamental were -6.9, -13.8, and -18.8 dB, respectively. The freefield correction for the microphone was +0.2 dB at the second harmonic and -0.5 dB at the third and fourth harmonics; it increased to +1.0 dB at the seventh harmonic. Because the energy contained in the harmonics above the fundamental was relatively low and other errors in the experiment were comparable or larger than the freefield corrections (especially when wind noise is accounted for), the input waveform to the computer was not corrected. However, all other measured harmonic levels were corrected for the freefield response.

The computed propagation curves are shown in Fig. 5-15. The general trend in the data is visible in this figure. Our predictions are too low for the fundamental and second harmonic and are slightly high for the third harmonic. The maximum deviation between experimental and computed values for each harmonic (at the distance the deviation occurred) are as follows: fundamental, +1.8 dB (at 76 m); second harmonic, +1.8 dB (at 21 m); and third harmonic, -0.7 dB (at 76 m). A positive deviation indicates that the measured spectral level is the higher of the two. The prevalence of underestimated levels would seem to be anomalous. That is, overestimations could rather easily be explained by additional losses that are not accounted for in the computer algorithm. The deviations were not

attributed to the selection of the step size parameters in the algorithm. We shall reconsider this discrepancy shortly.

The minimum computed separation between the fundamental and second harmonic was a value of 5.8 dB. This value, which occurred at a distance of 12 m, is 0.2 dB less than the value predicted for a sawtooth wave. Thus the relative levels of an initially distorted wave may possibly violate the limiting values applicable to an initially sinusoidal wave. An analysis by Webster[11] applicable to the preshock region may lend support to this suggestion. Webster has shown that, for a source with initial second harmonic distortion, the separation of the fundamental and second harmonic levels is less than it is in the case of a pure tone source. The amount of reduction depends on the relative phase of the fundamental and initial second harmonic. This behavior might carry over into the postshock region. In any case, because no definitive accuracy test of the computer program has been devised (except for the case of no atmospheric absorption), the 0.2 dB difference value described may not be significant.

The computed and measured time waveforms and spectra for representative distances are compared in Fig. 5-16. Note that, because of the characteristics of the condenser microphone, the electrical output signal is inverted with respect to the acoustic signal. The waveform was therefore restored to its proper appearance through use of the oscilloscope's inverting amplifier. The plot sizes of the experimental and computed waveforms are matched for the source waveform. The remaining plot axes are proportional in size to the source wave axes, according to the relative gain setting of the oscilloscope. The zero pressure line on

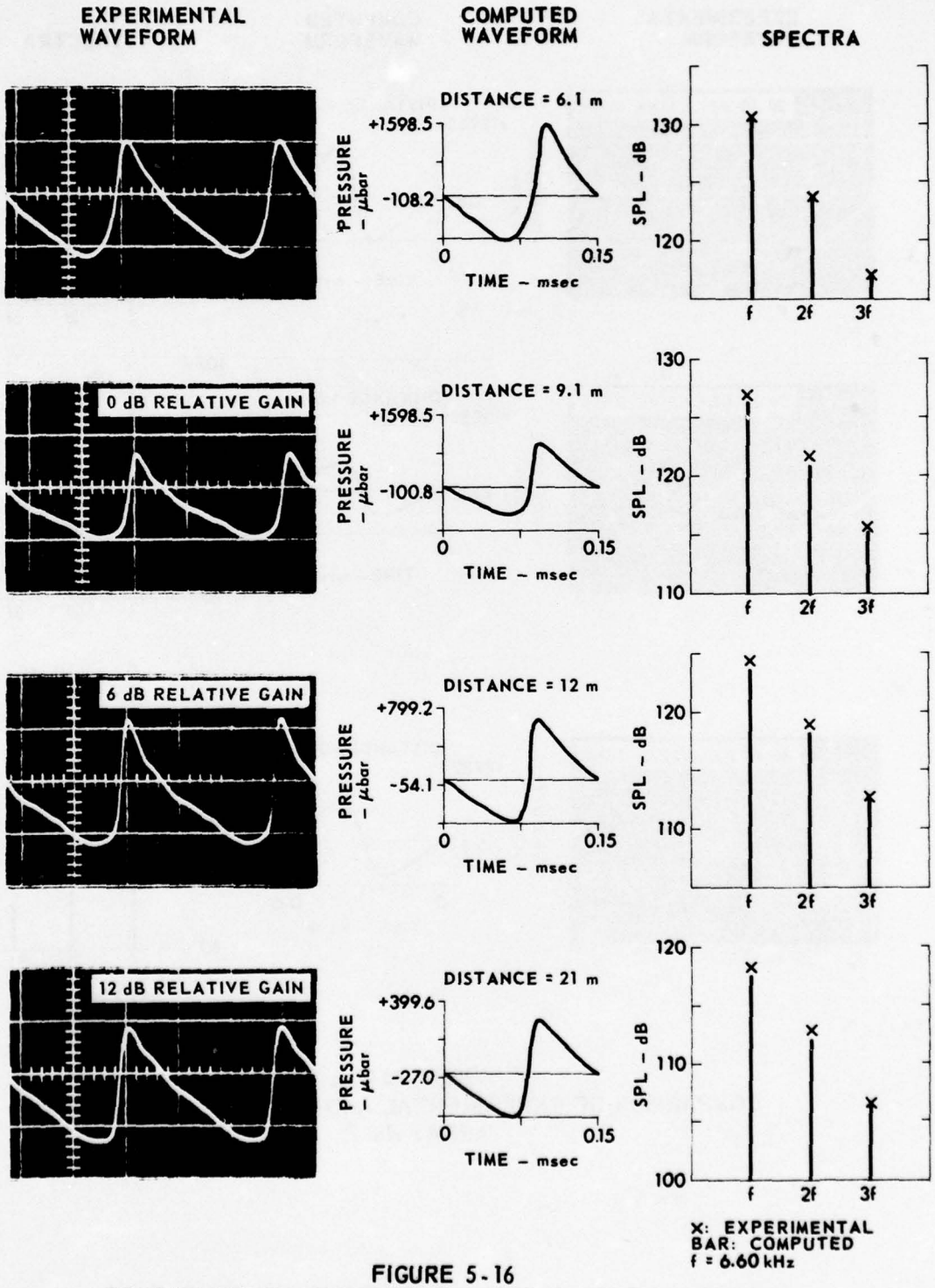

FIGURE 5-16
COMPARISON OF EXPERIMENTAL AND COMPUTED RESULTS
ARRAY No. 2

ARL - UT
AS-76-1693b
MAT - DR
12 - 21 - 76

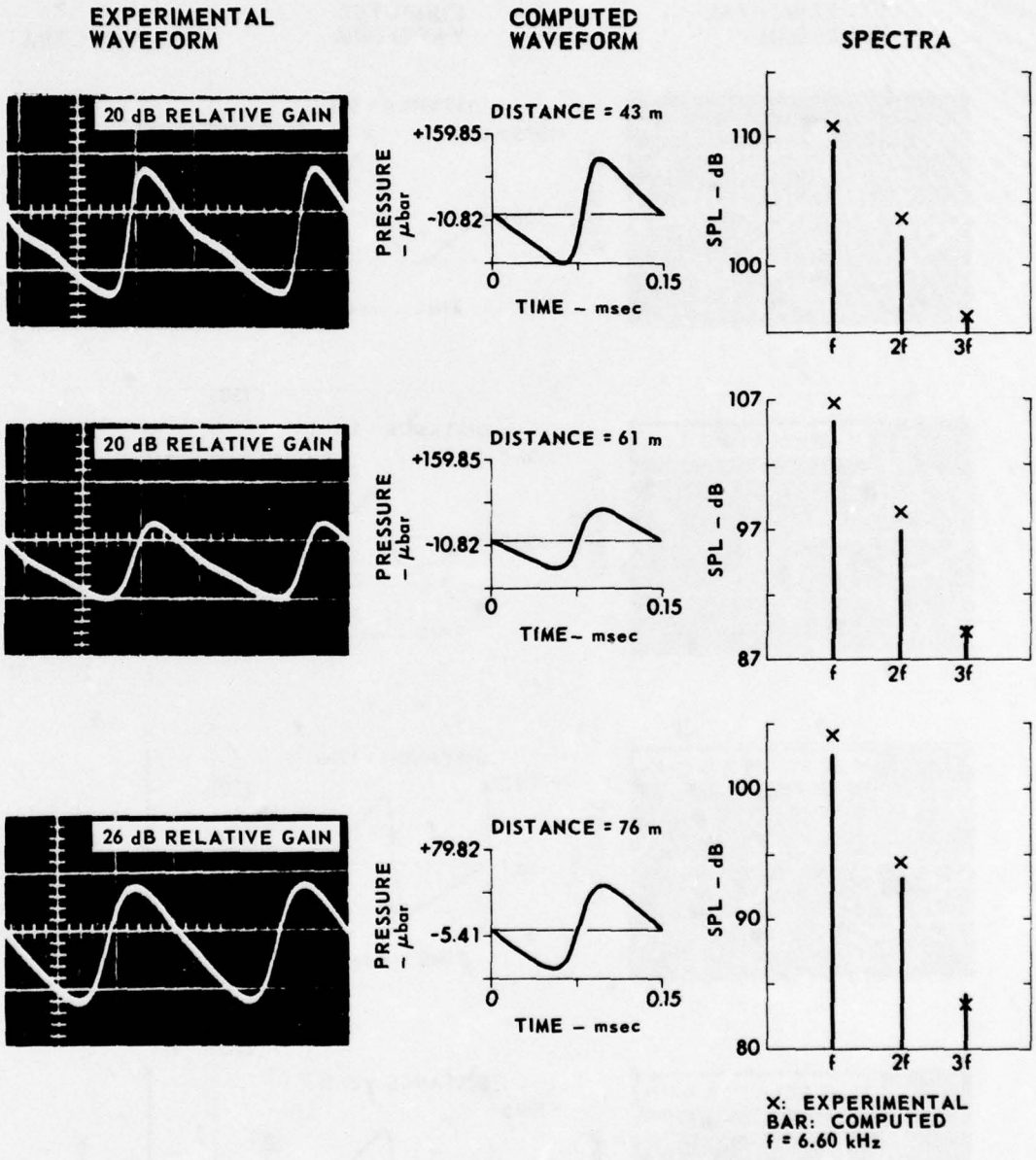

FIGURE 5-16 (Cont.)
COMPARISON OF EXPERIMENTAL AND COMPUTED RESULTS
ARRAY No. 2

ARL - UT
AS-76-1693a
MAT - DR
12 - 21 - 76

the oscillograms does not correspond to a grid mark. This apparent dc shift of the measured waveforms relative to the computed waveforms was caused by a maladjustment of the oscilloscope's vertical position control. For ease of comparison, the experimental and computed results for the first three spectral levels are repeated in this figure. Theoretical results are shown as solid bars; the measurements are indicated by crosses.

It is seen from Fig. 5-16 that the experimental waveforms out to a distance of approximately 61 m are more peaked on the positive half-cycle than are the computed waveforms; the negative half-cycles match quite closely. The experimental waveform at 76 m has the same wave shape as the computed waveform but has a higher amplitude. The differences in amplitude between the experimental and computed time waveforms become less dramatic when they are expressed in decibels. These differences increase with propagation distance, where the effects of the inhomogeneous medium were stronger. Because the oscillograms do not depict time averaged waveforms, the oscillograms show more variability than the spectral levels. Finally, because the computed results were all based on one initial waveform, small phase or amplitude variations in this waveform may be carried through the calculations.

A comparison between our measured values of the extra attenuation and the values predicted using the Merklinger et al. model was desired. The amplitude and radius of an equivalent spherical source of sinusoidal waves must be known for these computations. The relative levels of the first and second harmonics at a distance of 6.1 m indicate that a shock is already present. (The SPL of the second harmonic is

-6.9 dB, relative to the SPL of the fundamental. The difference in these levels for a newborn shock is -7.9 dB.) But the waveform is also asymmetric at this distance. Solutions were computed by assuming two extreme conditions: (1) a sine wave exists at r_o=6.1 m and (2) a newborn shock wave exists at r_i=6.1 m. (This assumption means that a sine wave exists at r_o=1.4 m.) These two assumptions lead to the two curves shown in Fig. 5-17. The measured data are effectively bracketed by the two predictions. This result is encouraging, especially when it is recalled that the experimental error for calm air is of substantial size on the scale of the figure.

It is appropriate, though somewhat difficult, to determine whether the beam from array No. 2 was affected by diffraction. (See the discussion in section B.3. of chapter II.) In current theoretical treatments,[28-30] the amplitude variation across the beam is assumed to be Gaussian. Although the variation is not Gaussian for the beam from the array, we may very roughly approximate it to be so by defining the effective beam radius b (see Eq. 2-12) in terms of the points on the measured beam pattern (see Fig. 5-13) at which the response is down 8.7 dB. Because the measured beam is narrower on one side than the other, the estimate for N, at 15 m, is a range of values rather than a specific value, namely

$$0.1 < N < 0.4 \quad .$$

Because the beam spreads spherically, b increases and ϵ decreases with propagation distance. The net effect on N (see Eq. 2-13) is to decrease as 1/r.

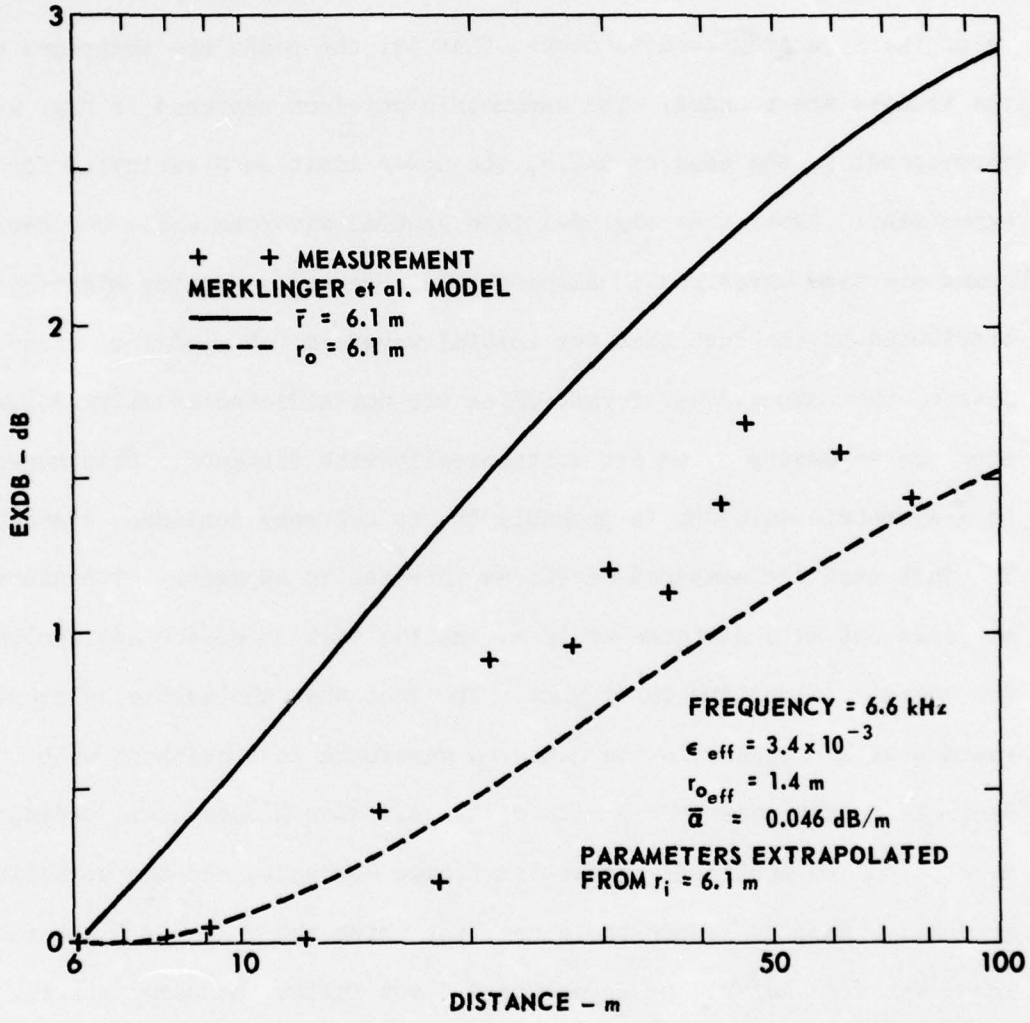

FIGURE 5-17
EXTRA ATTENUATION OF FUNDAMENTAL
ARRAY No. 2

ARL - UT
AS-76-1562
MAT - DR
12 - 2 - 76

Several characteristics of the experimental waveforms for our propagation experiments are in qualitative agreement with the predictions regarding the effects of diffraction.[28,30] The asymmetry of the waveforms is of the type predicted to occur, that is, the peaks are sharpened and the troughs are rounded. The asymmetric waveform sketched in Fig. 2-1 corresponds to the case of N=0.4, the upper limit on N estimated for our experiment. (Note that Fig. 2-1 is a spatial waveform while the oscillograms are time waveforms.) Although the observed asymmetry might be attributed to the fact that the initial waveform (at r_i=6.1 m) is asymmetric, the computed waveforms, which are not affected by diffraction, show the asymmetry dying out monotonically with distance. This reversion to a symmetric waveform is probably due to ordinary nonlinear distortion. The fact that the measured waveforms increase in asymmetry with distance, at least out to a distance of 12 m, implies that an effect not included in the computer algorithm is at work. The fact that the asymmetry eventually recedes with distance in the measured waveforms is consistent with the decrease in the parameter N with distance. When N decreases, ordinary absorption and nonlinear distortion become dominant, and the asymmetry is gradually "damped." When the siren, for which the value of N was much less, was used later, the asymmetry did not follow the same pattern. (See Fig. 6-10.) Although some initial asymmetry was present, it appeared to decay monotonically with distance in both the measured and computed waveforms. For these reasons, it is felt that the effects of diffraction may have been observed in the high amplitude propagation experiment in which array No. 2 was used.

We briefly summarize the general results of the array experiments. The expectations of wave behavior based on the position of the operating point on the SFL chart were borne out. Where theoretical predictions were applicable to the experiments, agreement with the data was reasonably good. This evaluation applies to the propagation curves, time waveforms, and the extra attenuation. The predicted harmonic levels were generally higher than the experimental levels; the measured extra attenuation was less than the expected values. Because the predictions used are intended for homogeneous media, it would appear that nonlinear effects are not completely neutralized by the random medium, at least for the conditions encountered during our experiments. Finally, the asymmetric distortion predicted by Rudenko et al. is demonstrated qualitatively in our recorded waveforms. The details of the effects of diffraction on initially asymmetric waves are unknown at the present time.

CHAPTER VI

SIREN EXPERIMENTS

A. Siren

A much more powerful acoustic source was needed in order to demonstrate much stronger nonlinear effects than those obtained with the arrays. Electrically driven sirens with external air compressors have been used to generate extremely high sound levels in open air.[37,38,64] A siren basically consists of two perforated plates, a fixed stator and a spinning rotor, and a supply of compressed air. When the holes (or ports) in the stator and rotor align, a burst of compressed air is emitted. Because the port diameter is normally much smaller than a wavelength, the port behaves like an acoustic monopole. The ports are commonly spaced equally in a circle on the rotor and stator plates. The siren is then expected to act as a ring.[65] The frequency with which the ports come into alignment, and thus the acoustic frequency, are determined by the motor speed and the number of plate perforations. The sound pressure output is a complex function of the port shape, size, and the pressure difference across the plates.[37]

We elected to construct a siren scaled down in size from the model described by Allen and Rudnick.[38] The main design criteria were that the siren operate at a frequency of approximately 12 kHz and produce nearby an SPL of 150 to 160 dB.* The final output level was to be determined by the air compressor available. The mechanical design was by

*The threshold of pain for humans is an SPL of approximately 120 dB. An SPL of 160 dB is found in the nearfield of a 10,000 lb thrust jet engine.[66]

J. Byers and L. Guyer of Applied Research Laboratories. A schematic diagram of the siren (sketch by W. N. Cobb) is shown in Fig. 6-1. The drive motor was a 1/2 hp tool post grinder (Precise model No. Super 60), which had an unloaded spindle speed of 45,000 rpm. By mounting the motor directly inside the air chamber, we hoped to use the siren air flow for extra cooling of the motor. It was believed that this arrangement would allow the motor to operate above its normally rated load. The rotor was machined from titanium for strength and safety. Twenty conical ports were drilled in the rotor and stator. The ports were equally spaced with centers on a circle of radius q=7.6 cm. The port diameters were: rotor, 0.87 cm input and 0.53 cm output; and stator, 0.53 cm input and 1.1 cm output. Assuming a loaded motor speed equal to 80% of its unloaded speed, we expected the maximum frequency to be 12 kHz. The siren output was coupled to the atmosphere through a 6.4 cm long conical horn (27° flare angle). The completed siren is shown in Fig. 6-2.

B. Siren Transmit System

The siren transmit system, shown in Fig. 6-3, had the following major components:

(1) General Radio 200 CU Variac. The siren speed was controlled by varying the ac voltage applied to the motor. The upper limit to the speed was set by the maximum motor current, which was 5.6 A.

(2) Pearson Electronics model No. 110 current transformer and Hewlett-Packard 400 EL ac voltmeter. These devices monitored the motor current so that overloading (and overheating) could be avoided.

(3) Davey 210 WDS-TS piston type air compressor (truck-mounted). The air supply for the siren was rated at 94 liters/sec at 6.8 atm (gauge).

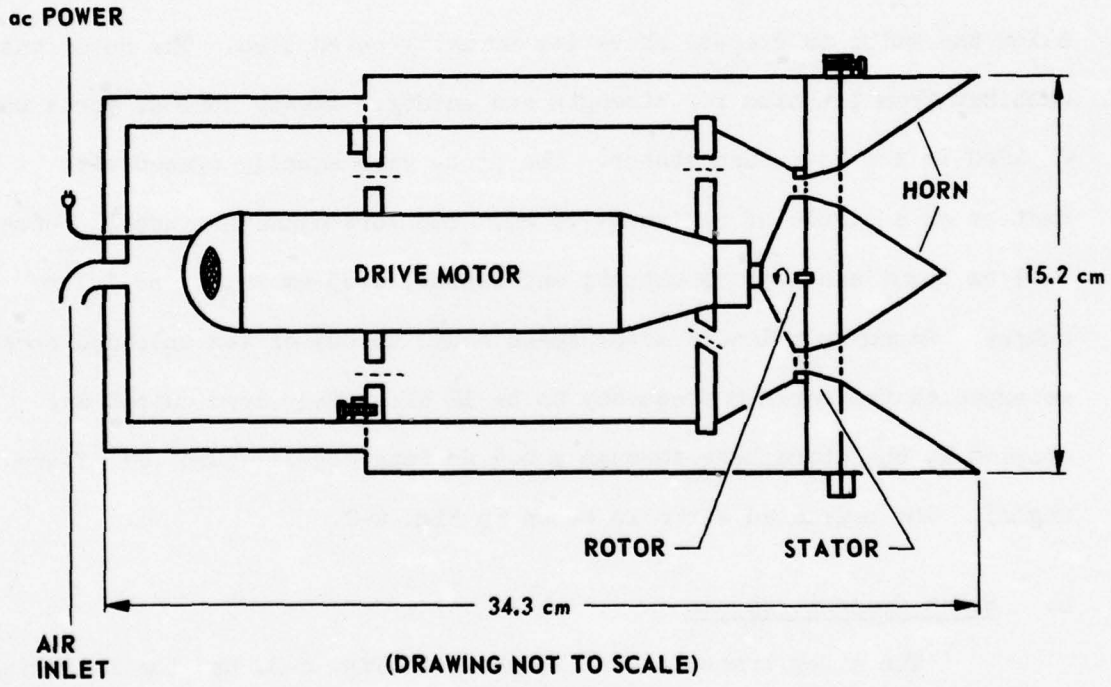

FIGURE 6-1
SCHEMATIC DIAGRAM OF SIREN

Previously reported by M. A. Theobald, D. A. Webster, and D. T. Blackstock (1976), Ref. 48

ARL - UT
AS-76-2301
MAT - DR
12 - 14 - 76

(a) SIDE VIEW

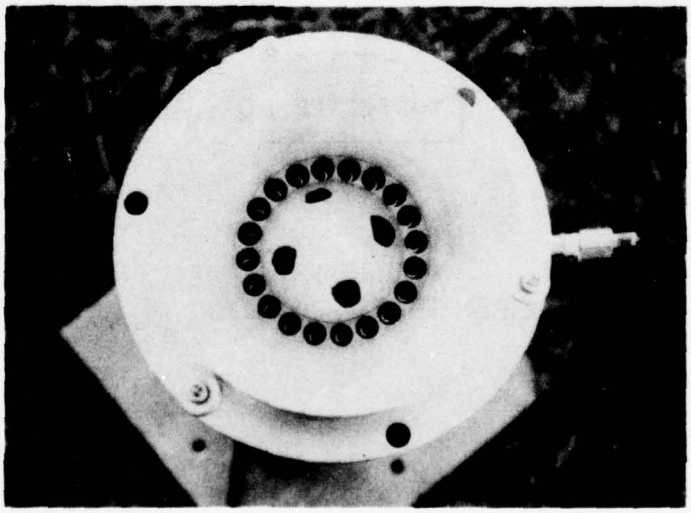

(b) VIEW OF SIREN PORTS AND CONICAL HORN

FIGURE 6-2
SIREN WITH HORN

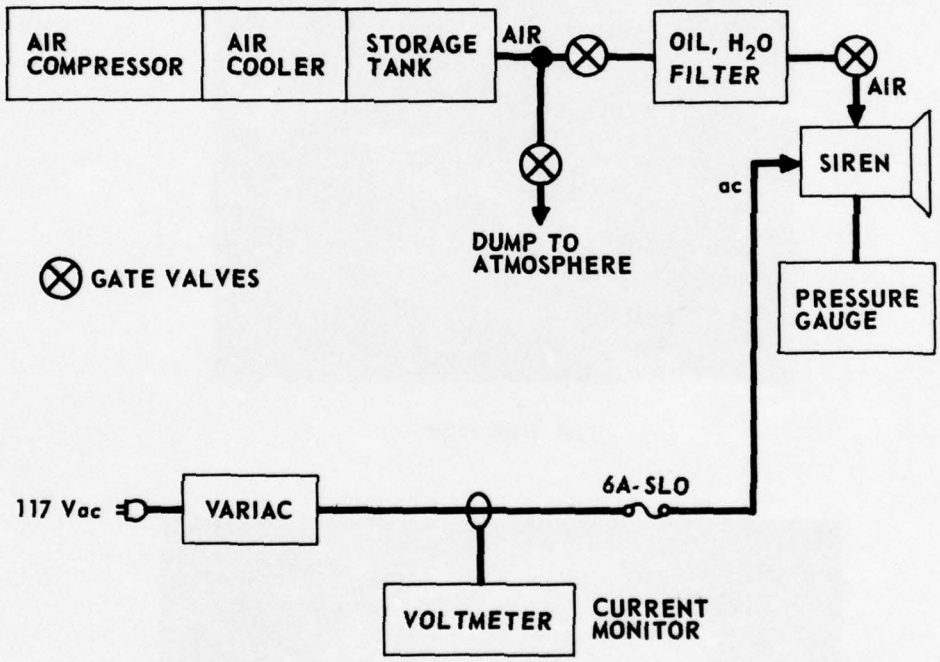

FIGURE 6-3
SIREN TRANSMIT SYSTEM

ARL - UT
AS-76-1330
MAT - DR
11 - 19 - 76

The supply included an air cooler and storage tank. The compressor could supply only enough air to charge the siren chamber to a maximum pressure of 1 atm (gauge). Because of pressure regulation problems, the chamber pressure could be reduced only to approximately 0.3 atm.

C. Siren Operation

Several problems were encountered during the initial testing of the siren. The loading on the motor was much higher than had been expected. We assume that the loading, which was found to increase with chamber pressure, was caused by air drag on the rotor. The design frequency, 12 kHz, could not be achieved. The maximum (stable) frequency was about 6 kHz at full chamber pressure and 8 kHz at minimum chamber pressure. At maximum acoustic output (full chamber pressure), the SPL of the fundamental (6.3 kHz) was 165 dB at a distance 19 cm from the stator plate. More serious than the drop in operating frequency, however, was the overheating of the motor that occurred when full chamber pressure was used. Operation at a motor current of 6 to 6.5 A (the rated maximum current was 5.6 A) eventually caused the motor windings to fail. After the motor was repaired, the motor current was carefully monitored. With the chamber pressure reduced to 0.7 atm, the current was an acceptable 4.9 A. Under these conditions the SPL (again at 6.3 kHz) at 19 cm was only 0.5 dB less than the value achieved when full chamber pressure was used. Thereafter the siren operated very reliably.

At low chamber pressures, which were needed for the small signal experiments, regulation of the air supply became a problem. Variations in the chamber pressure caused corresponding variations in the acoustic

output. The output variations were reduced to 0.2 to 0.3 dB by dumping excess air pressure into the atmosphere and running the compressor continuously. In this way stable operation at a chamber pressure as low as 0.3 atm was achieved.

D. Evaluation of the Siren as a Sound Source

In this section, we describe the important acoustical characteristics of the siren. The Rayleigh distance (based on the area) of the horn mouth was calculated to be 38 cm for a frequency of 6.1 kHz. Although the nearfield was not probed in detail, enough measurements were made to show that the waves were already spherically spreading at a distance r=19 cm. When the siren was operated at high amplitudes, a wave at this distance was approximately triangular in shape. The wave distorted into an asymmetric sawtooth by the distance r=38 cm. Finite amplitude effects are believed responsible for this distortion.

Microphone measurements made near the horn mouth were disturbed by air flow. We did not attempt to determine whether the dc air flow through the siren or the "sonic wind" effect described by Allen and Rudnick[38] was the main contributor to the disturbance. It is suggested that the atmospheric wind, which blew crosswise to the acoustic beam, may have acted to disperse any sonic wind present. (Allen[39] employed an electric fan for this purpose for his indoor experiments.) In any case, measurements made at r=38 cm and beyond were seemingly undisturbed by the air flow.

The conical horn attached to the siren provided a gain of approximately 8 dB over the siren alone. The gain measurement was made at a distance of 19 cm.

The beam pattern for the fundamental measured at a distance of 15 m is shown in Fig. 6-4. The siren was operated at a high amplitude (an SPL_{1m} of approximately 149 dB) for these measurements. A beamwidth of approximately 50° is indicated. The siren alone should be expected to act as a ring source. Data described by Allen and Rudnick for their siren are in good agreement with the predicted beam pattern for a ring source. Their measurements were made at a short distance (25 cm). The measured beamwidth of their siren increased when an exponential horn was added. With the addition of a horn, the source might be expected to behave as a baffled piston. The predicted beam patterns for both uniform ring and piston models for our siren are given in Fig. 6-4. The measured beam pattern does not confirm either model. However, in our discussion we have thus far neglected nonlinear effects. At a distance of 15 m, where the measurements were made, a significant loss due to nonlinear effects had already occurred (see section E of this chapter). It is suggested that the major lobe pattern has the blunted appearance characteristic of high amplitude sources. Indeed a 6 to 7 dB reduction, due to extra attenuation, at the center of the major lobe would cause the beam pattern for a piston-like source to resemble our measured results.

An estimate of the acoustic output of the siren at the fundamental frequency for high amplitude operation was desired. The power output may be estimated by integrating the received sound pressure of the fundamental over the area of the beam. Carrying out this calculation by using the information given in Fig. 6-4, one obtains a power of 60 W at the fundamental frequency. But, as noted above, extra attenuation has probably reduced the level by 6 to 7 dB, at least in the center of the

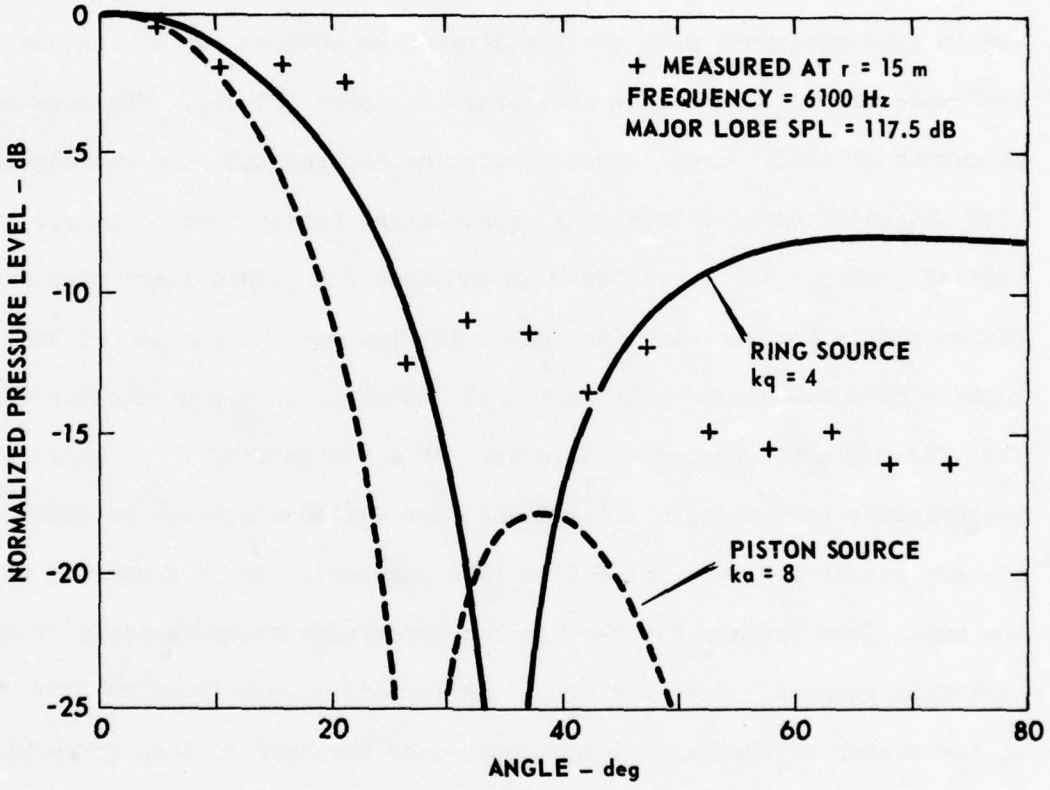

FIGURE 6-4
SIREN BEAM PATTERN (FUNDAMENTAL)

ARL - UT
AS-76-1332
MAT - DR
11 - 19 - 76

major lobe. If one instead extrapolates the pressure measured on-axis at 0.38 m (the Rayleigh distance of the horn) out to 15 m, and uses the same beam pattern measured there, a power rating of 410 W is obtained. The corresponding extrapolated SPL on-axis is 125.7 dB versus the 117.5 dB value measured at 15 m. Because nonlinear losses tend to square off the major lobe, the value 410 W may be an overestimate. If our estimate is correct, however, 85% (350 W) of the siren's power output (at the fundamental frequency) was lost within the first 15 m of propagation. In the future, for purposes of comparison, a small signal beam pattern for the fundamental should also be measured.

We were without an airflow meter during these experiments and the siren conversion efficiency was not measured. Efficiency was not a major concern in this application.

Because the acoustic output of the siren was an asymmetrical sawtooth-type wave even at very short propagation distances, we desired a check on whether low level sound from the siren would exhibit small signal behavior. When the chamber pressure was reduced to approximately 0.3 atm, we were able to conduct an experiment at 6.1 kHz at a source level SPL_{1m}=140 dB. The operating point on the SFL graph (Fig. 4-1) is point D (SFL=156 dB, $\alpha r_o = 8.5 \times 10^{-4}$, where $r_o = R_o/2$). The propagation curve (see Fig. 6-5) for the fundamental matches the linear theory extremely well. The deviation is less than 0.9 dB out to a distance of 46 m.

E. Propagation Experiments at Finite Amplitude

The data from three propagation experiments with the siren operating at high amplitudes are shown in Figs. 6-6, 6-7, and 6-8. The

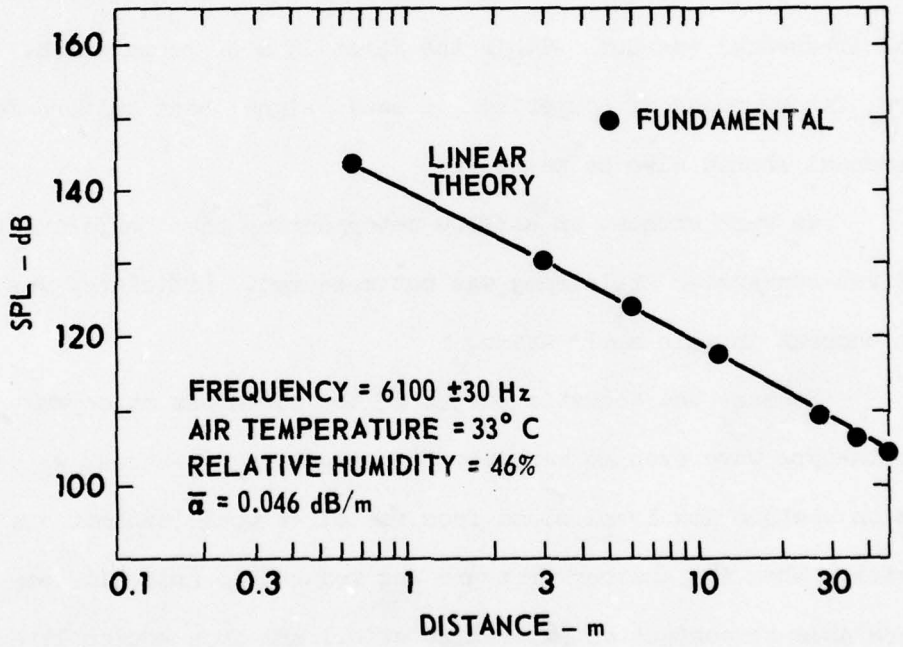

FIGURE 6-5
SIREN – SMALL SIGNAL PROPAGATION

ARL - UT
AS-76-1328-S
MAT - DR
11-9-76
REV 2-11-77

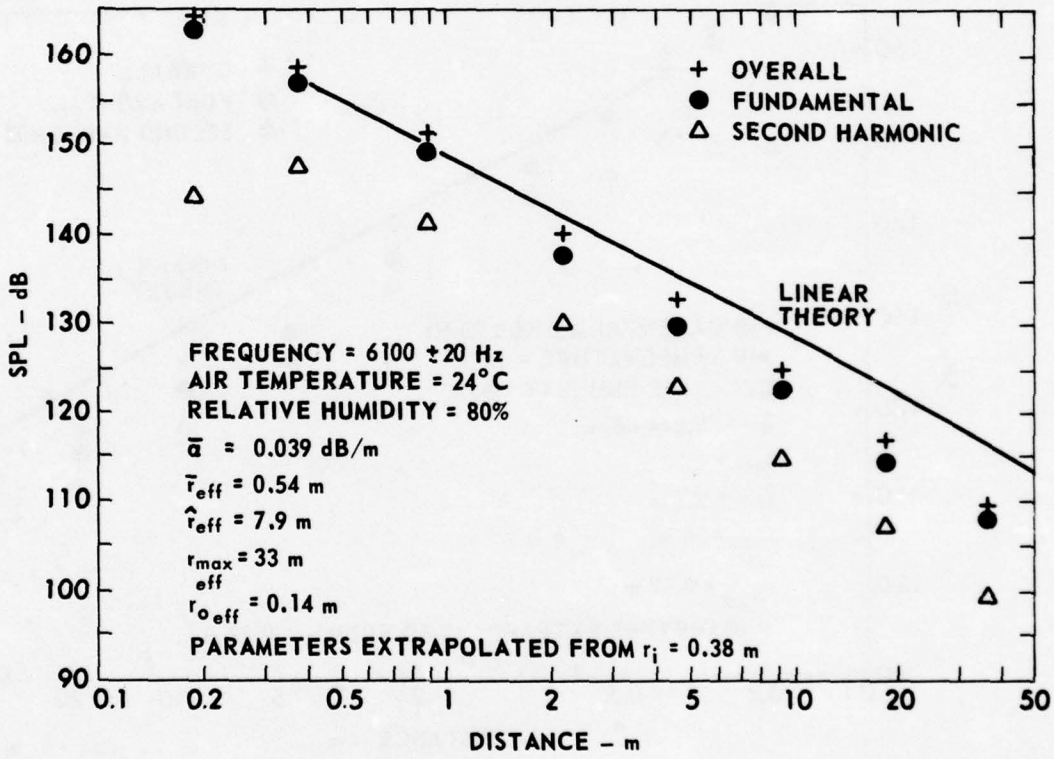

FIGURE 6-6
SIREN – FINITE-AMPLITUDE PROPAGATION No. 1

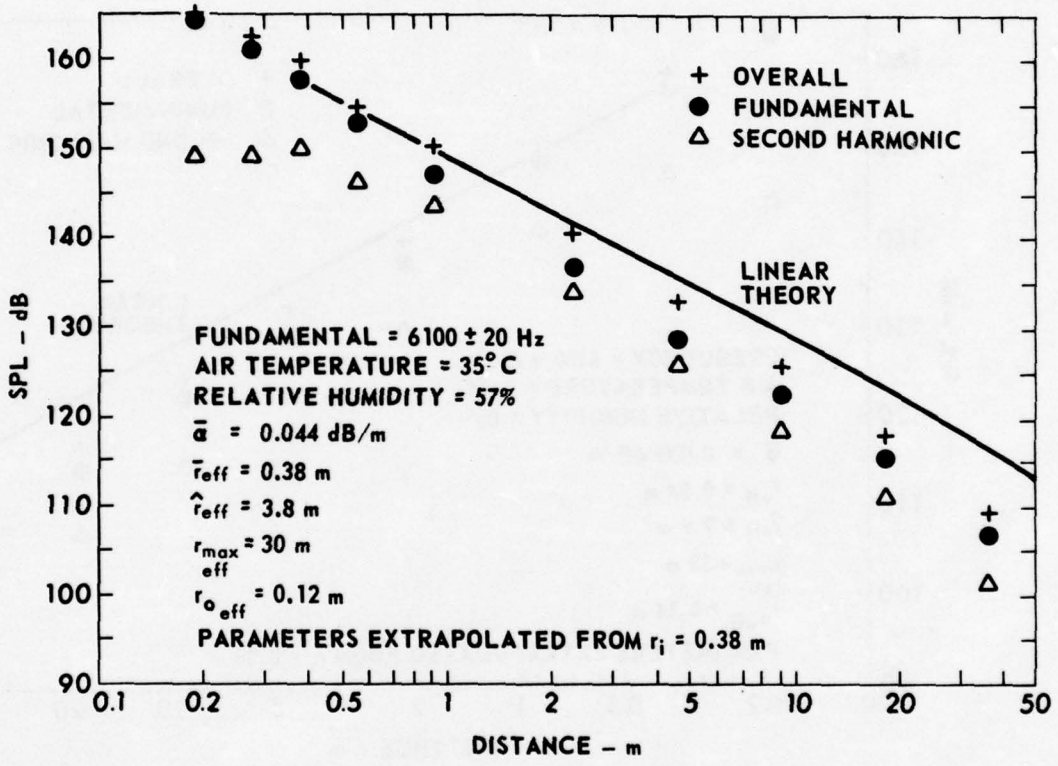

FIGURE 6-7
SIREN – FINITE AMPLITUDE PROPAGATION No. 2

ARL - UT
AS-76-1326
MAT - DR
11 - 19 - 76

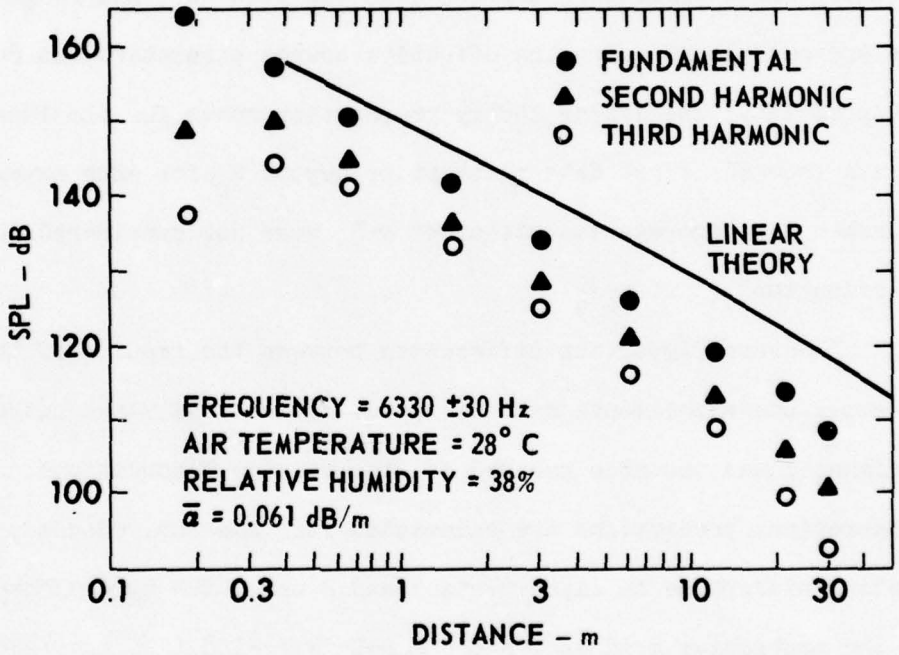

FIGURE 6-8
SIREN – FINITE AMPLITUDE PROPAGATION

ARL - UT
AS-76-1327-S
MAT - DR
11-9-76
REV 2-11-77

value of SPL_{lm} for all three runs was approximately 149 dB, where fundamental frequencies of 6.1 and 6.3 kHz were used. The corresponding points on the SFL chart are shown in Fig. 4-1. The variation in position of the three points results from the wide ranging values of α associated with varying weather conditions as well as from the slightly different fundamental frequencies used. The measured operating parameters and the calculated range parameters are shown in the figures. All range parameters are calculated using the effective source parameters, as described in chapter III. The linear theory propagation curve for the fundamental is drawn from the first data point at or beyond R_o for each experiment. Measurements at propagation distances $r<R_o$ were not considered in the data reduction.

Several important differences between the results of the three high amplitude experiments must be noted. First, the siren output during experiment 1 was unstable because of line voltage fluctuations. Therefore, no theoretical predictions are calculated for this run. Second, the traveling microphone in experiments 1 and 2 was a B&K type 4136 (1/4 in.) with the protective grid in place. A B&K type 4138 (1/8 in.) microphone without a grid was used in experiment 3. The angle of incidence was 90° in all cases. Waveforms received at similar distances for experiments 1, 2, and 3 are shown in Fig. 6-9. Although the distances are not all the same, one would expect the propagating wave to have about the same waveform in each case. Yet the three waveforms appear quite different. Analyzing the harmonic components of the waveform from experiment 1 on the Hewlett-Packard digitizer, we found that the fifth and sixth harmonics (30.5 and 36.6 kHz, respectively) were approximately 3 dB above the

160 N/m^2 – div

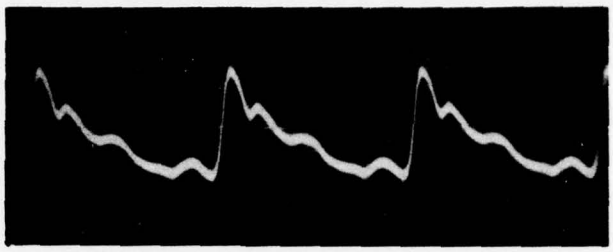

SIREN EXPERIMENT 1
DISTANCE = 4.6 m
1/4 in. MICROPHONE WITH GRID

150 N/m^2 – div

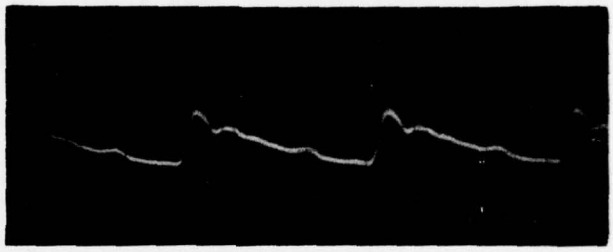

SIREN EXPERIMENT 2
DISTANCE = 9.1 m
1/4 in. MICROPHONE WITH GRID

510 N/m^2 – div

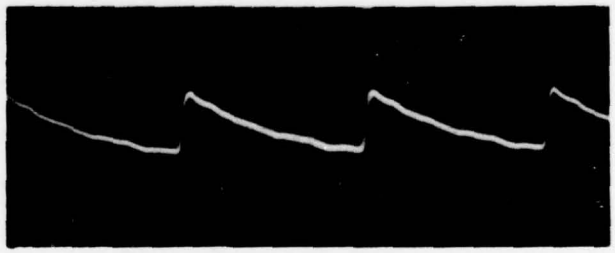

SIREN EXPERIMENT 3
DISTANCE = 3.0 m
1/8 in. MICROPHONE WITHOUT GRID

FIGURE 6-9
QUALITATIVE COMPARISON OF RECEIVED WAVEFORMS
FROM 3-SIREN EXPERIMENTS
ALL HORIZONTAL SCALES: 50 μsec/div

relative levels expected for a perfect sawtooth wave. The frequencies of these harmonics lie in a region in which there is a 3 dB response peak of the microphone (for 90° incidence with the protective grid in place). A few selected measurements were performed to show that the "enhancement" of the harmonics decreased when the protective grid was removed. But to ensure that the rise time of the shocks was not severely limited by the frequency response of the traveling microphone, we used the 1/8 in. model (without the protective grid) in experiment 3. It is clear that use of the 1/8 in. microphone gave much improved results. The "bumps" appearing in the output of the 1/4 in. microphone may probably be attributed to diffraction and reflection effects involving the slotted protective grid.

Third, a most curious result is provided by experiment 2. The second harmonic appears to have approached within 3 dB of the fundamental. For a perfect sawtooth wave, the second harmonic is 6 dB below the fundamental. We were perplexed by this discrepancy at the time the experiment was performed and sought to pinpoint the error source. The traveling microphone, a 1/4 in. model with grid, was replaced by a duplicate, but the same results were obtained. The meter readings were triple checked. Later, analysis of the oscillograms by the digitizer and calculator indicated that the difference in harmonic levels was actually close to 6 dB. We concluded that the unexpectedly close proximity of the second harmonic to the fundamental was caused by a malfunction in the heterodyne analyzer. Note, however, that the measured fundamental levels appear to be unaffected by the assumed malfunction. It is also noteworthy that the fundamental second harmonic separation in the other two experiments is close to 6 dB.

To obtain theoretical predictions to compare with data from experiment 3, we used the computer algorithm discussed in section B.1. of chapter III. The waveform measured at a distance of 0.38 m, where signal fluctuations caused by the dc air flow were small, was used as the input for the computer program. The freefield corrections for the traveling microphone are less than 0.5 dB out to a frequency of 70 kHz. The input wave was therefore not freefield corrected. The sizes for the distortion steps and the absorption correction steps in the computer program are constant. Because the propagation distance is nearly two orders of magnitude greater than the initial distance, a considerable amount of computer time was required for program execution. In computing the results for the first five range points, we used an absorption correction step size of 8 cm. The program was executed a second time with a step size of 61 cm to calculate predictions for the last three points. This change of step size apparently caused an offset in the computed results (see Fig. 6-8). The problem may be remedied in the future by allowing the step size to increase exponentially with propagation distance.

The computed curves and experimental propagation data for experiment 3 are compared in Fig. 6-8. (The data and predictions are also displayed in a different fashion in the third column of Fig. 6-10.) Agreement between theory and experiment appears to be quite good, although there is some indication that the agreement may deteriorate at large distances. The change in step size described in the previous paragraph is indicated by the break lines in the figure. The maximum deviations between computed and experimental results are as follows: fundamental, -1.6 dB (at 30 m); second harmonic, -1.4 dB (at 30 m); and third harmonic,

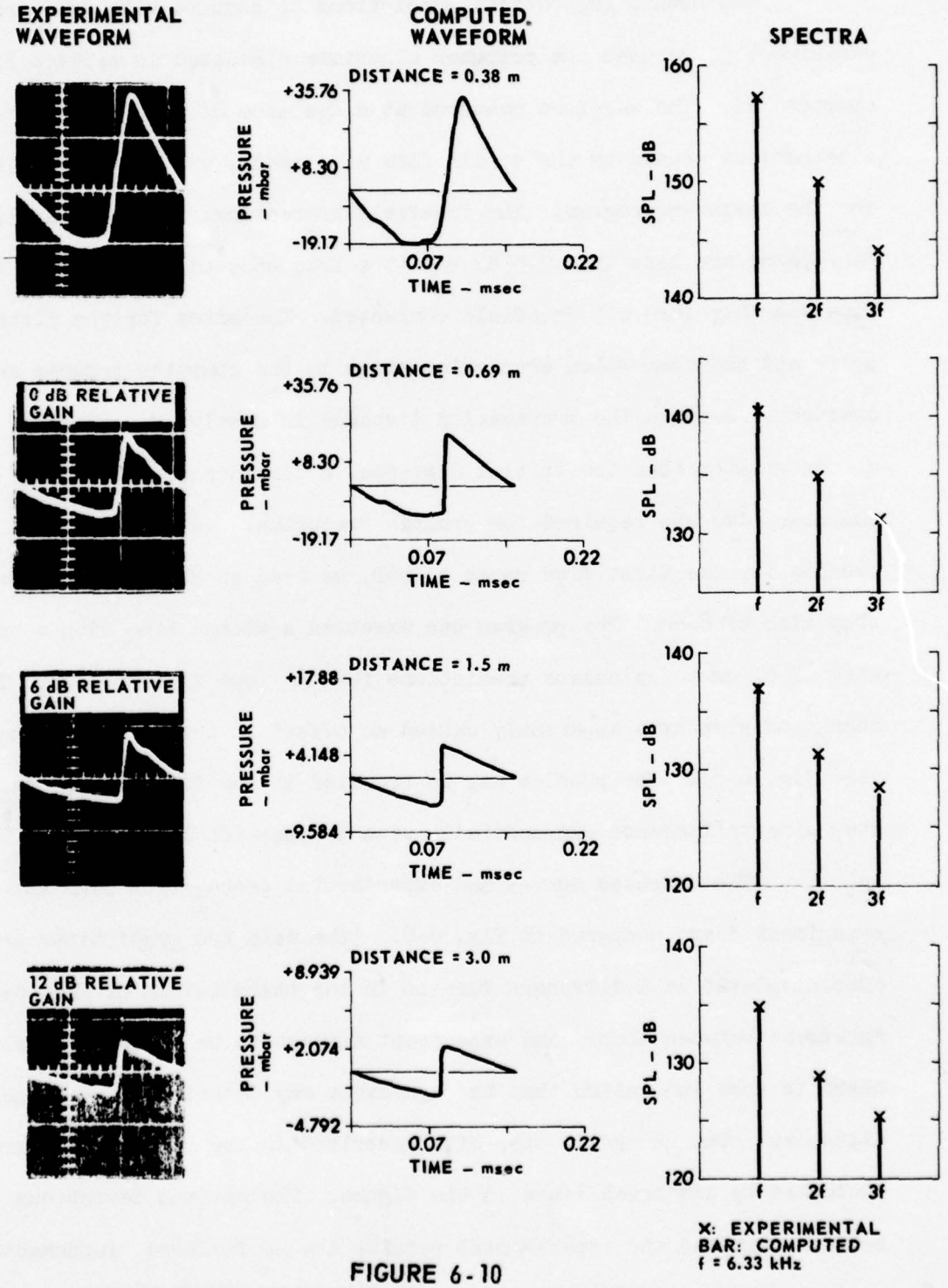

FIGURE 6-10
COMPARISON OF EXPERIMENTAL AND COMPUTED RESULTS
SIREN-FINITE AMPLITUDE PROPAGATION No. 3

ARL - UT
AS-76-1694a
MAT - DR
12 - 21 - 76

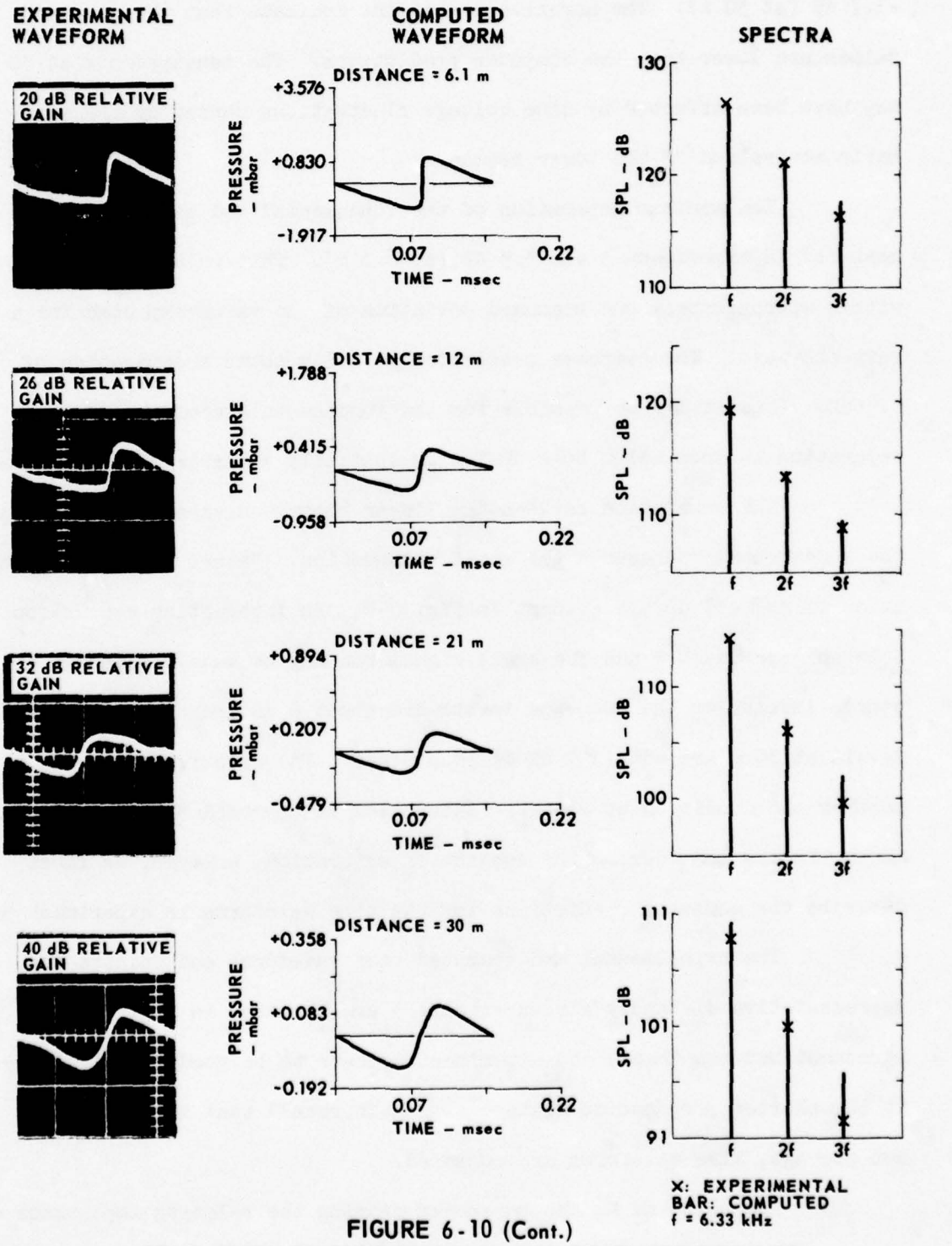

FIGURE 6-10 (Cont.)
COMPARISON OF EXPERIMENTAL AND COMPUTED RESULTS
SIREN-FINITE AMPLITUDE PROPAGATION No. 3

ARL - UT
AS-76-1694b
MAT - DR
12 - 21 - 76

-3.7 dB (at 30 m). The negative deviations indicate that the measured values are lower than the computer predictions. The measurements at 30 m may have been affected by line voltage fluctuations caused by the automatic activation of the tower beacon.

The minimum separation of the fundamental and second harmonic measured in experiment 3 was 5.5 dB (at 6.1 m). This value is again within approximately one standard deviation of the value expected for a sawtooth wave. The computer prediction at 6.1 m shows a separation of 5.4 dB. Thus it may be possible for the fundamental-second harmonic separation to drop below to 6 dB for an initially asymmetric strong wave.

The separation between the linear theory curve and the data for the fundamental represents the extra attenuation. Values of extra attenuation of up to 7 dB are evident in Fig. 6-8. An interesting comparison between experiment 3 and the small signal run may be made. Although the source levels for the two experiments are about 6 dB apart, the received levels at 30 m are within 1 dB of each other. The question arises as to whether the condition of acoustic saturation is approached in this experiment. Before considering the subject of saturation, however, we first describe the computer predictions for the time waveforms in experiment 3.

The experimental and computed time waveforms and spectra for representative distances for experiment 3 are compared in Fig. 6-10. Agreement between theory and experiment appears to be good, particularly at the shorter propagation distances. Again recall that instantaneous, not average, time waveforms are compared.

The value of N, the parameter gauging the relative importance of beam diffraction to nonlinear distortion, is estimated to be very small

for this experiment, namely N=0.023 at 15 m. Therefore, little, if any, beam diffraction effects are predicted. Although asymmetry is present in the waveforms, it is attributed to inherent characteristics of the siren source. Note, for example, the fact that the asymmetry is definitely greatest close to the source. Furthermore, in contrast to the asymmetry of the waveforms in the array No. 2 experiment, the asymmetry here decays rapidly and monotonically with distance.

We now take up the matter of acoustic saturation[2] as related to our siren experiment. The maximum amplitude attainable at a given distance, regardless of the acoustic power available at the source, is termed the saturation amplitude. While saturation theory for plane waves has met with considerable success, the theory for spherical waves has lagged behind. However, Laird (see, for example, Ref. 2) has found the saturation amplitude for diverging spherical waves in the sawtooth region. His result, adapted for the fundamental component of the acoustic pressure, is

$$p_{1(\text{saturation})} = \frac{2\rho_o c_o^2}{\beta k r} \ln\left(\frac{r}{r_o}\right) \quad . \tag{6-1}$$

As Shooter et al.[2] have pointed out, this formula is not expected to be accurate in the region beyond r_{max}. Shooter et al. proposed an improved formulation which takes small signal absorption into account for the range beyond r_{max}. However, because weak shock theory affords a reasonably accurate description of the received level of the fundamental for our experiments, even at distances beyond r_{max} (see below), we calculate the saturation level of the fundamental as a function of r on the basis of

Eq. 6-1. The value of r_o is determined by the extrapolation procedure outlined in section A of chapter III. The results are plotted in Figs. 6-11 and 6-12 for experiments 2 and 3, respectively. The measured data approach within 1 dB of the predicted saturation levels. By implication, therefore, an increase in acoustic output near the siren would hardly be noticed at distances exceeding, say, 5 m. The bounding of our experimental data by the saturation level is indeed an important result.

The measured level of the fundamental is compared to predictions based on linear theory, weak shock theory, and the Rudnick model in Figs. 6-11 and 6-12 for experiments 2 and 3, respectively. Both weak shock theory and the Rudnick model provide substantially better predictions than linear theory. The small effect of atmospheric absorption in these experiments may be seen by comparing the Rudnick model and weak shock theory curves. The difference in the predicted levels at a distance of 50 m is only about 2 dB. Although on theoretical grounds the Rudnick model would seem to be preferable, the data do not clearly indicate that it is. Additional experiments at longer propagation distances and/or higher frequencies are clearly needed. The effective source parameters used in making the calculations for Figs. 6-11 and 6-12 were extrapolated from waveforms at 0.55 and 0.69 m, respectively. These distances were the smallest at which sawtooth waves were indicated. The resulting values of ϵ_{eff}, the acoustic Mach number of a spherical sinusoidal source of radius $r_{o_{eff}}$, are very high. The values are in fact above the amplitude limit for the applicability of weak shock theory to plane waves.[7] But, because of spherical spreading and the small values of $r_{o_{eff}}$, the amplitude is quickly reduced to values within the region of applicability. It must be

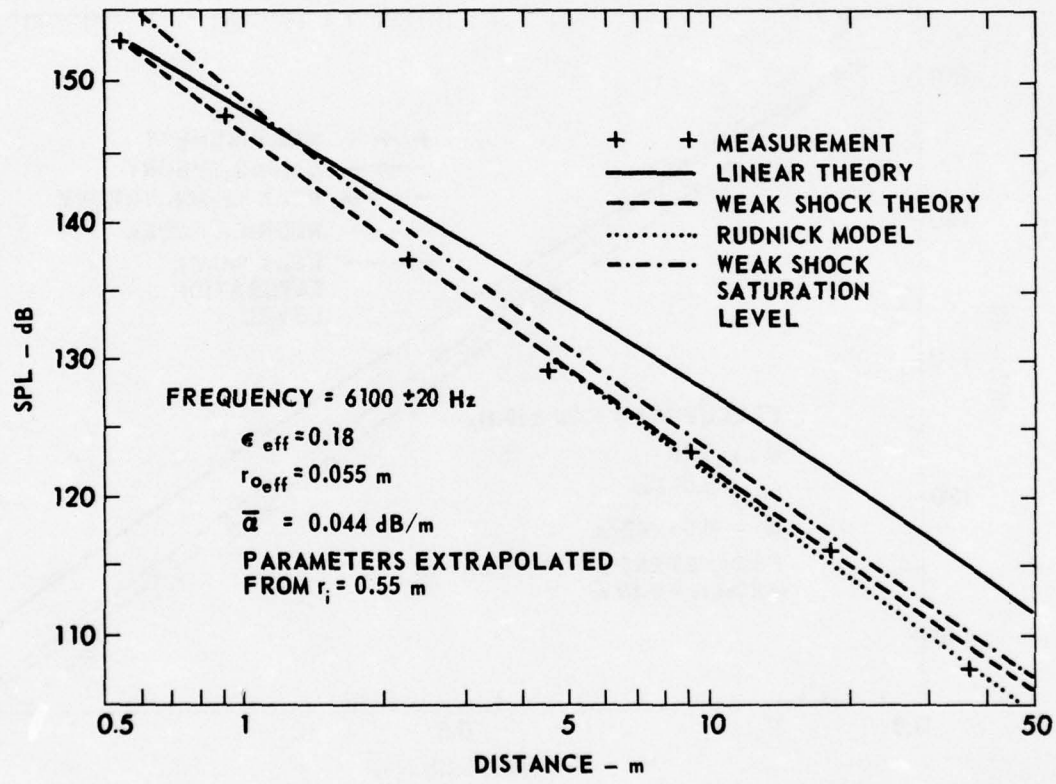

FIGURE 6-11
PROPAGATION CURVE FOR FUNDAMENTAL – SIREN EXPERIMENT No. 2

ARL - UT
AS-76-1553
MAT - DR
11 - 30 - 76

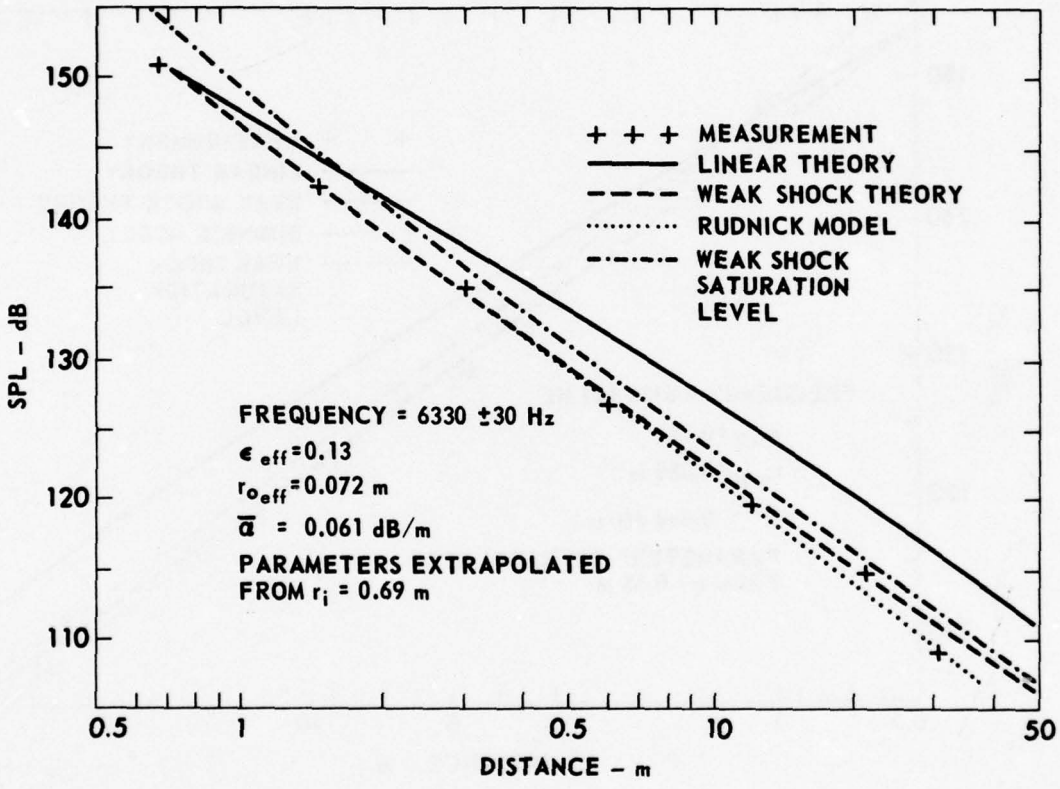

FIGURE 6-12
PROPAGATION CURVE FOR FUNDAMENTAL – SIREN EXPERIMENT No. 3

ARL - UT
AS-76-1554
MAT - DR
11 - 30 - 76

recognized that our extrapolation procedure was applied from a farfield point, where a convenient value of σ could be determined. There is some arbitrariness involved in the selection of the value of r_i. Because waves of very high amplitude quickly become sawtooth waves, however, much of the asymmetry in wave shape present near the siren is lost at larger distances. Therefore, basing the extrapolation on a farther rather than a nearer range point should be expected to improve the reliability of the parameters.

The measured extra attenuation is compared to that calculated by the Merklinger et al., Cary, and Rudnick models in Figs. 6-13 and 6-14 for experiments 2 and 3, respectively. The curves for the Cary model end at the limiting distance for the validity of the model. This limit is a distance analogous to r_{max}, occurring where

$$\left(\frac{r}{r_o}\right)\left(1 + \sigma_o \ln \frac{r}{r_o}\right) = \frac{(0.6)\beta\epsilon k}{\alpha} \quad .$$

The extra attenuation is assumed to reach a plateau value at the distance. The reader is reminded that the extra attenuation predictions plotted in Figs. 6-13 and 6-14 are referred to the level of the fundamental at the distance r_i from which the effective source parameters were extrapolated. The extra attenuation curve for the Rudnick model in Fig. 6-13 is an estimate only. The Rudnick model is applicable only in the sawtooth region ($r \geq 0.55$ m in experiment 2). The source parameters for use with the Rudnick model were therefore extrapolated from $r_i = 0.55$ m. Parameters for the other models were extrapolated from $r_i = 0.38$ m (just beyond the R_o). In order to maintain consistent sets of source parameters for all three

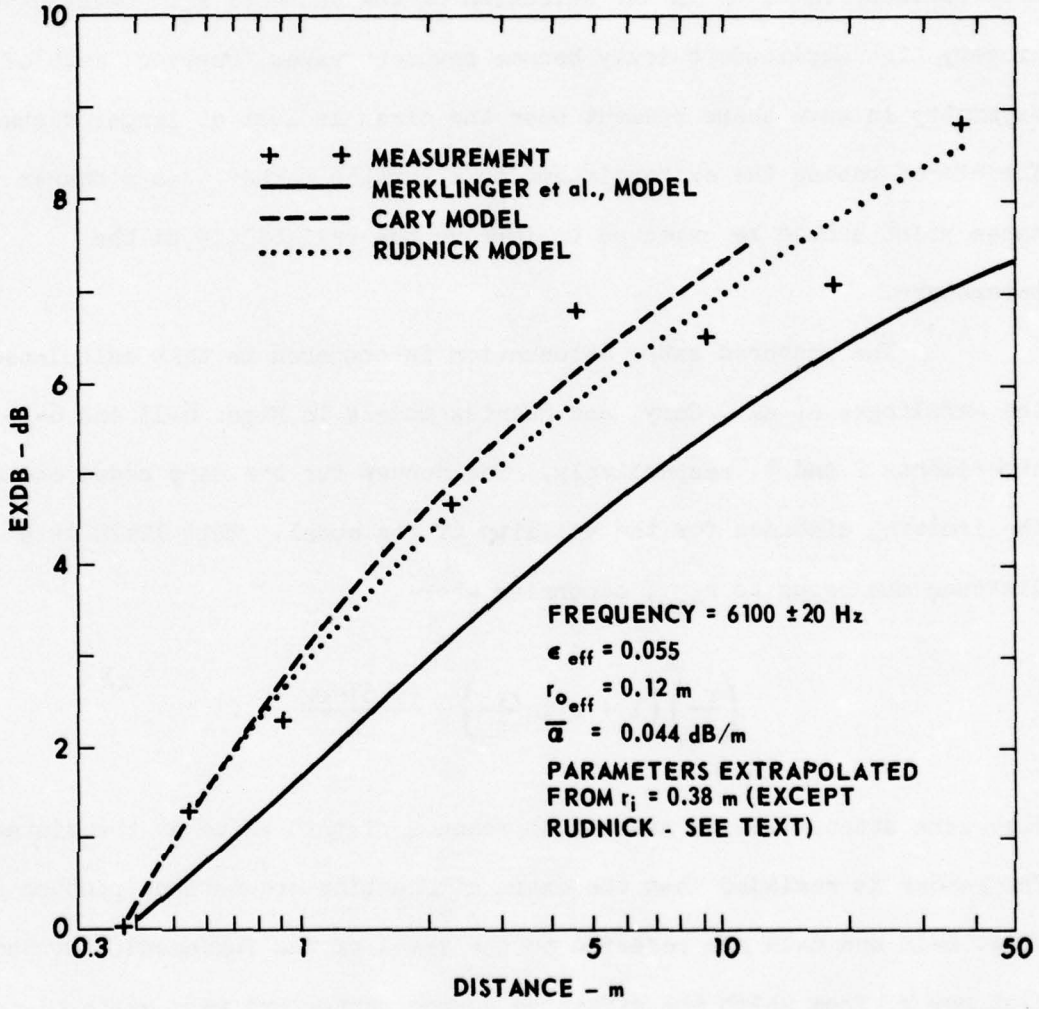

FIGURE 6-13
EXTRA ATTENUATION OF FUNDAMENTAL
SIREN EXPERIMENT No. 2

ARL - UT
AS-76-1563
MAT - DR
12 - 2 - 76

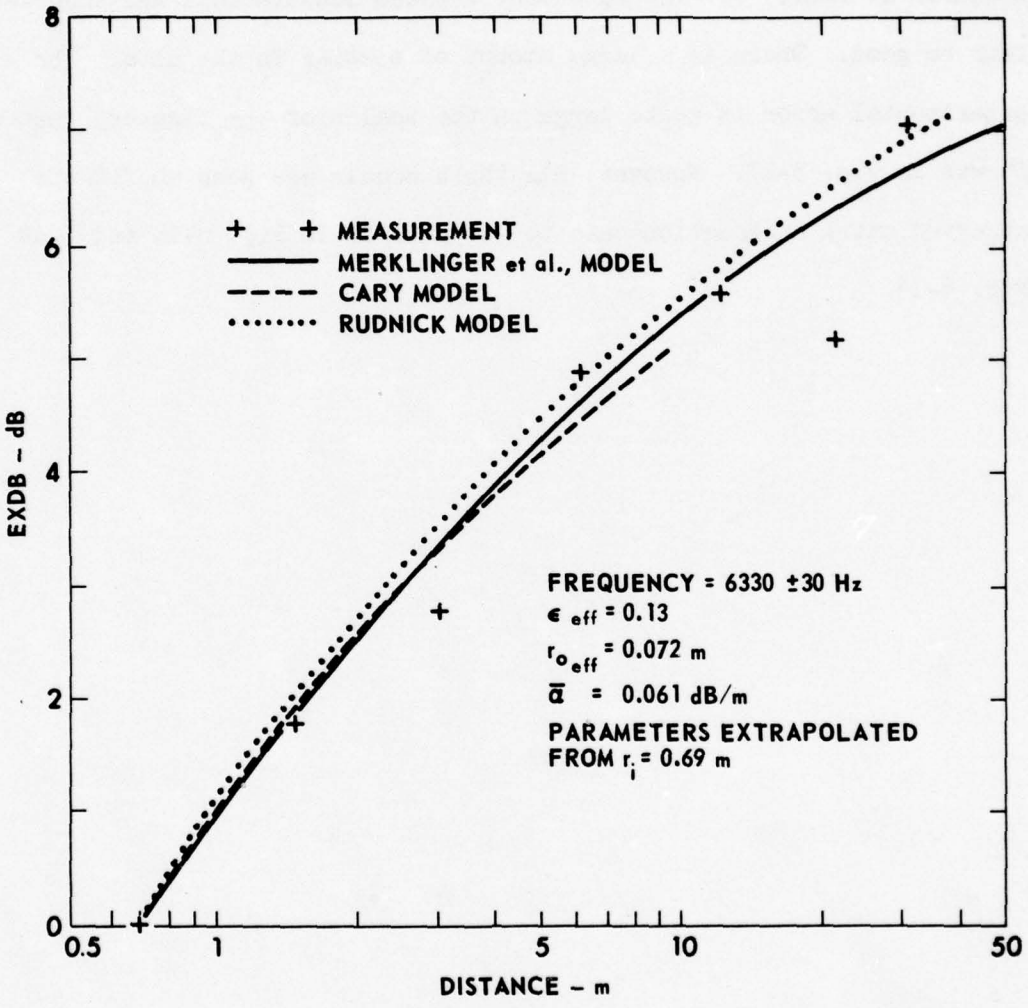

FIGURE 6-14
EXTRA ATTENUATION OF FUNDAMENTAL
SIREN EXPERIMENT No. 3

ARL - UT
AS-76-1564
MAT - DR
12 - 2 - 76

models and yet reference the results to the level at the range r=0.38 m, the EXDB predicted by use of the Rudnick model was added to the EXDB measured at r=0.55 m. The agreement between measurements and theories is fair to good. There is a large amount of scatter in the data. The experimental error is quite large on the scales of the figures, just as it was in Fig. 5-17. However, all three models are seen to fit the observed extra attenuation data to within 2 dB in Fig. 6-13 and 1 dB in Fig. 6-14.

CHAPTER VII

CONCLUSIONS

A summary of the results of our experiments is given in this chapter. Several further studies are planned for the future, and the direction of these studies is indicated.

We have carried out a series of experiments on the propagation of finite amplitude sound outdoors. The main purpose of the experiments was to determine the extent to which the outdoor environment, mainly the random inhomogeneity of the medium, affects finite amplitude propagation. Secondary purposes were to record and, if possible, explain any new nonlinear phenomena. The source frequency was generally in the range 6 to 8 kHz, and the source level SPL_{1m} varied from 140 dB to 149 dB. Two different sources were used: an array of either seven or ten horns and a siren. In terms of nonlinear effects, weak to moderate waves were generated by the arrays; strong waves were generated by the siren. The propagation path was vertical and parallel to an 85 m tower, whose elevator carried the traveling microphone. Maximum propagation distances used varied from 30 m to 76 m. Meterological conditions were as follows: temperature range 24 to 35°C, relative humidity range 38 to 40%, and wind speed (at ground level) 0 to 24 km/h. The measurements were made both during the day and at night and were mainly done during the months of August through October 1976.

Several theoretical approaches were used to explain the data. A graphical method, the SFL chart, was used to gauge the magnitude of the nonlinear behavior expected. The SFL chart proved to be a quite reliable

guide in predicting the gross importance of nonlinearity. Pestorius's computer model[6] for the propagation of finite amplitude plane waves was modified to include the effects of spherical spreading and atmospheric absorption. This algorithm enabled predictions of both time waveforms and spectra to be made over the propagation path. The ad hoc propagation models of Merklinger et al.,[17] Rudnick-Webster,[11] and Cary[13] were used where applicable. Predictions based on ordinary weak shock theory were checked against the siren data. A perturbation solution of Burgers' equation was compared with data for a horn array.

It was found that nonlinear propagation effects were modified by inhomogeneity of the medium in the following way. The atmospheric inhomogeneities did cause significant fluctuations in the instantaneous acoustic signal. These fluctuations were most apparent at large propagation distances. The waveforms varied both in amplitude and wave shape. However, with sufficient time averaging when the spectral measurements were made, the frequency domain data (i.e., the levels of the first three harmonic components) largely confirmed predictions based on theory for homogeneous media. There was a slight indication that these predictions may be less reliable at the longer propagation distances. Thus additional experiments need to be performed at larger distances.

The siren-generated sound waves were very intense and were greatly affected by nonlinearity. Intense sawtooth waves were produced very near the source. The propagation data for the fundamental came within 1 dB of the predicted saturation level (the prediction was based on weak shock throry). Extra attenuation up to about 8 dB was measured. Values of the extra attenuation (EXDB) predicted by use of the Rudnick,

Merklinger et al., and Cary models agreed with the measured values to within 2 dB. The Rudnick model and weak shock theory predictions of the level of the fundamental were within 1 and 2 dB, respectively, of the data for maximum propagation distances of 36 m. The computer algorithm predictions of the fundamental component were within 2 dB over the same distances.

The beam pattern for the siren, measured at finite amplitudes at a distance of 15 m, appeared to have the blunted major lobe characteristic of high amplitude sources. The siren's acoustic power output at the fundamental frequency was estimated to be 410 W. A small signal beam pattern for the siren should be measured as a check on these last two conclusions.

The results of the array experiments were less clear cut. The measured beamwidths of the arrays were from 6 to 8°. Nonlinear propagation distortion was produced. The maximum value of EXDB measured was approximately 1.5 dB, or approximately 1 dB less than the value predicted using the computer and Merklinger et al. models.

The received waveforms for the experiment in which array No. 2 was the source were initially asymmetric. The asymmetry first grew with propagation distance and then decreased at larger distances. This behavior is qualitatively compatible with the speculation that narrowbeam-type diffraction was important in the experiment. The computer algorithm, which did not contain the effects of diffraction, predicted a monotonic decrease of the asymmetry.

The results of an experiment described in Appendix B show the interaction of diffraction and nonlinear propagation distortion for the

radiation of intense sound from a circular horn. Both experimental results and theoretical predictions indicate that, for the conditions of the experiment, the diffraction and distortion stages of the propagation may be treated separately. Additional studies on this subject are needed to explore the cases where the two effects may not be handled separately.

Our project was planned as the prototype experiment for future studies on finite amplitude noise. The extension of this work is clear. Many aspects of the propagation of finite amplitude noise are experimentally and theoretically unexplored. One subject of significant practical interest is the change in spectral content of noise with propagation distance. This change gives rise to extra attenuation in some spectral bands but to apparent amplification in others. Another subject of interest is the effect of ground reflection on propagation of finite-amplitude noise. Finally, it would be of interest to carry out a basic study of the local effects of nonlinearity in the intense sound field near the siren and to make experiments on the focusing of intense sound waves in air.

APPENDIX A

AN ANECHOIC CHAMBER FOR USE AT HIGH AUDIO FREQUENCIES

A. Introduction

Careful freefield measurements of the performance of the horn drivers required the construction of an anechoic chamber. The requirement that the chamber be anechoic only for high frequencies, say, frequencies above approximately 1 kHz, considerably simplified the acoustical treatment needed. The chamber was to be constructed at absolute minimum cost, if possible utilizing Navy shipboard sound insulation materials available as government surplus. While many construction details were forced upon us by budget limitations, the results may be of possible use to others. We found the literature on anechoic chambers to be surprisingly limited.

A room on the second floor of Building 1A at Balcones Research Center, The University of Texas at Austin, was available for conversion to an anechoic chamber. The inside dimensions were 3.0 m (height) by 5.5 m (width) by 7.6 m (length). The walls were of glazed brick and the ceiling was made of prestressed concrete U-channels. (The inverted U shape gave the appearance of a beamed ceiling.) The floor was poured concrete and sloped at a 4% grade. Thus the height was actually 3.0 m at the door and 3.3 m at the end wall.

We first sought an estimate of the sound absorbing capabilities of the materials available to us. Although financial considerations ultimately forced the use of the shipboard insulation, some additional justification for our selection was desired. To explain the tests performed, we first define some terms commonly encountered in room acoustics.[67]

Sabine absorption coefficient α_{Sab}. This coefficient is the ratio of the sound energy absorbed by a material to the incident sound energy. For a given material, the ratio is a function of frequency and the angle of incidence. The coefficient is usually measured by comparing the reverberation times for a reverberation chamber with and without samples of the absorbing material present.

Reverberation time T. The reverberation time is the time required for a sound to decay by 60 dB. This time is a function of α_{Sab} and therefore is also a function of frequency. For a room that is not so large that atmospheric absorption becomes important, T is given in seconds by

$$T = \frac{(0.161)V}{S\,\overline{\alpha_{Sab}}} \quad , \tag{A-1}$$

where V is the room volume, S is the room's surface area, and $\overline{\alpha_{Sab}}$ is the average value of α_{Sab} for the room surfaces. All variables in Eq. A-1 are to be expressed in metric units.

Statistical (energy) sound absorption coefficient α_s. This coefficient is the ratio of absorbed-to-incident sound energy for a perfectly diffuse incident sound field. Morse and Ingard[68] state that the maximum value of α_s theoretically possible for a flat surface is about 0.96. By contrast, the value of α_s for a wedge-covered anechoic chamber wall may equal 0.996. The cutoff frequency of an anechoic chamber is defined as the frequency at which α_s drops to 0.99 (i.e., a sound reduction of 20 dB for one reflection).[69] Values of α_{Sab} obtained by reverberation room measurements usually exceed the true value of α_s; sometimes the

excess is 20 to 50%. For highly absorbing surfaces, measured values of α_{Sab} may exceed 1 (impossible by conservation of energy) by 20 to 30%. The excesses are attributed to diffraction around the sample and difficulties in producing a truly diffuse field.

Reverberation measurements were made in a similar room using a "slap board" (an enlarged version of the "horse whip" device used in orchestras) as a sound source, a B&K 1/2 in. condenser microphone, and the Hewlett-Packard 3580A analyzer (see chapter V) functioning as a narrowband graphic level recorder. The reverberation time in a 100 Hz bandwidth was recorded for the empty room for various frequencies. Several types of absorptive materials were sequentially added to the chamber and the reverberation measurements were repeated. The absorptive materials included Owens Corning types R-11 and R-19 industrial fiberglass insulation, Owens Corning type No. 703 acoustic insulation, and the shipboard fiberglass. The latter consisted of a 5 cm thick fiberglass mat with a perforated plastic masking on one side. The mats were 61 x 91 cm in size. The results of the reverberation measurements overestimated $\overline{\alpha_{Sab}}$ by as much as 500%. That is, $\overline{\alpha_{Sab}}$ values approaching 5 were obtained at certain frequencies. We made no attempt to diffuse the sound field, as is done in actual reverberation rooms. The presence of room modes plus the diffraction grating effect of the beamed ceiling may have caused the poor results.

Reflection coefficient measurements (normal incidence) were made in the progressive wave tube described in chapter V. The equipment used was that shown in Fig. 5-1, with the exception that the anechoic wedge termination was replaced by a sample of the test material backed by a

solid aluminum plug. The results for two layers (10 cm) of shipboard fiberglass, which was the thickness eventually used for the chamber, were as follows:

TABLE A-1

REFLECTION TESTS FOR TWO LAYERS OF SHIPBOARD FIBERGLASS
(PLASTIC MASKING TOWARD WALL)

Frequency (Hz)	200	400	800	1k	2k	3k	5k
Pressure Reflection Coefficient	0.63	0.33	0.19	0.23	0.17	0.05	0.1
Normal Incidence (Energy) Absorption Coefficient	0.60	0.89	0.96	0.95	0.97	1.0	0.99

Impedance tube measurements were not performed, although they might have improved our estimates greatly. In any case, for the frequency range of interest, we rated the shipboard fiberglass as the best absorber among the materials considered.

B. Construction

A small section at the front of the room (3.0 m (height) by 5.5 m (width) by 12.0 m (length)) was converted to an alcove to contain the required electronic equipment and personnel. Two separate walls of 1/2 in. gypsum board nailed to (separate) 2 in. x 4 in. studs were installed between the anechoic chamber proper and the equipment room. The space between the walls was filled with fiberglass. The partition provided sufficient acoustic isolation for the personnel at high frequencies,

although no detailed sound transmission data were taken. Entry to the chamber from the equipment alcove was through two solid wooden doors, one for each wall. The doors had weather-stripped seals. Electrical connections to equipment used in the chamber were made via an offset "feed-through panel."

The fiberglass panels were attached to the walls and ceiling by using Tactoo self-adhering insulation hangers made by AGM Industries. These hangers were essentially nails, 11 cm long, with self-adhesive base plates. The insulation was impaled on the nails. Small friction-fit retainers held the insulation tightly in place. Use of the hangers simplified construction greatly. Several alternative mounting methods were considered, but all would have required more installation time.

The poured concrete floor was treated as follows. Floor drains were plugged and caulked to prevent sound transmission to other parts of the building. Water condensing on the floor would eventually have soaked any fiberglass in direct contact; therefore heavy plastic sheeting was put down, followed by a layer of soft rubber, 2 to 5 cm thick. The rubber, which was also government surplus material, would serve to mechanically isolate vibrating sources from the building. Finally, two layers of the fiberglass panels were simply laid on the rubber. The panels were arranged to leave open a 0.6 m wide walkway along the room diagonal. The walkway was covered while experiments were under way by a roll of Owens Corning R-19 fiberglass.

An overhead monorail support for microphones was suspended from the ceiling along the room diagonal. The total unobstructed path length

was 9.1 m. A window-type air conditioner helped maintain a constant comfortable temperature and humidity.

C. Performance Test

The traditional performance test for anechoic chambers is the inverse square law test. The following test was performed using a bare horn driver (no horn), which acted as an approximately hemispherical source, except at the highest frequencies used. The propagation path was the room diagonal, and the source was placed approximately 1.5 m above the floor. The microphone was carried by the monorail system. The measurements were accurate to ±0.5 dB. The propagation data are plotted in Fig. A and compared against the theoretical predictions for spherical spreading. Air absorption was negligible over such short distances and was not included in the calculations. We note that deviations from spherical spreading were within ±3.0 dB for propagation distances out to 5 m for frequencies between 250 Hz and 16 kHz. At the final propagation (6.4 m), the microphone was pushed against the chamber corner. The effect of reflections near the corner are evident in the data. The results are a considerable improvement over those reported by Bedell (see, for example, Ref. C) who also used flat absorbers rather than wedges, which are more effective but are also more expensive. Bedell noted deviations of ±3 dB out to 1.5 m and ±5 dB out to 3 m for the frequency range 300 Hz to 5 kHz. Our check was performed under steady state conditions.

Hedegaard[70] suggests a method by which anechoic chamber performance may be improved. Standing waves in a chamber may be reduced to negligible amplitudes by driving the device under test with a warble-tone

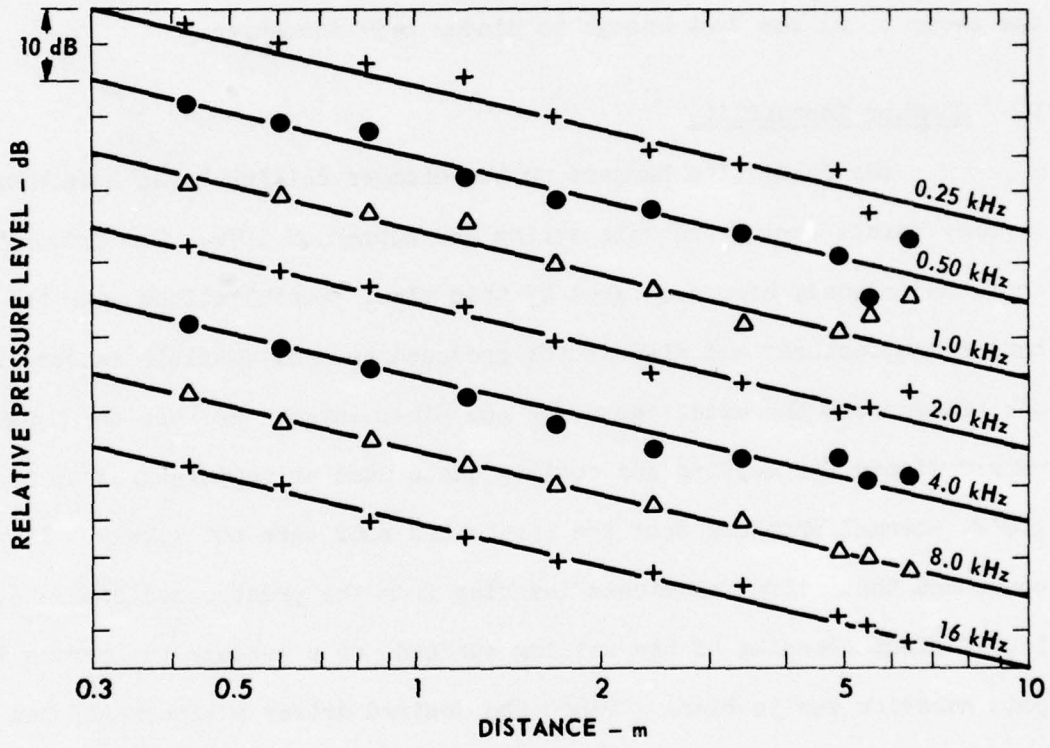

FIGURE A
INVERSE SQUARE LAW MEASUREMENTS

ARL - UT
AS-76-1335
MAT - DR
11 - 19 - 76

and analyzing the signal with a slave filter. The changing frequency components are variably phase shifted on reflection at the wall and therefore cancel and compensate each other. In other words, a steady state condition is never attained. The swept frequency response tests of the drivers in the chamber were influenced by this effect, if we assume the sweep speed was fast enough to hinder mode formation.

D. Chamber Instability

The insulation hangers on the chamber ceiling began loosening at many points during the late spring and summer of 1976. The driver tests had already been completed by this time. Consultations with the hanger manufacturer and distributor produced several possible reasons for the problem but the exact cause was not pin-pointed. Because the hangers were designed for heating and cooling ducts used at temperatures up to 180°F, thermal problems from the sun-heated roof were not likely. It was concluded that either chemicals leaching from the prestressed concrete, insufficient cleaning of the ceiling surface, or a surface too porous for good adhesion was to blame. Since the desired driver measurements had already been made by this time, no serious hindrance to the progress of the outdoor experiments was caused. At any rate, we took consolation in some words expressed by Alfred H. Sommer:[71] "The best equipment is one that falls apart after the last experiment; any effort to make it more durable is a waste of time and effort."

APPENDIX B

RADIATION OF HIGH INTENSITY SOUND WAVES FROM A HORN

In this appendix we discuss the effects of diffraction and nonlinear propagation distortion on the radiation of high intensity sound from a circular horn. Our interest in the subject was triggered by two stimuli. First, while investigating the performance of various horn driver and horn combinations, we were surprised to observe high amplitude waveforms that did not seem to distort according to nonlinear theory predictions. Second, Ostrovsky and Sutin have recently published a series of papers dealing with the effects of diffraction on nonlinear propagation.[72,73,74] We briefly cite the conclusions of linear theory for diffraction by a circular horn, describe the results of a diffraction experiment performed at high sound levels, and finally note the predictions which follow for the experiment from the theory of Ostrovsky and Sutin.

It was stated earlier in this thesis that a common model for radiation from a horn is the assumption that a "slug" of air oscillates uniformly at the horn mouth. This model is equivalent to the model of a vibrating circular piston mounted in a plane infinite baffle, probably because the back wave is suppressed in both cases. The circular piston model is in turn mathematically equivalent to the diffraction of a plane wave by a circular aperture in a plane screen. The solution for the diffraction of a plane wave may be described by a Green's function formulation as (see, for example, Ref. 9)

$$p = \frac{\rho_o}{2\pi} \int \frac{\dot{u}(t-r'/c_o)}{r'} \, dS \quad , \qquad \text{(B-1)}$$

where p is the acoustic pressure, u is the piston velocity or the particle velocity wave incident upon the aperture, t is time, the dot indicates a time derivative, and the integral is over the aperture area. Here r' is the distance from an infinitesimal area segment in the aperture to the axial field point. The exact solution for the pressure at the axial position x is

$$p = \rho_o c_o \left[u\left(t - \frac{x}{c_o}\right) - u\left(t - \frac{r}{c_o}\right)\right] \quad , \qquad \text{(B-2)}$$

where $r = \sqrt{x^2+a^2}$ and a is the aperture radius. A result of Eq. B-2 is that the axial pressure signal in the farfield (Fraunhofer zone) is the time derivative of the source wave.[75] The point at which farfield behavior begins is known as the Rayleigh distance $R_o [= A_m/\lambda$, where A_m is the piston or aperture area and λ is the wavelength].

A more realistic description of horn radiation may be based on the Helmholtz-Kirchhoff diffraction theory for spherical waves. The waves radiated by a horn actually have a finite curvature. Thus an incident spherical wave is diffracted by a plane circular aperture, as shown in Fig. B-1. Here r_o is the radius of curvature of the waveform, Q is the observation point, I is the wavefront just filling the aperture, and r_1 and r_2 are the distances shown. The Kirchhoff diffraction integral (see, for example, Ref. 14) may be evaluated for this situation to yield

$$p(Q,t) = \frac{r_o}{r_o + r_1} \left\{ p\left(I, t - \frac{r_1}{c_o}\right) - \frac{1 + \cos \Phi}{2} \, p\left(I, t - \frac{r_2}{c_o}\right) \right\} \quad . \qquad \text{(B-3)}$$

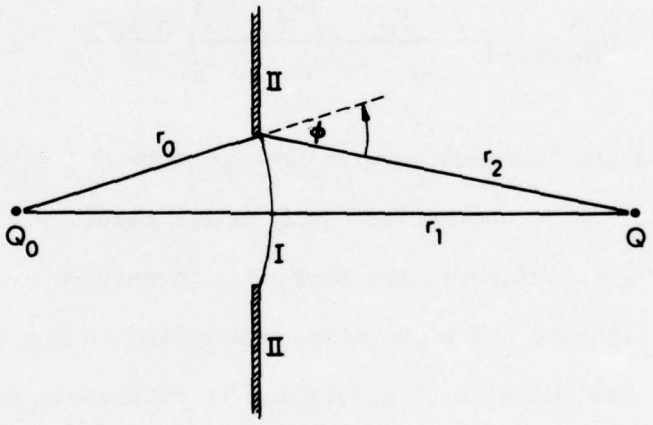

FIGURE B-1
DIFFRACTION OF SPHERICAL WAVE
BY AN APERTURE

The solution is interpreted as follows: The farfield pressure signal is the sum of a direct wave traveling along the axis and a phase inverted diffracted wave from the aperture rim. The diffracted wave is scaled by the obliquity factor $(1+\cos\varphi)/2$. This result is only an apparent one formed by the addition of waves from all points in the aperture. In the farfield the obliquity factor is approximately equal to one. The farfield axial pressure then reduces to

$$p_{farfield} \doteq \frac{r_o}{r_o + r_1}\left(\frac{r_2 - r_1}{c_o}\right)\frac{\partial\, p(\tau)}{\partial\tau} \quad , \qquad \text{(B-4)}$$

where $p(\tau)$ is the incident wave in the aperture and $\tau=t-(r_1/c_o)$ is the retarded time. Thus the earlier qualitative result for piston radiation, the wave differentiation in the farfield, is carried over. We have ignored nonlinearity and atmospheric absorption in the preceding discussion. The omission of absorption is reasonable for audio frequencies over the short distances considered here. The role of nonlinearity is discussed presently.

The experimental arrangement for the measurement of the waveforms on the axis of a circular horn is shown in Fig. B-2. (The photograph was taken in the anechoic chamber at Cockrell Hall, The University of Texas at Austin; the particular set of measurements described here were actually made outdoors). The horn was the unit described in chapter V. The sound source was a JBL 2470 horn driver (2.5 cm throat diameter). A flared connector joined the horn and driver. The waveforms received are shown in Fig. B-3. The SPL on axis at the horn mouth was 132 dB. The waves within the horn were sufficiently

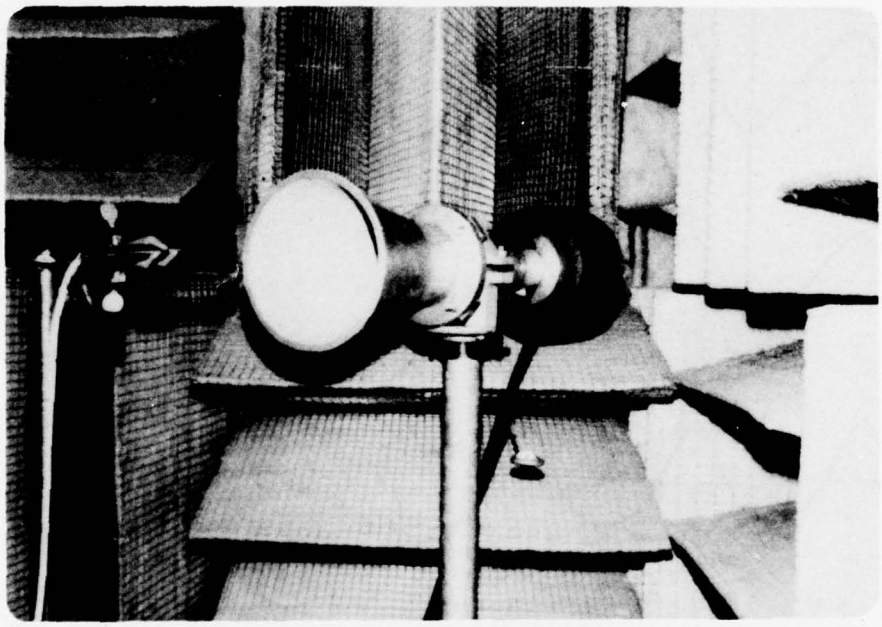

FIGURE B-2
APPARATUS TO MEASURE ACOUSTIC SIGNAL
ON THE AXIS OF A HORN

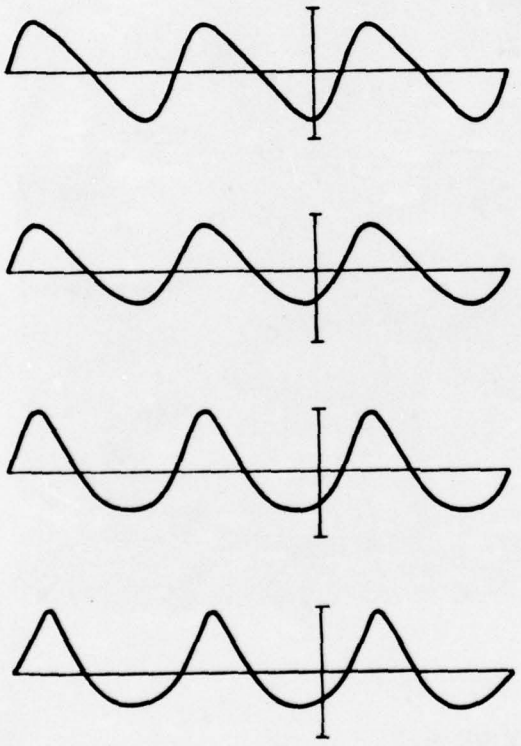

DISTANCE (m)	OSCILLOSCOPE GAIN (dB)
0	0
0.30	0
0.61	6.0
3.05	19.3

FIGURE B-3
OSCILLOGRAMS OF RECEIVED ACOUSTIC SIGNAL
versus AXIAL DISTANCE FOR f = 7.36 kHz

Previously reported by Theobald, Webster,
and Blackstock (1976). Ref. 48

intense to have suffered substantial nonlinear distortion by the time they reached the horn mouth. Further distortion would have tended to sharpen the waveforms into a sawtooth shape. Instead, the propagating waves exhibited an asymmetrical shape. The waveform at a distance of 3 m strongly resembled the time derivative of the mouth waveform (distance=0). Unfortunately, the mouth waveform also contained a contribution from the diffracted wave such that the source wave could not, in general, be observed directly.

Because the boundary conditions for the Kirchhoff solution (Eq. B-3) are not exact, i.e., the solution cannot reproduce the assumed conditions in the aperture plane, then the solution can only be approximately correct near the aperture. We may get an indication of the expected behavior in the aperture for large source wave curvatures, r_o, by examining the plane wave solution (Eq. B-2). The exact plane wave solution on-axis in the aperture is

$$p(t)_{\text{aperture}} = p(t) - p\left(t - \frac{a}{c_o}\right) \quad . \tag{B-5}$$

We note that the horn radius for our experiment was 7.8 cm and the time delay corresponding to a/c_o was very nearly (3/2) T, where T is the period. By periodicity, we expect that the pressure amplitude on-axis at the mouth was twice the amplitude of the incident wave. The wave shape is expected to remain unchanged. We assume that the source wave calculated here may be used for the spherical diffraction problem.

As a rough quantitative check on the applicability of the above analysis, we calculated the peak-to-peak amplitude of the source wave

based on the experimental farfield signal. This particular course was followed because it is much simpler to numerically integrate than to differentiate. The relation employed is

$$p_{aperture} = \frac{r_o + r_1}{r_o} \quad \frac{c_o}{r_2 - r_1} \int_o^T p_{farfield}\, dt \qquad \text{(B-6)}$$

The farfield signal at a distance of 3.0 m was integrated and scaled as in Eq. B-6 to predict a mouth waveform of a peak-to-peak pressure amplitude 170 N/m^2. The pressure amplitude measured at the horn mouth was 240 N/m^2 (p-p). We have shown that the actual incident wave should have an amplitude of about half that of the wave at the mouth, or 120 N/m^2(p-p). The agreement is within 3 dB. While the error is fairly large, it is not too surprising, considering the variablility in the horn mouth pressure distribution noted in chapter V, and that the microphone was aligned with the horn by eye and the measurements were made outdoors. Nonlinearity should not have played a large role following diffraction because the amplitude was sharply reduced from an originally marginal level by spherical spreading.

We now briefly discuss a few points from Ostrovsky's work on diffraction problems in nonlinear acoustics. A geometry shown below is assumed.

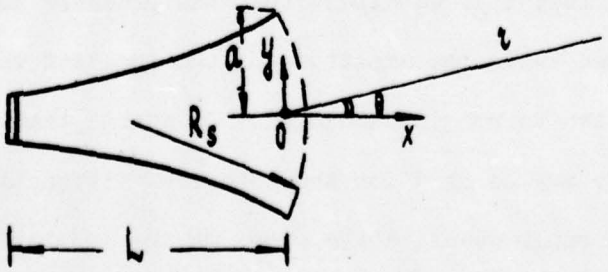

FIGURE B-4 DIFFRACTION FROM A HORN (after Ostrovsky and Sutin[73])

Consider a horn radiating finite amplitude sound generated by a vibrating piston in the horn throat. The source wave has the curvature R_s. The distortion variable, expressed in stretched coordinates, for propagation through the horn to the mouth is (see, for example, Ref. 4)

$$\sigma = \beta\epsilon k \int_{-L}^{o} \sqrt{\frac{A_o}{A(x)}}\, dx \quad , \tag{B-7}$$

where A_o is the throat area $A(x)$ is the cross sectional area at the position x, and quasiplane wave propagation through the horn is assumed. Ostrovsky and Sutin base their analysis on the hypothesis that, for certain geometries, frequencies, and source levels, the diffraction and nonlinear distortion stages may be separated. The stated condition for separability is

$$\beta\epsilon \ll \left[\frac{\lambda(1-\sigma)}{a}\right]^2 \quad , \tag{B-8}$$

where σ is defined in Eq. B-7 and ϵ is measured at the horn throat. (Shock formation is precluded here. For cases involving the diffraction of shock waves, see Ref. 74.) We offer a physical reason in support of the idea of separability. The only nonlinear effect considered here, namely, propagation distortion, is an effect cumulative with distance. Diffraction, on the other hand, is a localized phenomena. If the wave is not too strong, the propagation distortion in the Fresnel zone will be negligible and the diffraction and distortion may be considered separately. Van Buren and Breazeale[76] have utilized a parallel hypothesis

in describing the reflection of short finite amplitude sound pulses from rigid boundaries.

The values of the parameters for the measured waveforms shown in Fig. B-3 relevant to the theory of Ostrovsky and Sutin were as follows: $\beta\epsilon \doteq 2.8\times10^{3}$, $\sigma \doteq 0.5$ (calculated value), $R_s = 23$ cm, and $R_o = 41$ cm. Under these conditions, the diffraction and nonlinear distortion stages are predicted to be separable. The solution given by Ostrovsky and Sutin reduces to Eq. B-3, where the obliquity factor is equal to one. A second solution applicable for observation points off the horn axis is also given. We have not experimentally investigated this case for lack of time.

REFERENCES

1. D. F. Pernet and R. C. Payne, "Non-linear propagation of signals in air," J. Sound Vib. 17, 383-396 (1971).

2. J. A. Shooter, T. G. Muir, and D. T. Blackstock, "Acoustic saturation of spherical waves in water," J. Acoust. Soc. Am. 55, 55-62 (1974).

3. C. G. Little, "Acoustic sounding of the lower atmosphere," Meteorological Monographs 11, 397-404 (1970).

4. D. T. Blackstock, "Nonlinear Acoustics (Theoretical)," in Amer. Inst. Phys. Handbook, D. E. Gray, ed. (McGraw-Hill Book Co., Inc., New York, 1972), 3rd ed., pp. 3-183/ - /3-205.

5. D. T. Blackstock, "Propagation of plane sound waves of finite amplitude in nondissipative fluids," J. Acoust. Soc. Am. 34, 9-30 (1962).

6. F. M. Pestorius, "Propagation of Plane Acoustic Noise of Finite Amplitude," Applied Research Laboratories Technical Report No. 73-23 (ARL-TR-73-23), Applied Research Laboratories, The University of Texas at Austin (1973). (AD 778 868)

7. F. M. Pestorius and S. B. Williams, "Upper limit on the use of weak-shock theory," J. Acoust. Soc. Am. 55, 1334-1335 (L) (1974).

8. D. T. Blackstock, "Connection between the Fay and Fubini solutions for plane sound waves of finite amplitude," J. Acoust. Soc. Am. 39, 1019-1026 (1966).

9. J. C. Lockwood, "Two Problems in High-Intensity Sound," Applied Research Laboratories Technical Report No. 71-26 (ARL-TR-71-26) Applied Research Laboratories, The University of Texas at Austin (1971).

10. D. T. Blackstock and J. G. Willette, "The Effect of Nonlinear Propagation Distortion on High-Power Low Frequency Sonars" (U), Applied Research Laboratories Technical Report No. 71-11 (ARL-TR-71-11), Applied Research Laboratories, The University of Texas at Austin (March, 1971). (CONFIDENTIAL)

11. D. A. Webster, "Saturation of Plane Acoustic Waves and Notes on the Propagation of Finite Amplitude Spherical Waves," Master's Thesis, The University of Texas at Austin (1976), Applied Research Laboratories Technical Report No. 77-4 (ARL-TR-77-4), Applied Research Laboratories, The University of Texas at Austin (1977).

12. K. A. Naugol'nykh, S. I. Soluyan, and R. V. Khokhlov, "Spherical waves of finite amplitude in a viscous heat conducting medium," Sov. Phys.-Acoust. 9, 42-46 (1963).

13. B. B. Cary, "Nonlinear losses induced in spherical waves," J. Acoust. Soc. Am. 42, 88-92 (1967).

14. M. O. Anderson, "The Propagation of a Spherical N Wave in an Absorbing Medium and its Diffraction by a Circular Aperture," Applied Research Laboratories Technical Report No. 74-25 (ARL-TR-74-25), Applied Research Laboratories, The University of Texas at Austin (1974). (AD 787 878)

15. M. H. Safar, "The propagation of spherical acoustic waves of finite amplitude in fresh and sea water," J. Sound Vib. 13, 1-7 (1970).

16. D. F. Pernet and R. C. Payne, "Non-linear propagation of signals in air," J. Sound Vib. 17, 383-396 (1971).

17. H. M. Merklinger, R. H. Mellen, and M. B. Moffett, "Finite-amplitude losses in spherical sound waves," J. Acoust. Soc. Am. 59, 755-759 (1976).

18. P. J. Westervelt, "Self-Scattering of High Intensity Sound," Proceedings of the Third International Congress on Acoustics, Stuttgart, 1959, L. Cremer, ed. (Elsevier, Amsterdam, 1961), Vol. I, pp. 316-321.

19. I. Rudnick, "Theory of the Attenuation of Very High Amplitude Sound Waves," Technical Report No. 42, Soundrive Engine Co., Los Angeles, California (1952). See also I. Rudnick, J. Acoust. Soc. Am. 25, 1012-1013(L) (1953).

20. N. N. Romanova, "The vertical propagation of short acoustic waves in the real atmosphere," Izv. Acad. Sci. USSR Atmos. Ocean. Phys. 6, 134-145 (1970).

21. T. W. Carlton and D. T. Blackstock, "Propagation of Plane Waves of Finite Amplitude in Inhomogeneous Media with Applications to Vertical Propagation in the Ocean," Applied Research Laboratories Technical Report No. 74-31 (ARL-TR-74-31), Applied Research Laboratories, The University of Texas at Austin (1974).

22. A. H. Nayfeh, "Finite-amplitude plane waves in ducts with varying properties," J. Acoust. Soc. Am. 57, 1413-1415 (1975).

23. R. H. Kraichnan, "The scattering of sound in a turbulent medium," J. Acoust. Soc. Am. 25, 1096-1104 (1953).

24. G. W. Ford and W. C. Meecham, "Scattering of sound by isotropic turbulence of large Reynolds number," J. Acoust. Soc. Am. 32, 1668-1672 (1960).

25. A. N. Malakhov, E. N. Pelinovsky, A. I. Saichey, and V. E. Fridman, "Propagation of Intensive Acoustic Waves in Randomly Inhomogeneous Media," Proceedings of the 6th International Symposium on Nonlinear Acoustics, Moscow, 1975, R. Khokhlov, ed. (Moscow University Press, Moscow, 1976), Vol. I, pp. 139-149.

26. V. E. Fridman and E. N. Pelinovsky, "Spectral Theory of the Intensive Acoustic Waves in Media with Large-Scale Fluctuations," Abstracts of 7th International Symposium on Nonlinear Acoustics, Blacksburg, Virginia, 1976, pp. 47-50.

27. M. Aubry, F. Baudin, A. Weill, and P. Raintreau, "Measurement of the total attenuation of acoustic waves in the turbulent atmosphere," J. Geophys. Res. 79, 5598-4605 (1974).

28. O. V. Rudenko, S. I. Soluyan, and R. V. Khokhlov, "Confinement of a quasiplane beam of periodic perturbations in a nonlinear medium," Sov. Phys.-Acoust. 19, 556-559 (1974).

29. N. S. Bakhvalov, I. M. Zhileikin, E. A. Zabolotskaya, and R. V. Khokhlov, "An acoustic beam in a nonlinear medium," Proceedings of the 6th International Symposium on Nonlinear Acoustics, Moscow, 1975, R. Khokhlov, ed. (Moscow University Press, Moscow, 1976), Vol. I, pp. 88-96.

30. O. V. Rudenko, S. I. Soluyan, and R. V. Khokhlov, "Nonlinear theory of paraxial sound beams," Sov. Phys. Dokl. 20, 836-837 (1976).

31. H. H. Hubbard (Chairman), Sonic Boom Symposium, 3 November 1965, St. Louis, Missouri, J. Acoust. Soc. Am. 39, S1-S80 (1966).

32. H. S. Ribner, ed., Sonic Boom Symposium, 3 November 1970, Houston, Texas, J. Acoust. Soc. Am. 51, 671-798 (1972).

33. W. E. Baker, Explosions in Air (University of Texas Press, Austin, 1973).

34. M. W. Widener and T. G. Muir, "Experiments on parametric arrays in air," J. Acoust. Soc. Am. 55, 429(A) (1974).

35. T. G. Muir, "Nonlinear Parametric Transduction in Underwater Acoustics," Proceedings of IEEE Ultrasonics Symposium, Milwaukee, Wisconsin, November 1973, 603-612.

36. L. V. King, "On the propagation of sound in the free atmosphere and the acoustic efficiency of fog-signal machinery," Phil. Trans. A 218, 211-293 (1919).

37. R. C. Jones, "A fifty horsepower sirens," J. Acoust. Soc. Am. 18, 371-387 (1946).

38. C. H. Allen and I. Rudnick, "A powerful high frequency siren," J. Acoust. Soc. Am. 19, 857-865 (1947).

39. C. H. Allen, "Finite Amplitude Distortion in a Spherically Diverging Sound Wave in Air," Ph.D. Dissertation, The Pennsylvania State University (1950).

40. Y. Shin, "Attenuation of Repeated Spherical Shock Waves," Technical Report No. 22, Department of Physics, University of California, Los Angeles, California (1963), (AD 413 346).

41. H. W. St. Clair, "An electromagnetic sound generator for producing intense high frequency sound," Rev. Sci. Instr. 12, 250-256 (1941).

42. D. E. Watson, Applied Research Laboratories, The University of Texas at Austin, 1975 (unpublished).

43. H. E. Bass, "Study of Sound Propagation in Air," Final Technical Report U. S. Army Research Office, University of Mississippi, University, Mississippi (1976).

44. F. H. Fenlon, "Approximate Methods for Predicting the Performance of Parametric Sources at High Acoustic Reynolds Numbers," Proceedings of 1973 Symposium on Finite-Amplitude Wave Effects in Fluids, Copenhagen, L. Bjørno, ed. (IPC Science and Technology, Guildford, England, 1974), pp. 160-167.

45. M. Abramowitz and I. Stegun, Handbook of Mathematical Functions, National Bureau of Standards Applied Mathematics Series 55, Government Printing Office (1964), Eq. 5.1.53, p. 231.

46. D. T. Blackstock, Applied Research Laboratories, The University of Texas at Austin, 1971 (unpublished).

47. E. L. Stiefel, An Introduction to Numerical Mathematics (Academic Press, New York, 1963), pp. 164-168.

48. M. A. Theobald, D. A. Webster, and D. T. Blackstock, "The importance of finite-amplitude distortion in outdoor propagation experiments," paper presented at the 7th International Symposium on Nonlinear Acoustics, Virginia Polytechnic Institute, State University, Blacksburg, Virginia, 19-21 August 1976.

49. H. D. Parry and M. J. Sanders, Jr., "The design and operation of an acoustic radar," IEEE Trans. Geosci. Electron. GE-10, 58-64 (1972).

50. F. F. Hall, Jr., and J. W. Wescott, "Acoustic antennas for atmospheric echo sounding," J. Acoust. Soc. Am. 5, 1376-1382 (1974).

51. J. A. Gallego Juarez and G. Rodriguez Corral, "Piezoelectric transducer for air-borne ultrasound," Acustica 29, 234-239 (1973).

52. W. T. Fiala, J. K. Hilliard, J. A. Renkus, and J. J. Van Houten, "Electropneumatic acoustic generator," J. Acoust. Soc. Am. 38, 956-964 (1965).

53. "Atmospheric Physics and Sound Propagation," Final Report by Acoustics Laboratory, The Pennsylvania State University, under Signal Corps Contract W36-039-SC-32001 (September 1950) (AT I 94971), pp. 25-146.

54. Y. Y. Borisov, "Acoustic gas-jet generators of the Hartmann type," in Sources of High-Intensity Ultrasound (Vol. 1), L. D. Rozenberg, ed. (Plenum Press, New York, 1969), pp. 3-162.

55. H. F. Olson, Acoustical Engineering (D. Van Nostrand, Inc., Princeton, New Jersey, 1957) pp. 108-109.

56. L. E. Kinsler and A. P. Frey, Fundamentals of Acoustics (John Wiley and Sons, Inc., New York, 2nd ed., 1962), pp. 166-183.

57. H. Stenzel and O. Brosze, Leitfaden zur Berechnung von Schallvorgängen (Springer-Verlag, Berlin, 1958), p. 89.

58. G. J. Thiessen, "Resonance Characteristics of a finite catenoidal horn," J. Acoust. Soc. Am. 22, 558-562 (1950).

59. R. D. Finch and P. W. Higgins, "Optimizing the monotone performance of electrodynamic drivers using tubular couplers," J. Acoust. Soc. Am. 60, 937-943 (1976).

60. W. R. Peterson, "Audio applications of the RCA-HC200 H hybrid linear power amplifier," RCA Application Note AN-4474, RCA Solid State Division, Somerville, New Jersey.

61. Instructions and Applications for 4135/4136 Condenser Microphones, Bruel and Kjaer, Copenhagen, 1963.

62. P. V. Brüel, "Aerodynamically induced noise of microphones and wind screens," Brüel and Kjaer Technical Review No. 2, pp. 3-26 (1960).

63. Instructions and Applications for 4138 Condenser Microphones, Brüel and Kjaer, Copenhagen, 1967.

64. J. N. Cole, R. G. Powell, H. L. Oestreicher, and H. F. von Gierke, "Acoustic siren for generating wide-band noise," J. Acoust. Soc. Am. 35, 173-191 (1963).

65. H. F. Olson, Acoustical Engineering (D. Van Nostrand, Inc., Princeton, New Jersey, 1957) p. 43.

66. "Giant horn simulates sound of Saturn firing," Sound 2, 34-36 (1963).

67. T. F. W. Embleton, "Sound in large rooms," in Noise and Vibration Control, L. L. Beranek, ed. (McGraw-Hill Book Company, Inc., New York, 1971) pp. 221-224.

68. P. M. Morse and U. Ingard, Theoretical Acoustics (McGraw-Hill Book Company, Inc., New York, 1968) p. 580.

69. L. L. Beranek and H. P. Sleeper, Jr., "The design and construction of anechoic sound chambers," J. Acoust. Soc. Am. 18, 140-150 (1946).

70. P. Hedegaard, "Freefield response of sound level meters," Brüel and Kjaer Technical Review No. 2, 3-24 (1976).

71. A. H. Sommer, Letter to the Editor in Phys. Today 29, 9 (1976).

72. L. A. Ostrovsky and A. M. Sutin, "Diffraction and focusing of nonlinearly distorted waves," Proceedings of the 6th International Symposium on Nonlinear Acoustics, Moscow, 1975, R. Khokhlov, ed. (Moscow University Press, Moscow, 1976), Vol. F., pp. 97-108.

73. L. A. Ostrovsky and A. M. Sutin, "On radiation of intensive acoustic horns," Abstracts of the 7th International Symposium on Nonlinear Acoustics in Blacksburg, Virginia, pp. 222-225 (1976).

74. L. A. Ostrovsky and A. M. Sutin, "Diffraction and radiation of sawtooth sound waves," Sov. Phys. Acoust. 22, 49-52 (1976).

75. P. M. Morse, Vibration and Sound (Mcgraw-Hill Book Company, Inc., York, Pennsylvania, 1948), pp. 344-346.

76. A. L. Van Buren and M. A. Breazeale, "Reflection of finite-amplitude ultrasonic waves, I. phase shift," J. Acoust. Soc. Am. 44, 1014-1020 (1968) and "II. Propagation," J. Acoust. Soc. Am. 44, 1021-1027 (1968).

May 1977

DISTRIBUTION LIST FOR
ARL-TR-77-5
UNDER CONTRACT NAS1-14160, CONTRACT F44620-76-C-0040,
CONTRACT N00014-75-C-0867, and GRANT 04-5-022-12
UNCLASSIFIED

AFOSR/NA (16)
Attn: L/C L. W. Ormand
Bldg 410
Bolling AFB, DC 20332

NASA Langley Research Center (5)
Acoustics and Noise Reduction Division
Attn: J. M. Seiner, Mail Stop 460
Hampton, VA 23365

Office of Naval Research (3)
Physics Program Office (Code 421)
Attn: L. E. Hargrove
800 N. Quincy Street
Arlington, VA 22217

National Oceanic and Atmospheric Administration (20)
Environmental Research Laboratories
Attn: F. F. Hall
Boulder, CO 80302

AFAPL (1)
Attn: Paul Shahady
Wright-Patterson AFB, OH 45433

Naval Research Laboratory (1)
Underwater Sound Reference Division
Attn: P. H. Rogers
P. O. Box 8337
Orlando, FL 32806

New London Laboratory (1)
Naval Underwater Systems Center
Attn: M. B. Moffett
New London, CT 06320

Brown University
Department of Physics
Attn: R. T. Beyer (1)
P. J. Westervelt (1)
Providence, RI 02912

Georgia Institute of Technology (1)
School of Mechanical Engineering
Attn: A. D. Pierce
Atlanta, GA 30332

Hendrix College (1)
Department of Physics
Attn: R. L. Rolleigh
Conway, AR 72032

Kalamazoo College (1)
Department of Physics
Attn: W. M. Wright
Kalamazoo, MI 49008

The Pennsylvania State University (1)
Institute for Science and Engineering
Applied Research Laboratory
Attn: F. H. Fenlon
P. O. Box 30
State College, PA 16801

Raytheon Company (1)
Attn: Jim Lockwood
W. Main Road
Portsmouth, RI 02871

The Dept of Physics and Astronomy (1)
University of Tennessee
Attn: M. A. Breazeale
Knoxville, TN 37916

Distribution list for ARL-TR-77-5 (Cont'd)

Office of Naval Research (6)
Code 101 1P (ONR/L)
800 N. Quincy Street
Arlington, VA 22217

Naval Research Laboratory (6)
Code 2627
Washington, D.C. 20375

Commanding Officer (1)
Office of Naval Research
Branch Office
536 South Clark Street
Chicago, IL 60605

Office of Naval Research (1)
Resident Representative
Room No. 582
Federal Building
Austin, TX 78701

Yale University (1)
Mason Laboratory M4
Attn: R. E. Apfel
New Haven, CT 06511

LCDR F. M. Pestorius (1)
2310 Wofford Road
Charleston, SC 29407

US Army Construction Engineering (1)
Research Laboratory
Attn: Paul Schomer
P. O. Box 4005
Champaign, IL 61820

University of Toronto
Institute of Aerospace Studies
Attn: H. S. Ribner (1)
I. I. Glass (1)
4925 Dufferin Street
Downsview, Ontario
Toronto, CANADA, M3H 5T6

Defence Research Establishment (1)
Atlantic
Attn: H. M. Merklinger
P. O. Box 1012
Dartmouth, Nova Scotia
CANADA

Technical University of Denmark (1)
Fluid Mechanics Department
Attn: L. Bjørnø
Building 404
DK-2800 Lyngby
DENMARK

University of Birmingham (1)
Electronic and Electrical
Engineering Department
Attn: H. O. Berktay
P. O. Box 36 B
Birmingham B15 2TT
ENGLAND

University of Toronto (1)
Mechanical Engineering Department
Attn: David S. Scott
Toronto, Ontario
CANADA M5S 1A4

University of Southampton (1)
Institute of Sound and Vibration
Research
Attn: C. L. Morfey
Southampton SO9 5NH
ENGLAND

Centro de Investigaciones Fisicas (1)
"L. Torres Queredo"
Attn: J. A. Gallego Juarez
Serrano 144
Madrid -6
SPAIN

Hans Strohm (1)
852 Erlangen
Mozartstrasse 32
WEST GERMANY

ARL Reserve (30)